

EVALUATION OF REGIONAL SEISMIC DISCRIMINANTS USING THE  
INTELLIGENT SEISMIC EVENT IDENTIFICATION SYSTEM

AD-A258 936



Douglas Baumgardt  
Jeanne Carney  
Michael Maxson  
Sam Carter

DTIC  
ELECTE  
DEC 3 1992  
S C D

SEMI-ANNUAL TECHNICAL REPORT

SAS-TR-93-38

October 23, 1992

DISTRIBUTION STATEMENT A  
Approved for public release  
Distribution Unlimited

Sponsored by:

Defense Advanced Research Projects Agency (DoD)  
Nuclear Monitoring Research Office

ARPA Order 6731, AMD #14

Issued by:

Phillips Laboratory  
Contract F29601-92-C-0009

406167

92-30705



10388

Name of Contractor: ENSCO, Inc.  
Effective Date of Contract: 26 March 1992  
Contract Expiration Date: 31 December 1993  
Reporting Period: 1 April 1992 - 1 October 1992

Principal Investigator: Dr. D.R. Baumgardt  
Phone Number: 703-321-9000

DISCLAIMER

"The views and conclusions contained in this document are those of the authors and should not be interpreted as representing the official policies, either expressed or implied, of the Defense Advance Research Projects Agency or the U.S. Government."

UNCLASSIFIED

SECURITY CLASSIFICATION OF THIS PAGE

REPORT DOCUMENTATION PAGE				
1a. REPORT SECURITY CLASSIFICATION UNCLASSIFIED			1b. RESTRICTIVE MARKINGS	
2a. SECURITY CLASSIFICATION AUTHORITY			3. DISTRIBUTION/AVAILABILITY OF REPORT Unlimited	
2b. DECLASSIFICATION/DOWNGRADING SCHEDULE				
4. PERFORMING ORGANIZATION REPORT NUMBER(S) SAS-TR-93-38			5. MONITORING ORGANIZATION REPORT NUMBER (S)	
6a. NAME OF PERFORMING ORGANIZATION ENSCO, Inc.		6b. OFFICE SYMBOL (If applicable)	7a. NAME OF MONITORING ORGANIZATION Phillips Laboratory/PKRA	
6c. ADDRESS (CITY, STATE, AND ZIP CODE) 5400 Port Royal Road Springfield, VA 22151-2388			7b. ADDRESS (CITY, STATE, AND ZIP CODE) Directorate of Contracting Kirtland AFB, NM 87117-5320	
8a. NAME OF FUNDING/SPONSORING ORGANIZATION DARPA/NMRO		8b. OFFICE SYMBOL	8. PROCUREMENT INSTRUMENT IDENTIFICATION NUMBER F29601-92-C-0009	
8c. ADDRESS (City, State, and Zip Code) 3701 North Fairfax Drive Arlington, VA 22203-1714			10. SOURCE OF FUNDING NUMBERS	
			PROGRAM ELEMENT	PROJECT NO.
11. TITLE (Include Security Classification) Evaluation of Regional Seismic Discriminants Using the Intelligent Seismic Event Identification System				
12. PERSONAL AUTHOR(S) Dr. Douglas Baumgardt, Ms. Jeanne Carney, Mr. Michael Maxson, Mr. Sam Carter				
13. TYPE OF REPORT Semi-Annual Report	13b. TIME COVERED FROM 26 Mar 92 TO 30 Sep 93		14. DATE OF REPORT (Year, Month, Day) 1992 October 23	15. PAGE COUNT 96
16. SUPPLEMENTARY NOTATION				
17. COSATI CODES			18. SUBJECT TERMS (Continue on reverse if necessary and identify by block number)	
FIELD	GROUP	SUB-GROUP	Discrimination, Regional, Seismic, High Frequency, Regional Arrays, Features, Chernov Faces, Multivariate Stars	
19. ABSTRACT (Continue on reverse if necessary and identify by block number)  In this study, the effectiveness of several regional waveform discriminants and processing methods are being evaluated using a large database of regional waveforms. ISEIS has been installed at the Center for Seismic Studies (CSS) where it is being used to process and analyze discriminants for seismic events formed by the Intelligent Monitoring System (IMS). The system has undergone a number of modifications to interface with the CSS databases and to improve the processing efficiency of the system in the CSS environment. Also, a number of new features have been added to facilitate the processing of the data and discrimination research, including automated feature extraction and processing, improved plotting displays for reviewing IMS and analyst phase				
20. DISTRIBUTION/AVAILABILITY OF ABSTRACT <input type="checkbox"/> UNCLASSIFIED/UNLIMITED <input checked="" type="checkbox"/> SAME AS REPORT <input type="checkbox"/> DTIC USERS			21. ABSTRACT SECURITY CLASSIFICATION UNCLASSIFIED	
22a. NAME OF RESPONSIBLE INDIVIDUAL			22b. TELEPHONE (Include Area Code)	22c. OFFICE SYMBOL

DD FORM 1473, 84 MAR

UNCLASSIFIED

SECURITY CLASSIFICATION OF THIS PAGE

UNCLASSIFIED

SECURITY CLASSIFICATION OF THIS PAGE

Block 19:

identification, data viewing displays for reference events plotted in scatterplots, a new top-level display for viewing ISEIS processing results, multichannel coherence and deconvolution processing interfaces, and a research interface for multivariate classification using a simulated neural network approach.

A comprehensive study of regional seismic discriminants, using a variety of multivariate analysis and visualization methods, has been commenced using the large IMS database. This study has revealed two interesting dilemmas: (1) The most effective discriminants between explosions and earthquakes are broad-band (2-16 Hz)  $Pn/Sn$  and  $Pn/Lg$  amplitude ratios, where earthquakes generate more shear-wave energy relative to compressional-wave energy than explosions. However, the ratios have much larger variances, a factor of two or more, for known mine explosions located in the same mine, compared with earthquakes distributed over a large geographic area, which exhibit much less variation. Some mine explosions generate as much shear-wave energy as earthquakes. (2) Performance of the single-phase spectral-ratio discriminant, first discovered for  $Lg$  by Murphy and Bennett (1982) for western U.S. earthquakes and explosions, exhibits extreme regional variation. In Scandinavia, there is little difference in the spectral ratios of mine explosions, nuclear explosions, and earthquakes, as has been reported in other shield regions of the world in other studies. However, the discriminant does effectively separate regionally recorded mine explosions and earthquakes in Germany. A possible explanation of dilemma (1) is that mine explosions may induce associated shear by ripple-firing, which increases the fracture efficiency of the blasting and makes many mine blasts resemble earthquakes. Dilemma (2) may be due to regional variations in geologic differences between shallow structure, where explosions occur, and deep structure, where earthquakes are located. In unstable platform areas, such as the western U.S. and Germany, these geologic differences may cause the shallow blasts to have higher single-phase spectral ratios (less high frequency content) than the deeper earthquakes. Such differences may be less extreme in stable shield areas, such as Scandinavia, where there is less of a difference in single-phase ratio between explosions and earthquakes. Variation in the depth separation of blasts and earthquakes (less in the shield regions) may also partly explain the dilemma.

UNCLASSIFIED

SECURITY CLASSIFICATION OF THIS PAGE

## TABLE OF CONTENTS

SECTION	PAGE
ABSTRACT .....	iii
1.0 INTRODUCTION .....	1
1.1 OBJECTIVES .....	1
1.2 SUMMARY.....	2
1.2.1 Research Accomplished .....	2
1.2.2 Overall Conclusions.....	3
1.2.3 Organization of Report.....	4
2.0 NEW DEVELOPMENTS IN THE INTELLIGENT SEISMIC EVENT IDENTIFICATION SYSTEM AND INSTALLATION AT THE CENTER FOR SEISMIC STUDIES.....	5
2.1 INTRODUCTION .....	5
2.2 INSTALLATION AT THE CSS - ISSUES .....	6
2.2.1 Automated Processing.....	6
2.2.2 Automated Phase Selection.....	8
2.2.3 Faulty Channel Data and Their Elimination .....	9
2.2.4 Removing Intermediate Database Results .....	11
2.2.5 Improvement of Efficiency.....	12
2.3 NEW DEVELOPMENTS IN ISEIS .....	14
2.3.1 PhaseSelect Interface.....	14
2.3.2 Scatterplot Displays - ViewEvts.....	17
2.3.3 Top Level Summary (TLS) Interface .....	29
2.3.4 ISEIS Interface to the NMRD Map Process.....	32
2.3.5 Coherence, Deconvolution, and Neural Networks.....	35
3.0 COMPARATIVE STUDY OF DISCRIMINATION OF MINE EXPLOSIONS AND EARTHQUAKES IN THREE DIFFERENT GEOGRAPHIC REGIONS .....	37
3.1 BACKGROUND AND OBJECTIVES.....	37
3.2 DATA AND ANALYSIS PROCEDURES.....	38

## TABLE OF CONTENTS (CONTINUED)

SECTION		PAGE
3.3	DATA ANALYSIS RESULTS.....	43
3.3.1	Phase Selections and Incoherent Beams.....	43
3.3.2	Visualization Methods - Southern Norway Events.....	45
3.3.3	Discrimination of Steigen Earthquakes and Kola Blasts - ARCESS.....	56
3.3.4	Discrimination of Vogtland Earthquakes and Blasts - GERESS.....	63
3.4	DISCUSSION.....	73
3.4.1	High Amplitude Ratio Variance in Blasts.....	73
3.4.2	Variability in Performance of the <i>Lg</i> Spectral Ratio Discriminant.....	83
3.5	CONCLUSIONS.....	93
4.0	REFERENCES.....	94

**DTIC QUALITY INSPECTED 2**

Accession For	
NTIS <del>ORIS</del>	<input checked="" type="checkbox"/>
DTIC TAB	<input type="checkbox"/>
Unannounced	<input type="checkbox"/>
Justification	
By _____	
Distribution/	
Availability Codes	
Dist	Avail and/or Special
A-1	

## ABSTRACT

In this study, the effectiveness of several regional waveform discriminants and processing methods are being evaluated using a large database of regional waveforms. ISEIS has been installed at the Center for Seismic Studies (CSS) where it is being used to process and analyze discriminants for seismic events formed by the Intelligent Monitoring System (IMS). The system has undergone a number of modifications to interface with the CSS databases and to improve the processing efficiency of the system in the CSS environment. Also, a number of new features have been added to facilitate the processing of the data and discrimination research, including automated feature extraction and processing, improved plotting displays for reviewing IMS and analyst phase identification, data viewing displays for reference events plotted in scatterplots, a new top-level display for viewing ISEIS processing results, multichannel coherence and deconvolution processing interfaces, and a research interface for multivariate classification using a simulated neural network approach.

A comprehensive study of regional seismic discriminants, using a variety of multivariate analysis and visualization methods, has been commenced using the large IMS database. This study has revealed two interesting dilemmas: (1) The most effective discriminants between explosions and earthquakes are broad-band (2-16 Hz)  $Pn/Sn$  and  $Pn/Lg$  amplitude ratios, where earthquakes generate more shear-wave energy relative to compressional-wave energy than explosions. However, the ratios have much larger variances, a factor of two or more, for known mine explosions located in the same mine, compared with earthquakes distributed over a large geographic area, which exhibit much less variation. Some mine explosions generate as much shear-wave energy as earthquakes. (2) Performance of the single-phase spectral-ratio discriminant, first discovered for  $Lg$  by Murphy and Bennett (1982) for western U.S. earthquakes and explosions, exhibits extreme regional variation. In Scandinavia, there is little difference in the spectral ratios of mine explosions, nuclear explosions, and earthquakes, as has been reported in other shield regions of the world in other studies. However, the discriminant does effectively separate regionally recorded mine explosions and earthquakes in Germany. A possible explanation of dilemma (1) is that mine explosions may induce associated shear by ripple-firing, which increases the fracture efficiency of the blasting and makes many mine blasts resemble earthquakes. Dilemma (2) may be due to regional variations in geologic differences between shallow structure, where explosions occur, and deep structure, where earthquakes are located. In unstable platform areas, such as the western U.S. and Germany, these geologic differences may cause the shallow blasts to have higher single-phase spectral ratios (less high frequency content) than the deeper

earthquakes. Such differences may be less extreme in stable shield areas, such as Scandinavia, where there is less of a difference in single-phase ratio between explosions and earthquakes. Variation in the depth separation of blasts and earthquakes (less in the shield regions) may also partly explain the dilemma.

## **1.0 INTRODUCTION**

### **1.1 OBJECTIVES**

This report describes the results of a project to examine many seismic discriminants for small events recorded at regional distances using the newly assembled regional seismic databases at the Center for Seismic Studies (CSS) and to evaluate new knowledge-based approaches to seismic event characterization. In the context of monitoring worldwide low-yield comprehensive testban treaties and proliferation of nuclear weapons, the reliable identification of small seismic events is a key issue. National technical means must be developed to identify small earthquakes and economic explosions in a number of different geographic regions and to discriminate between these expected normal seismic events and nuclear tests, which may be in violation of existing treaties. Moreover, seismic identification of nuclear testing activity in any country, previously assumed not to be nuclear-weapons capable, provides the final confirmation of nuclear-weapons proliferation to such states.

The overall objective of this project is to utilize a new research prototype for seismic discrimination, called the Intelligent Seismic Event Recognition System (ISEIS) and described by Baumgardt et al (1991a, b), to evaluate regional seismic discrimination methods utilizing the databases produced by the Intelligent Monitoring System (IMS), described by Bache et al (1991). The IMS detects regional seismic events, recorded primarily by the four regional seismic arrays, NORESS, ARCESS, FINESA, and GERESS, as well as selected three-component stations, identifies key regional seismic phases, and locates events using combined phase travel times and array-parameter measurements. This process has been running online at NORSAR processing data from all four arrays since the beginning of 1991 and has produced waveform edits for many thousands of regional seismic events in Scandinavia, southern Europe, and western Russia which have been stored at the Center for Seismic Studies (CSS) in an Oracle database. Our goal in this study is to interface the ISEIS system with this database at the CSS and evaluate waveform discrimination techniques on this very large database.

There are, specifically, three overall objectives in this study:

- (1) Process through ISEIS the large database of waveforms in the IMS database, extract and store in a database numerous regional waveform features which may be useful discriminants, and test the discriminatory performance of the current rules in ISEIS on events of known identity.
- (2) Use multivariate and statistical analysis techniques to identify those waveform features which are most discriminatory.

- (3) Revise the rules in the ISEIS expert system to utilize the best discriminant features which optimize event identification performance.

## 1.2 SUMMARY

During this reporting period, a number of different projects were initiated, both in the improvement and CSS implementation of ISEIS and in the use of ISEIS to investigate in detail multivariate waveform discriminants. In Section 1.2.1, we summarize the work that has been completed and in Section 1.2.2, we present the conclusions of the research studies accomplished to date.

### 1.2.1 Research Accomplished

In this report, we describe the activities and results of the first six months of this 18 month study. The specific tasks which have been accomplished in this first period include the following:

- (1) ISEIS has been installed at the Center for Seismic Studies to process data from any Oracle database in automated and/or interactive modes. Improvements have been made to the user interfaces to reduce wait times for data and displays and to increase processing efficiency. Additional features have been added to the interface to efficiently review processing results, including review of previous phase identifications and to allow corrected and/or additional phase selections to be made if necessary.

- (2) A new *Top Level Summary (TLS)* interface has been added, in addition to the *Spreadsheet* interface, which provides the user with a simple review of ISEIS processing results and an interface to input event identifications and information interactively.

- (3) New facilities have been added to both the automated and interactive processes to "clean" the database of sometimes voluminous secondary data for events which have been identified in order to save disk space.

- (4) Additional features have been added to the "phase-selection" user interfaces, which include display of phase picks of the analyst from the Analyst Review Station (ARS), as well as predicted arrival times, automatic phase selection based on phase picks, including start time and/or duration, zooming options, and optional display of RMS incoherent beams with and without taking the logarithm. The phase pick displays have also been added to the individual waveform display user interfaces.

(5) A new user interface, called *ViewEvs*, has been added to the scatterplot displays to allow the user to immediately call up waveforms, incoherent beams, and spectra for selected events which appear in the scatterplot.

(6) Two new research interfaces, *Deconvolution* and *Coherence*, have been added, both of which are based on the work Zoltan Der and Robert Shumway. The former deconvolves teleseismic *P* and coda into source and receiver functions for closely spaced groups of events, recorded at a large array, for purposes of extracting source information, particularly *pP* depth information. *Coherence* provides a user interface for computing multichannel coherence functions between reference events and new events for "case-based" event characterization, as described by Der et al (1990). A third interface, *Neural Networks*, has also been developed which implements a three-layer perceptron neural network simulator for multivariate event classification.

(Note: The *Deconvolution* interface itself was initially developed under another project and was simply interfaced to ISEIS in this project. Because it is a teleseismic discrimination technique and this project will focus primarily on regional discriminants, there are no plans under this project for extensive research using this interface. The *Coherence* interface, on the other hand, directly relates to regional event identification in that it provides a multichannel method for characterizing events in terms of the similarity to previously recorded events in the same geographic region.)

(7) About one month (January) of data from the four-array database at the CSS (IMS2) from 1992 have been processed through ISEIS automatically and are currently being reviewed interactively. Also, the months of February and March have been processed with autoISEIS although they have not yet been interactively reviewed. Also, known events from an earthquake swarm in the Steigen region of northern Norway, presumed mine explosions on the Kola Peninsula and in Sweden, and events in the Vogtland region in Germany, including known earthquakes and explosions, have been processed through ISEIS using information being accumulated at the CSS in a specially prepared "ground truth" database (Grant and Coyne, 1992). The Vogtland data were previously studied by Wuster (1992) in a discrimination study and the results of the ISEIS processing of these events are being compared with those of the Wuster study.

### **1.2.2 Overall Conclusions**

(1) Incomplete, inconsistent, and sometimes inaccurate phase identifications in the IMS2 database makes automated discrimination processing problematic without analyst review of all events. Complete phase identifications (not just those needed for event location) need to be made in order to provide sufficient consistent waveform features for discriminant evaluation.

(Note: In the current ongoing research, data from the time period of February through April, 1991, are being processed through ISEIS, a time period when the Norwegian analysis procedure was optimized and when the most thorough analysis of all the events was made (Ryall, personal communication). A record is being kept of the when and how phase identifications of the ARS analyst are changed by the ISEIS analyst and statistics will be produced to quantify the degree of discrepancy between what is required by the ISEIS process in phase identification and what is currently being produced by the IMS analysis procedures. Hopefully, this study will provide some guidance on how phase identification procedures in the IMS can be improved, if necessary, in order to adequately support automated event-identification processing.)

(2) Analysis of  $Pn/Sn$  and  $Pn/Lg$  amplitude-ratio discriminants in three completely different regions has shown that earthquakes are very similar, in terms of the broad-band variations, as revealed by Chernov faces and star displays. Amplitude ratios for earthquakes in Scandinavia and Germany have extremely low variance, less than a factor of two, for events spread over hundreds of km. By contrast, mine explosions have much greater variance, a factor of three or more, even for events in the same mine or mine district. Many mine blasts generate strong shear waves, perhaps due to fracturing of rocks by the ripple-firing or associated mine tremors. It is possible that many of the events assumed to be mine blasts may actually be rock bursts. Although high frequency  $Pn/Sn$  and  $Pn/Lg$  ratios are good discriminants, this large variance for the mine blasts causes many blasts to overlap the earthquake populations.

(3) The  $Lg$  spectral ratio discriminant does not seem to work well in Scandinavia. However, preliminary results of processing the GERESS data for Vogtland indicates that it does separate mine blasts and earthquakes at a distance range of about 150 to 200 km. Such regional variation may be due to regional differences in the geology of the local blasting sites.

### 1.2.3 Organization of Report

Section 2.0 of this report describes the configuration of the implementation of ISEIS at the CSS and some of the processing issues which had to be addressed in this effort. Section 3.0 describes the results of a research study of seismic discriminants in two different geographic regions, the results of which were summarized above. Note that the ISEIS analysis of the four months of data in 1991, alluded to in conclusion (1) above, and the study of the new *Coherence*, *Deconvolution*, and *Neural Network* interfaces are still in progress and will be discussed in detail in subsequent reports.

## 2.0 NEW DEVELOPMENTS IN THE INTELLIGENT SEISMIC EVENT IDENTIFICATION SYSTEM AND INSTALLATION AT THE CENTER FOR SEISMIC STUDIES

Douglas Baumgardt, Jeanne Carney, Michael Maxson, and Sam Carter

### 2.1 INTRODUCTION

This project follows up earlier work on the development of a prototype research system for regional seismic discrimination, the Intelligent Seismic Event Identification System (ISEIS). ISEIS provides numerous graphics interfaces for extracting and analyzing seismic waveform features from regional seismic events. In this study, the effectiveness of several regional waveform discriminants and processing methods are being evaluated, using the large database of regional waveforms generated by the Intelligent Monitoring System (IMS), currently operating continuously in Norway on signals detected by the four regional arrays, NORESS, ARCESS, FINESA, and GERESS. Waveform features are to be measured with the Intelligent Event Identification System (ISEIS), which has been developed as an automatic and interactive backend system to identify events formed by the IMS (Baumgardt et al, 1992).

The ISEIS processing approach, as applied to regional arrays, is described in detail by Baumgardt et al (1991a, b). In brief, the processing steps include: (1) *incoherent beam* computation in nine primary filter bands, ranging from 0.5-2.5 Hz (for possible *Rg* phases analysis) to 8-16 Hz; (2) *stapick* selection for key phases and amplitude computation (maximum and average) within the *stapick* windows; (3) amplitude-ratio computation (same frequency) for selected phases; (4) array-stacked spectral density computation in the *stapick* windows; (5) spectral ratio computation for all phases; (6) cepstrum calculation for ripple-fire detection and depth estimation; (7) storage of all key features to an Oracle database; (8) rule-based processing, using rules coded in the NASA expert systems shell, CLIPS, to identify events on the basis of individual discriminants extracted from the database; and (9) overall event identification using a voting scheme.

A number of new capabilities have been added to ISEIS, beyond those discussed by Baumgardt et al (1991a, b), in order to facilitate the processing of data at the CSS. A number of other changes were made in order to improve interactive processing, in particular, to reduce wait times for acquisition of data from the database and to bring up displays. Other changes were made to facilitate the analysis of the data in the discrimination research study. The details of the CSS installation and issues which we had to confront in this effort are discussed in the next section.

## 2.2 INSTALLATION AT THE CSS - ISSUES

The flow diagram in Figure 1 shows the details of the ISEIS implementation at the CSS. This diagram shows how data from the CSS Oracle databases is migrated into the ISEIS database and processed through ISEIS, both in automated and interactive modes. Database relations, including event parameters (*origin*, *originerr*) analyst phase picks (*arrival*, *assoc*), and waveform pointers (*wfdisc*, *wftag*), are copied from a CSS Oracle database to the ISEIS\_IMS database for selected events of interest. The formats and descriptions of these standard CSS 3.0 database schema relations are described by Anderson et al (1990).

ISEIS processing is keyed initially to phase identifications and time picks made by the Intelligent Monitoring System (IMS) and/or the analyst review in the Analyst Review Station (ARS). ISEIS computes incoherent beams, makes phase selections, computes spectra and cepstra, and extracts features based on the phase picks. Initial event identifications by an expert system uses rules coded in the NASA expert system shell, CLIPS, and results are displayed in two user faces, *Spreadsheet* and *Top Level Summary (TLS) Interface*. Examples of the *TLS* are shown below. Interactive ISEIS provides the capability to review the automated phase selections and change them, and then automated ISEIS can be rerun with the corrected phase selections. It is essential that complete and consistent phase selections be made in order for reliable discriminants to be extracted. So far, in order to have consistency in phase selections, we have found it necessary to interactively review all events and reselect many phase picks because of inaccurate and/or incomplete phase identifications in the IMS. As mentioned earlier, we are now collecting statistics on how often phase identifications in the IMS are changed in ISEIS.

### 2.2.1 Automated Processing

ISEIS was originally intended to serve both as a discrimination-research and special-event analysis system, as well as a prototype for routine event-identification processing. The ISEIS design places primary emphasis on interactive processing and data visualization. However, in order to utilize ISEIS for routine, online processing, an automated mode of processing was required. Moreover, the automated processing in ISEIS was required in the research and special-event analysis, as well as in order to allow the analyst to avoid the many tedious processing steps in ISEIS.

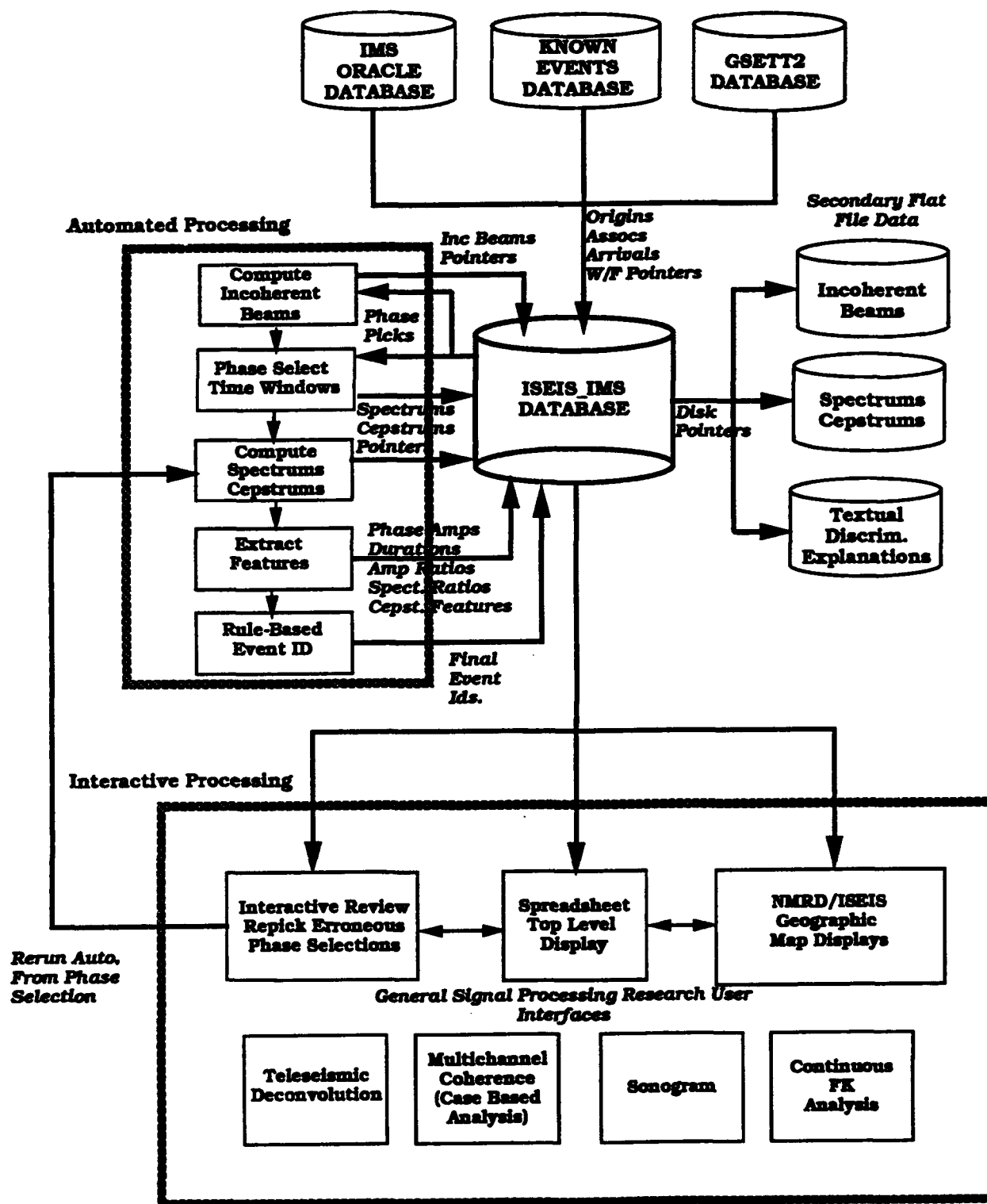


FIGURE 1: Functional flow diagram of the ISEIS implementation at the CSS.

Two new processes were developed for automated processing in ISEIS. First, *autoISEIS* accesses the *timestamp* relation in the database to determine which origin-ids (*orids*) in the database to process. Then, *autoDS* is either started from the *Spreadsheet* display or from a script in background. From the *Spreadsheet*, *autoDS* is started by selecting a range of events and then either selecting EXECUTE AUTO/SELECT or EXECUTE AUTO/ALL from the *Spreadsheet*. This method will probably not be used that much since the Spreadsheet must remain active during the course of automatic processing. Another more convenient script-based method is also available for background processing.

The procedure for submitting a batch of events for background automated processing is as follows:

- (1) Run the *TLS* or *Spreadsheet* process and select the OPEN\_DB function from the FILE menu and select events based upon the desired criteria.
- (2) Run the MakBatch.csh script to produce an autoDS script from the given eventFile.d file. Execute as:

```
MakBatch.csh $HOME/tmp/eventFile.d batch_file_name
```

- (3) Execute the newly created script as:

```
batch_file_name >& /dev/null &
```

We have found in general that for four-array data, about 30 to 40 minutes is required to completely process one event. This time varies depending on the length of the seismograms and the number of recording arrays.

### **2.2.2 Automated Phase Selection**

Automated phase selection is required by *autoDS* for two reasons: (1) the start time for computing the incoherent beams must be determined and (2) the onset times and window lengths for extracting regional phase features must be determined. For phase amplitude discriminants, such as amplitude ratios, the time window must be selected for finding the maximum phase amplitude or for computing average absolute value or rms averages. For spectral discriminants, the phase-selection windows give the time windows for computing spectra. As was mentioned above, the automated ISEIS process *autoDS* keys entirely off the phase identifications provided

by the IMS expert system or the analyst picks in the ARS. However, accurate phase identification and onset timing is critical for the success of this procedure.

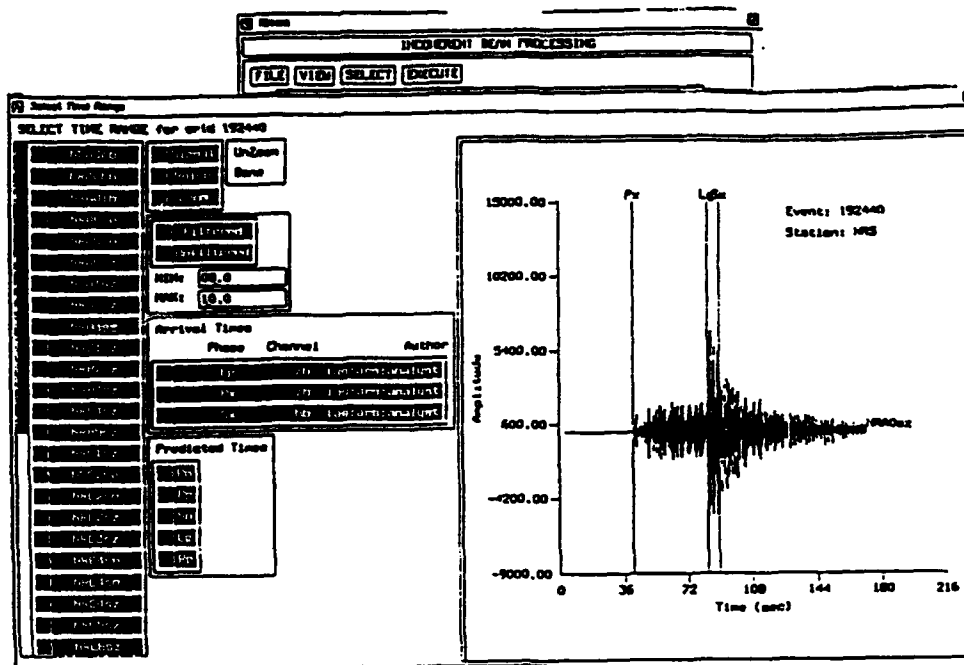
To accomplish the first purpose, the initiation of the incoherent beam processing, the phase time from the IMS for the first *P* phase associated with the event is used to select the start time for computing the incoherent beams. The actual start time is set at least 30 seconds in the noise before this first *P* time if this much noise is available in the waveform edit generated by the IMS. This makes it easier to see the onset time of the phase. For this purpose, accurate phase identification and timing is not so critical as long as there is sufficient noise available ahead of the first *P* onset.

Figure 2 shows an example of an earthquake recorded at NORESS for which the first arrival compressional phase was labeled *Px*. *Px* is an IMS phase identification for "generic regional *P*" for which a precise identification could not be made. Figure 2a shows an example of an interactive waveform view display from ISEIS with the analyst phase picks marked on the waveform and listed in the legend to the left of the main window. In Figure 2b, the blackened-in regions show the time windows for which the incoherent beams are computed. The identification of the first phase as *Px* is not a problem in computing incoherent beams. However, amplitude ratios in ISEIS require that either a *Pn*, *Pg*, or *P* be identified.

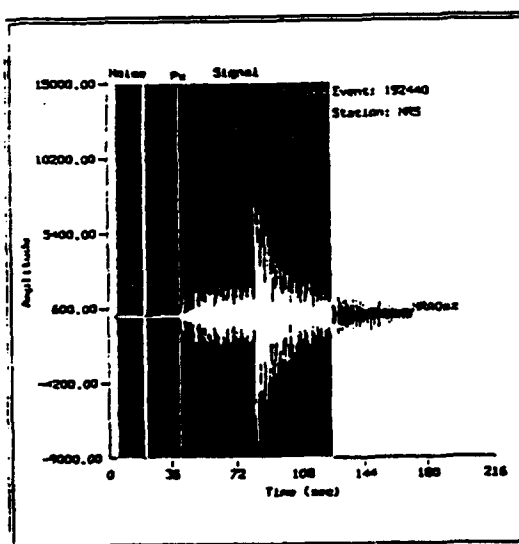
Figure 2c shows a display of the resultant incoherent-beam in the *PhaseSelect* interface, which will be described later (Section 2.3.1). This phase identified by IMS as *Px* appears on the incoherent beam to be *Pn* and was so identified interactively in ISEIS. The darkened regions indicate the *stapick* windows which will be used for the subsequent feature extraction. In this example, the *Pn* phase has been identified and a *Pg* phase, not detected by IMS, can be clearly observed in the incoherent beams and is so labeled. After repicking the phases, the rest of the processing steps can be redone automatically, using the "-nphase" option in *autoDS*. Correct phase identification and event location is vital in order for subsequent event identification to be successful.

### **2.2.3 Faulty Channel Data and Their Elimination**

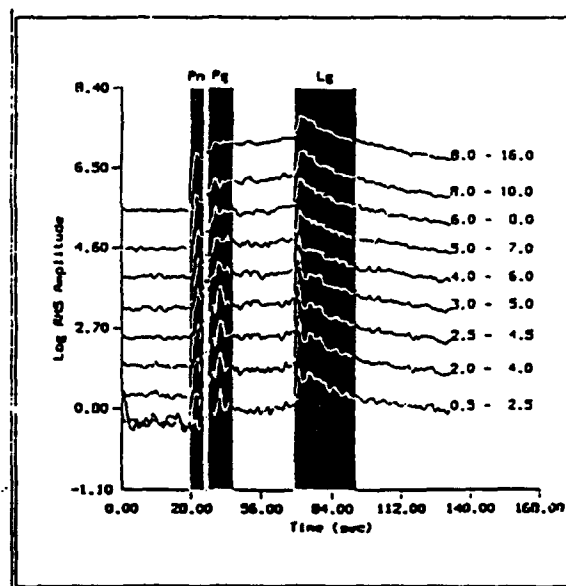
A major problem in automated seismic processing is the identification and elimination of faulty channels prior to processing. Faulty data consists of channels containing system noise, i.e., spikes, dropouts and glitches, missing channels, or channels which are bad because of other known problems. The system noise problem seems to be particularly severe in the case of the GERESS array, perhaps due to the fact that the data is transmitted from Germany to Norway via land telephone line (Jan Wuster, personal communication). Such noise can be a major problem,



(a)



(b)



(c)

**FIGURE 2: (a) Display of the waveform display of an earthquake recorded at NORESS. Note that the first phase is identified as *Px*, which means generic *P* but unidentified. (b) Time range on the incoherent beam selected for computation of the incoherent beam. (c) The resultant incoherent beams, with blackened regions showing the "phase selections" made by the ISEIS analyst.**

particularly for array-averaged spectral analysis if the noise is prevalent on many of the channels. Missing channels are less of a problem since the data in these channels are all zeros or the channel is not there at all, although such channels still should not be processed.

The GERESS array also has another known problem; some of the array elements were sited inadvertently on weathered sedimentary rocks. These sites have significant noise caused by resonances in the sediments. This problem was first noted when the ripple-fire discriminants applied to GERESS data identified all events as ripple-fired mine blasts (Sereno, 1992). The GERESS channels which have this problem are A0, A3, B3, B5, C1, D5, and D9 (Jan Fyen, personal communication). This problem can be corrected by simply not using these channels in all processing, which is what was done in ISEIS. However, it is unfortunate that so many channels must be dropped out in addition to the channels which must be eliminated because of glitches. In future work, receiver functions should be developed for these resonances and deconvolved from the data so that all the channels can be used.

In the interactive version of ISEIS, a channel review facility has been provided in the incoherent beam (IBeam) and spectral analysis (fsdisplay) interfaces. In this interface, the user can scroll through all the channel waveforms, identify channels which are faulty, and delete the corrupted channels in a top level pull-down menu. This process can be very tedious and time consuming, necessitating an automated procedure for accomplishing this. The IMS signal analysis function (SIGPRO) has subroutines for the automatic elimination of faulty channels, which must be done before beamforming and FK analysis. Unfortunately, no facility has been provided in the CSS 3.0 database to retain a record of which channels are bad, so that this process must be repeated for all subsequent processing of the waveform edits generated by IMS.

The ISEIS automated process, *autoDS*, uses a channel removal algorithm to throw out corrupted channels. This algorithm, modified from the IMS version, was originally used in RONAPP (Mykkeltveit and Bungum, 1984). Each channel's maximum amplitude is compared with the average amplitudes across the array. Any channel whose maximum amplitude exceeds the array average is considered to have a large spike. Although this algorithm is very simple and may not work in all cases, such as when all channels have large spikes, we have found it to work in most instances.

#### **2.2.4 Removing Intermediate Database Results**

Because of the limited disk storage at the CSS, it is not feasible to permanently store all the relations and disk files produced by ISEIS. Thus, if an event has been processed and identified,

these data can be deleted if the event is not to be kept as a reference event. The *Spreadsheet* display has a database cleanup interface, an example of which is shown in Figure 3, which provides the capability of deleting all or some of the processing data and features produced by ISEIS. The user selects CLEAN\_DB from under the FILE menu and selects items for deletion. This interface produces a list of database relations/files which are to be deleted by mouse-selecting the check boxes on the left of each. The *Def* button in the upper right sets the default values to be deleted. Incoherent beam files (\*.sta) and spectral/cepstral files (\*.fs, \*.mc, \*.fc) consume the bulk of disk space and can be easily reconstructed for an event. These relations are deleted by default. Feature data, such as *stapicks* or amplitude ratios, take up less space in the Oracle database and may be kept longer as reference, which can be compared with new events or used as training events in a discrimination procedure. However, these may also be eliminated if desired. In addition to the interactive interface, the clean function is also applied in the automated processing when an event is reprocessed. All of the old database relations and intermediate disk files are deleted, except for the original waveform data, the IMS *origin*, *arrival*, and *assoc* relations, and incoherent beams and phase selections if the "-nphase" option is invoked.

### **2.2.5 Improvement of Efficiency**

In the spring of 1992, the ISEIS software was modified to increase program performance. Specifically, database access software was modified to reduce access time. Changes in index usage, frequency of database access, and relation-ordering generated a marked improvement in program performance.

Database indices were created for all relations used by ISEIS. A database index reduces access time by providing direct access to rows in a table. Hence, creating indices on the elements most frequently accessed in each relation improved ISEIS performance substantially.

Further, program performance was increased by reducing the frequency of database access. Database queries found in loops were targeted in particular. Multiple database queries were sometimes combined into one statement. For a relation frequently accessed (such as *wfdisc*), programs were restructured to read the relation's information at the beginning of the program. The relation information was then readily available in memory until program completion. Further, certain database routines were found to access the same data twice. This was done in an effort to count the number of database elements, to allocate space for them, then to read them in from the

[illegible]

**FIGURE 3: Display of window produced by the *DB CLEAN* selected under the *OPEN* menu on the Spreadsheet. Each bar corresponds to a specific database relation or intermediate disk file which can be selected for deletion.**

database. To overcome this problem of duplicate database access, memory allocation routines were written which provide memory as data is read in. Hence, the data is only accessed once.

Finally, relation names were reordered in joint database queries. When relations were arranged from those with the largest number of elements to those with the smallest, database access time decreased. It was found that placing the *affiliation* relation in a joint database query decreased performance substantially when this query was made repeatedly in a programming loop. Hence, in these instances, the software was rewritten to access the affiliation relation a single time outside the programming loop. The SQL "IN" operator then played an important role in incorporating the *affiliation* relation's information into the database queries made in the programming loop.

## 2.3 NEW DEVELOPMENTS IN ISEIS

A number of new features were added to the basic ISEIS system, in addition to the changes discussed above for the installation of the system at the CSS and automated processing. These additions were made to improve visualization capabilities of the system and to allow more efficient review of processing results.

### 2.3.1 PhaseSelect Interface

The *PhaseSelect* interface is one of the most important functions in ISEIS. It provides a method for "phase selecting," which amounts to setting the start and stop times of specified phases, called *stapicks*, on incoherent beams, as opposed to "phase picking," which just sets the precise onset time of the phase. It is important to realize that *stapicks* are only meant to designate phase windows for purposes of subsequent feature extraction for waveform discrimination purposes. The start times of *stapicks* are probably not more precise than IMS phase picks since the former are on incoherent beams, not waveforms, and they may in fact be intentionally early in order to ensure that the maximum phase energy is centered in the *stapick* window.

The original interactive interface, described in the ISEIS User's Manual (Baumgardt, 1991a), was implemented as a subprocess under two primary processes which relied heavily on phase selections, ampratio, and dynamic time warping (DTW), and was initiated by mouse selection of the PHASE option. However, it can now be directly invoked from the top level *Spreadsheet* display under the EXECUTE pull-down menu. A number of new features have been added to the *PhaseSelect* interface to provide more visibility to the IMS and ARS analyst phase picks, the results of the automated phase selection, and various display options for the incoherent beams.

Figure 4 shows an example of a *PhaseSelect* window, which is a screen dump of a color display. This window contains a plot of incoherent beams with previously stored *stapicks* highlighted. To the upper left of the main window is a set of checkboxes containing drag types. To magnify an area of the incoherent beams, the user selects the drag type "Zoom" with the left mouse button, highlights the desired area by dragging the mouse with the left button depressed, and clicks the left mouse button on the "Zoom" button to the right of the plot. The user may select areas and zoom as many times as desired. To restore the original incoherent beams, the user clicks on "UnZoom" with the left mouse button.

Prior to defining a new phase window, the user may want to clear the old phase selections from the plot which is accomplished by clicking the left mouse button on the phase name displayed above the highlighted phase region on the plot.

To define new phase windows, the user clicks the left mouse button on the "Signal" drag type. To the left of the drag type checkboxes is a set of checkboxes containing phase names. The user selects the checkbox of the desired phase with the left mouse button. Then, the user drags the mouse on the desired plot area with the left button depressed.

Arrival and predicted times aid the user in identifying phase start times. Checkboxes for both are displayed below the phase name checkboxes. Phase arrival times are those times previously picked in the IMS/ARS and stored in the database. The arrival time checkboxes are labeled with the phase name, the channel on which the phase was identified, and the name of the user who made the pick. If phase times were not picked in the IMS/ARS, checkboxes for the arrival times will not appear on the display. Phase arrival times are marked on the incoherent beam plot in red. Predicted times are computed based on phase velocity. These times are marked on the incoherent beam plot in blue.

To automatically compute phase windows, the user clicks on "Auto" with the left mouse button. The program will then use the earliest phase arrival times to set phase start times. If an arrival time is not found for a phase, the predicted start time will be used. Phase lengths are computed based on phase velocity ranges. The user may be dissatisfied after selecting new phase windows. If so, clicking the left mouse button on "Restore" returns the original phase selections to the incoherent beams.

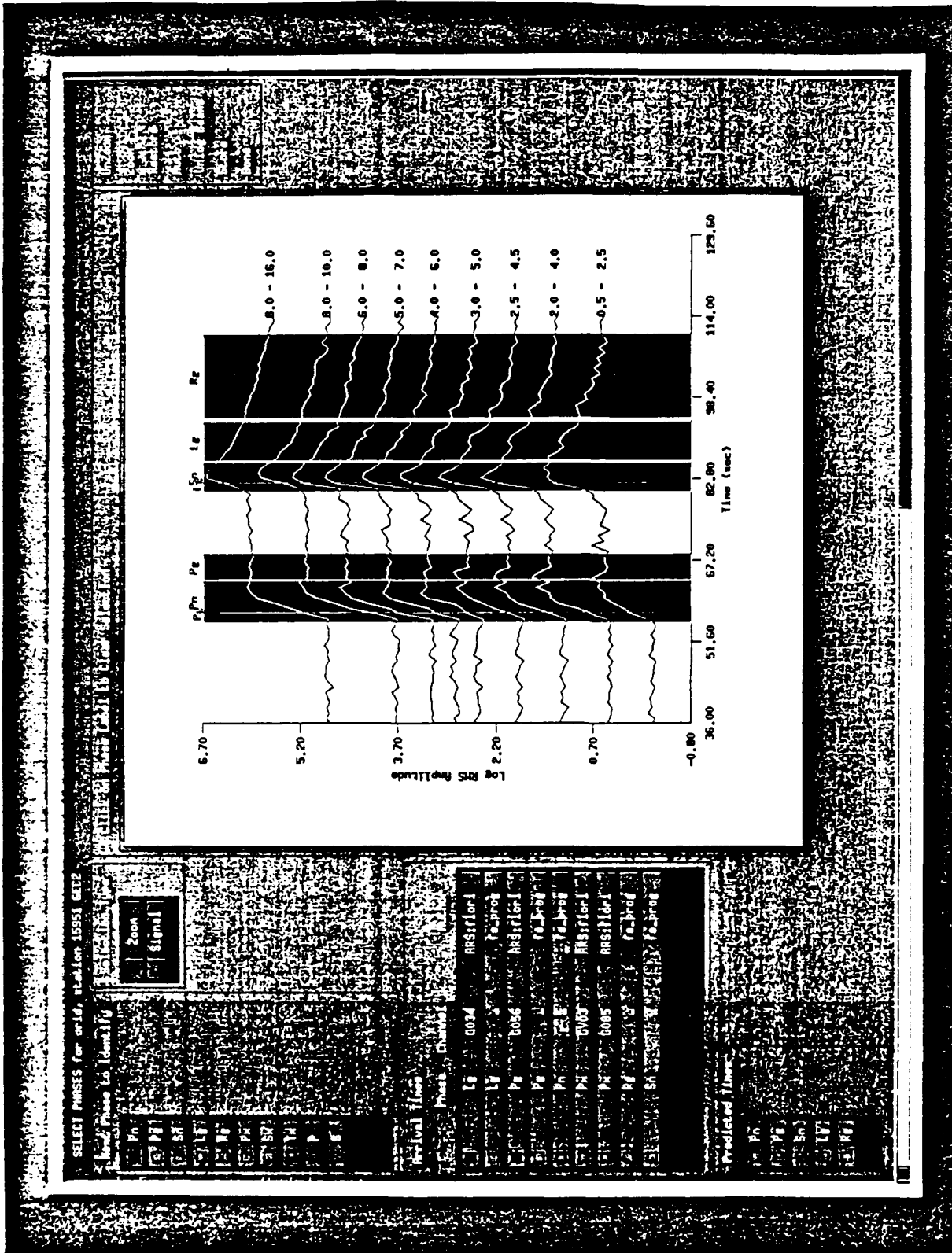


FIGURE 4: Screen dump of the Phase Select interface. The incoherent beams are those computed for one of the Vogtland events, discussed in Section 3.0.

The y-axis of the plot displays the incoherent beams' logged root-mean-square (rms) amplitude values. To display the rms amplitude values (unlogged), the user clicks on "Unlog Beams" with the left mouse button. The unlogged beams are then displayed, and the "Unlog Beams" button is relabeled "Log Beams." The unlogged beams more closely resemble the original waveforms than the logged beams. However, if there is a large amplitude difference between the largest and smallest beam amplitudes, the log plot reduces this large dynamic range. The user may restore the logged beams by clicking on "Log Beams" with the left mouse button.

The user may store the selected phase windows by clicking on "Store Times" with the left mouse button. *Stapick* features are then computed, i.e., maximum and average amplitudes in the phase windows, and stored in the database. If the user exits the PHASES window without clicking on "Store Times," all the phase window selections he/she has made will not be recorded.

The user may exit the PHASES window by clicking on "Done" with the left mouse button.

### **2.3.2 Scatterplot Displays - ViewEvts**

One of the primary visualization displays in ISEIS are the scatterplot displays which compare feature measurements for a particular event (CURRENT EVENT) with those made for reference events. The features which can be plotted include amplitude ratios (ARDISPLAY), which can be displayed as a function of reference region, distance, magnitude, signal-to-noise ratio, and frequency, and spectral ratio (SRDISPLAY), which can be plotted as a function of all of the above except for frequency. In each case, the user selects one or more reference regions from which to take a reference event which are plotted along with the same measurements for the current one. Detailed descriptions of these interfaces can be found in the ISEIS Users Manual (Baumgardt, 1991a).

In the course of doing analysis, we have found that it would be useful to immediately view signal information for the current event and reference events from which the features being viewed in the scatterplots were extracted. For this reason, a new facility, called *ViewEvts*, has been developed which can be initiated directly from any of the scatterplot displays. In this section, we discuss in detail the *ViewEvts* interface as it appears in the VIEW-BY-MAGNITUDE display for amplitude ratios when it is invoked under the VIEW menu of the ARDISPLAY. The same interface appears for all the other VIEW functions in ARDISPLAY and SRDISPLAY. More details about the ARDISPLAY and SRDISPLAY display interfaces and how they are initiated can be found in the Users Manual (Baumgardt, 1991a).

Figure 5a shows the display which appears after the VIEW-BY-MAGNITUDE has been selected and reference events from a specific region have been selected. (Note: This display is a black-and-white screen dump of a color display, where the dark areas are actually red on the display. Each window contains a table of options which can be selected by mousing on the boxes to the left of each option. In the actual display on a color monitor, the red boxes are filled in as black. However, on the display in Figure 5a, all boxes appear filled in because red appears as black on a black-and-white screen dump.) Note that this option has been selected for a particular event, designated by an origin id (orid) of 192692. The new option in Figure 5a is the SELECT PLOT INFO table on the far right, under which appears the checkbox option Plot Orids. By mouse-selecting this option, along with 6.0-8.0 under SELECT FILTERS, *Pn/Lg* under SELECT RATIOS, MAX under SELECT METHODS (i.e., display ratios computed from maximum amplitudes in the *stapick* windows on the rms incoherent beams), and *ml* under SELECT PLOT MAGNITUDE (i.e., select local magnitude as computed by the IMS), the scatterplot display shown in Figure 5b appears. This plot shows the current event as a circle with a star on the extreme lower right of the plot, with local magnitude of 3.2, compared with all the reference events in the reference region called K2. (Note: K2 is the Helsinki designation for a particular mine on the Kola Peninsula.). As shown, each point is labeled by a number which is the orid designation for the event. This plot shows that the *Pn/Lg* ratios range from 0.3 to 2.8 and that the current event is on the lower end of the range. We may wish to examine the data for orid 192692 to check this low value or perhaps to examine some of the data for the larger values, such as for orid 206744.

To view the data for any of the events in the scatterplot, the user can mouse the View Events button on the extreme upper right of the plot. This initiates the *ViewEvts* process which displays the interface menubar shown in Figure 6. The SELECT menu has one option, *REFERENCE EVENT*, which, when selected, brings up the checkbox table shown in Figure 6. This table contains a list of all the orids, shown in the scatterplot in Figure 5b, in order of the values of the feature shown in the plot. Thus, selecting any one of the boxes on the left of each orid number will bring in the data for the event designated by the orid.

The VIEW menu has three options, *BEAMS*, *TIME SERIES*, and *SPECTRA*, which will display, respectively, incoherent beams, single-channel seismograms, and array-stacked spectra for the event selected from the *REFERENCE EVENT* orid selected in the table in Figure 6. Selecting the *BEAMS* option brings up the display shown in Figure 7a, which is a plot of all the log-rms incoherent beams computed for the event. The first display shows all the filtered beams on the same axis. As can be seen in Figure 7a, the beams overlap each other although the

**VIEW RESULTS BY INDUSTRY for Q1 1993**

19

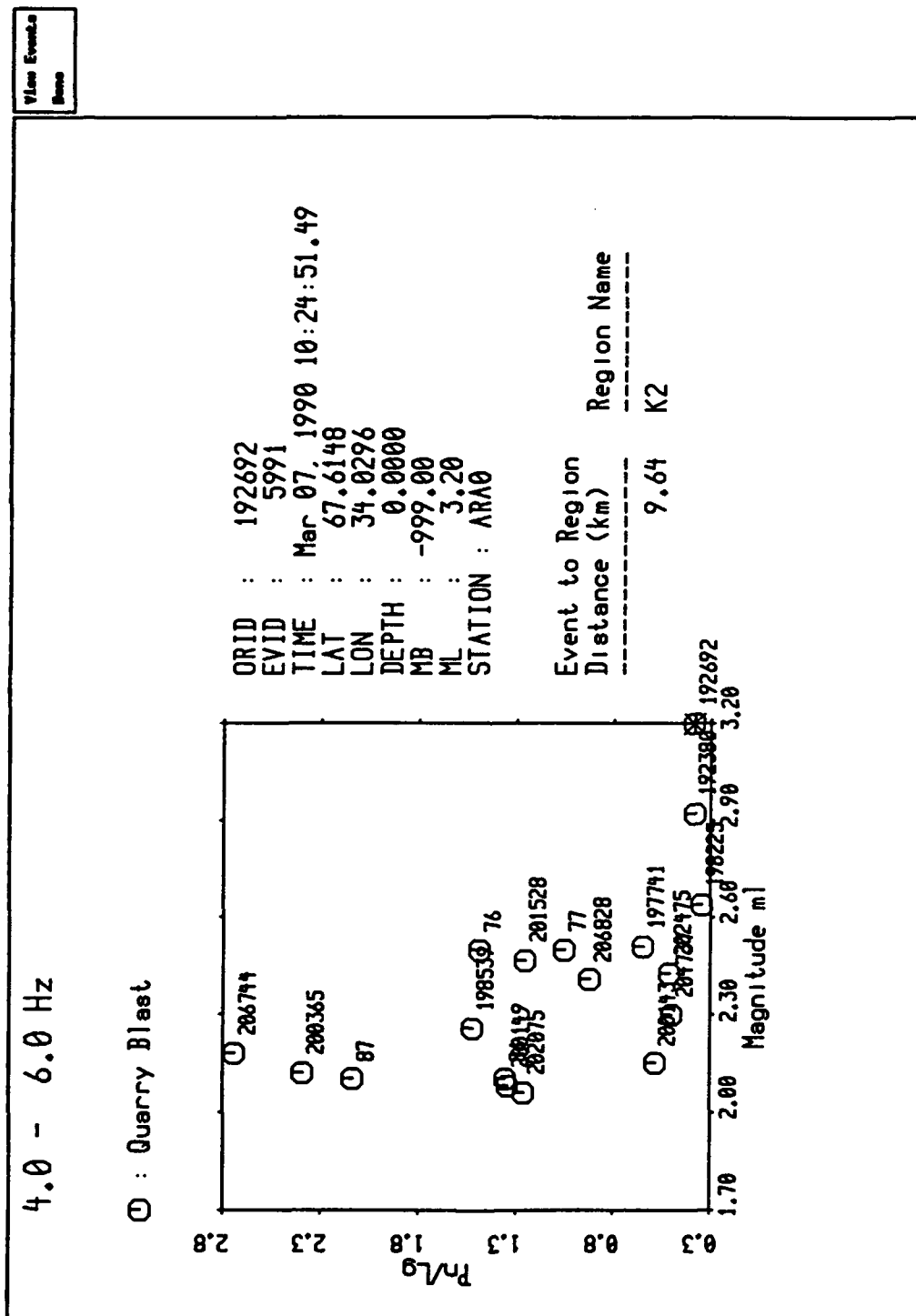


FIGURE 5(b): Scatter plot of  $P_n/L_g$  amplitude ratios plotted as a function of local magnitude, ML. The numbers plotted to the right of each symbol are the origin ids (orid) which are plotted when the Plot Orids box is selected under SELECT PLOT INFO window in Figure 5a.

id	ratio	region
100025	0.14	P2
100100	0.38	P2
100002	0.43	P2
200217	0.50	P2
200305	0.51	P2
200143	0.49	P2
100231	0.45	P2
200063	0.30	P2
22	1.05	P2
200283	1.25	P2
200025	1.26	P2
200191	1.44	P2
26	1.45	P2
26	1.40	P2
100000	1.52	P2
07	2.14	P2
200005	2.49	P2
200241	2.78	P2

**FIGURE 6:** *ViewEvs* top level interface and a checkbox table which appears when *REFERENCE EVENT* is selected under the *SELECT* menu. The table shows the orids of the events in the scatterplot in Figure 5b plotted in increasing order of the value of the  $Pn/Lg$  ratio in the 6.0 to 8.0 Hz band. When any of the checkboxes are selected, all the data (incoherent beams, waveforms, and spectra) are read in from the database.

Shift Plot  
 Holog Beam  
 Zoom  
 UnZoom  
 Done

VIEW NEWS for orid 198225, sta 0000

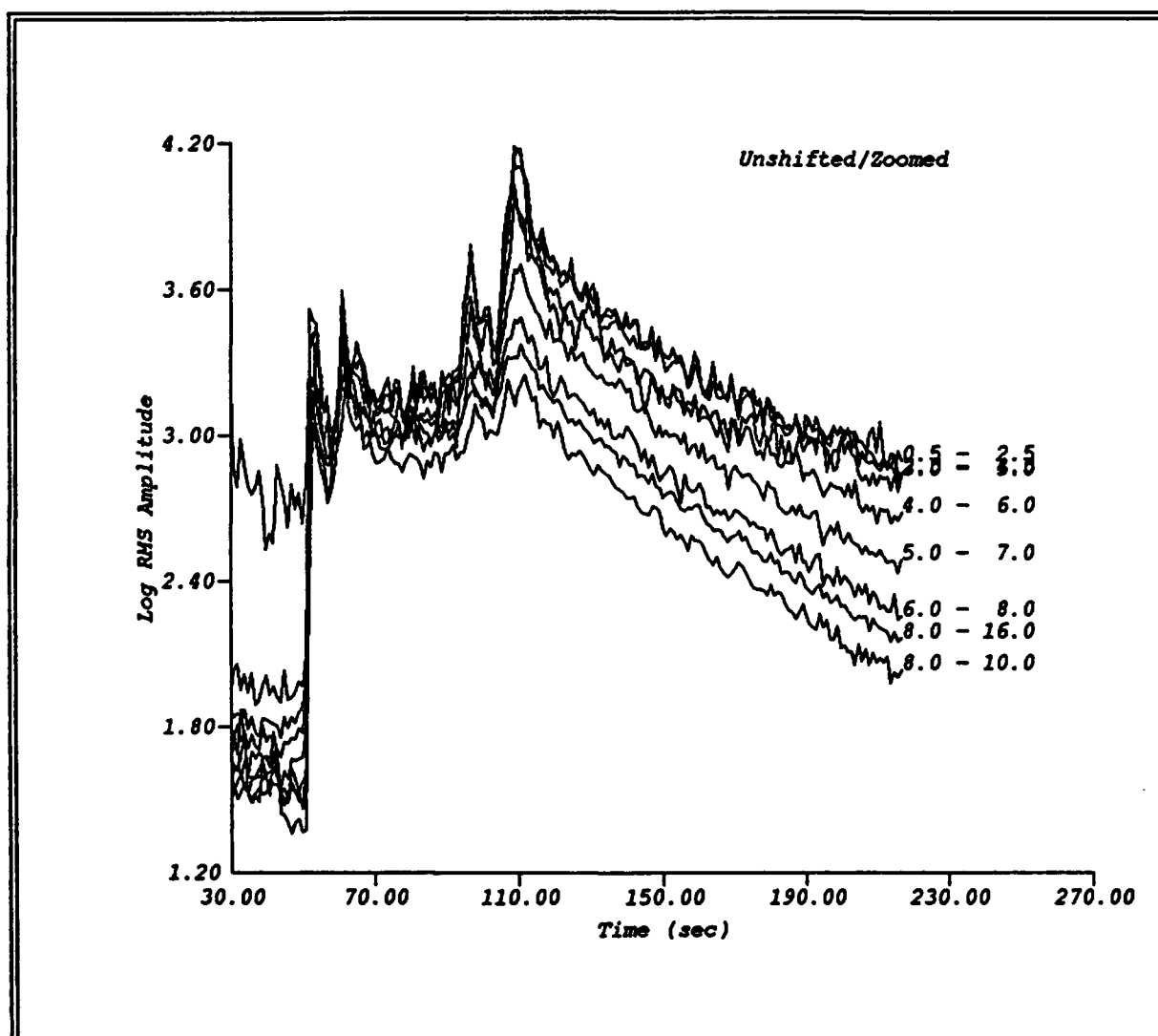


**FIGURE 7(a):** Plot of "unshifted" incoherent beams for selected orid=198225 which appears when *BEAMS* under the *VIEW* menu is selected in the *ViewEvs* interface.

dominant energy, particularly in the background noise ahead of the first onset, dominates in the low frequency band, 0.5 to 2.5 Hz. To get a clearer view of all the beams, a Shift Plot button is provided in the box in the upper right which separates each of the beams by 1/4 of the maximum to minimum values of all the beams, which gives the view shown in Figure 7b. This plot clearly shows the existence of an *Rg* phase on the 0.5 to 2.5 Hz beam, which is hard to see in Figure 7a because it is covered up by the overlapping beams. Selecting Unlog Beams produces the unlogged rms beam plots shown in Figure 7c. This action can be reversed by selecting Log Beams. Clearly, logging the rms beams reduces the contrast between the largest amplitude *Lg* phase and the other phases, which is much stronger on the unlogged plots in Figure 7c. In addition to these functions, a Zoom/UnZoom button provides an horizontally expanded plot of any portion of the incoherent beam plots.

Figure 8 shows the result of selecting *TIME SERIES*, which is the standard waveform review interface provided in the incoherent-beam and spectral computation interfaces. The checkboxes on the left select the channel to display. Other checkboxes allow display of analyst phase picks, predicted phase picks, and the application of bandpass filters. Phases plotted in Figure 8, with "fs\_prog" as author, are the start times of the phase selections (*stapicks*) made for this event.

Finally, selecting *SPECTRA* produces plots shown in Figures 9a and 9b. Figure 9a shows the spectra plotted on the same axis for the four phases, *Pn*, *Pg*, *Sn*, and *Lg*, and background noise to *Pn*. These spectra, which are clearly modulated due to ripple fire, are reasonably well separated. However, quite often, the spectra overlap so much it is hard to resolve details. The Shift Plot option in the box in the upper left produces the display shown in Figure 9b, where the spectra are shifted by 1/8 of the difference between the maximum and minimum amplitudes. This separation allows the user to more clearly view the details of each spectrum separately but on the same plot. This view can be reversed by selecting Unshift Plot. The other option in the box, Correct Spectra, allows the display of spectra corrected for instrument and/or anelastic attenuation, if they have been computed.

All the options discussed above are available in other interfaces. The intent of *ViewEvs* is to provide them quickly so that the user can review them in connection with the feature values displayed in the scatter plots. This capability allows the user, in a research mode, to check original waveforms, beams, and spectra for events with unusual features to determine if the values are reasonable or to better understand the cause of anomalous feature values.

Unshift Plot
Unlog Scale
Zoom
UnZoom
Done

VIBR DEMS for grid 150225, etc 0000

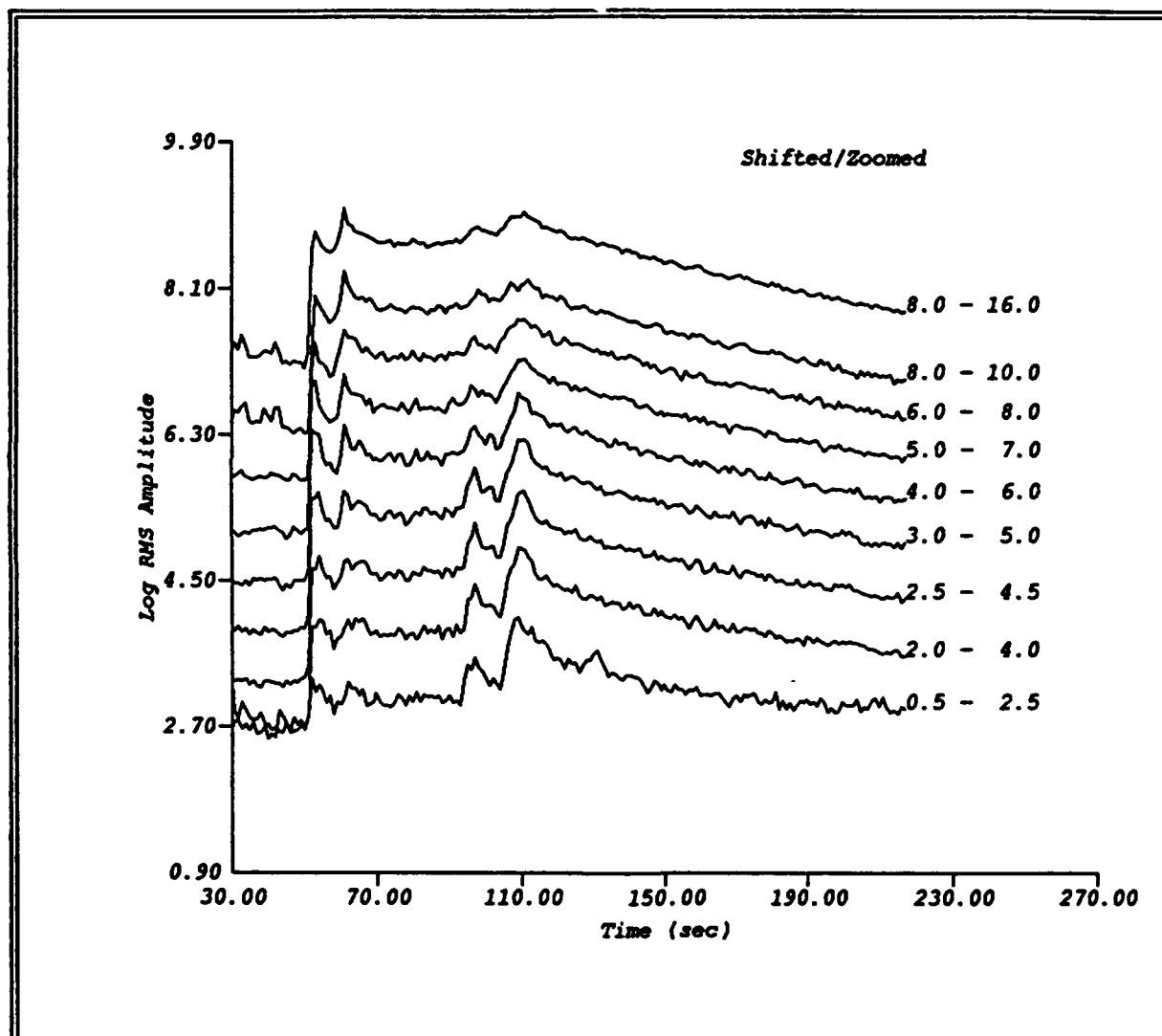


FIGURE 7(b): Same plot as Figure 7a after Shift Plot button is selected.

Unshift Flat
Log Beams
Zoom
UnZoom
Done

VIBR BEAMS for grid 150225, sta 0000

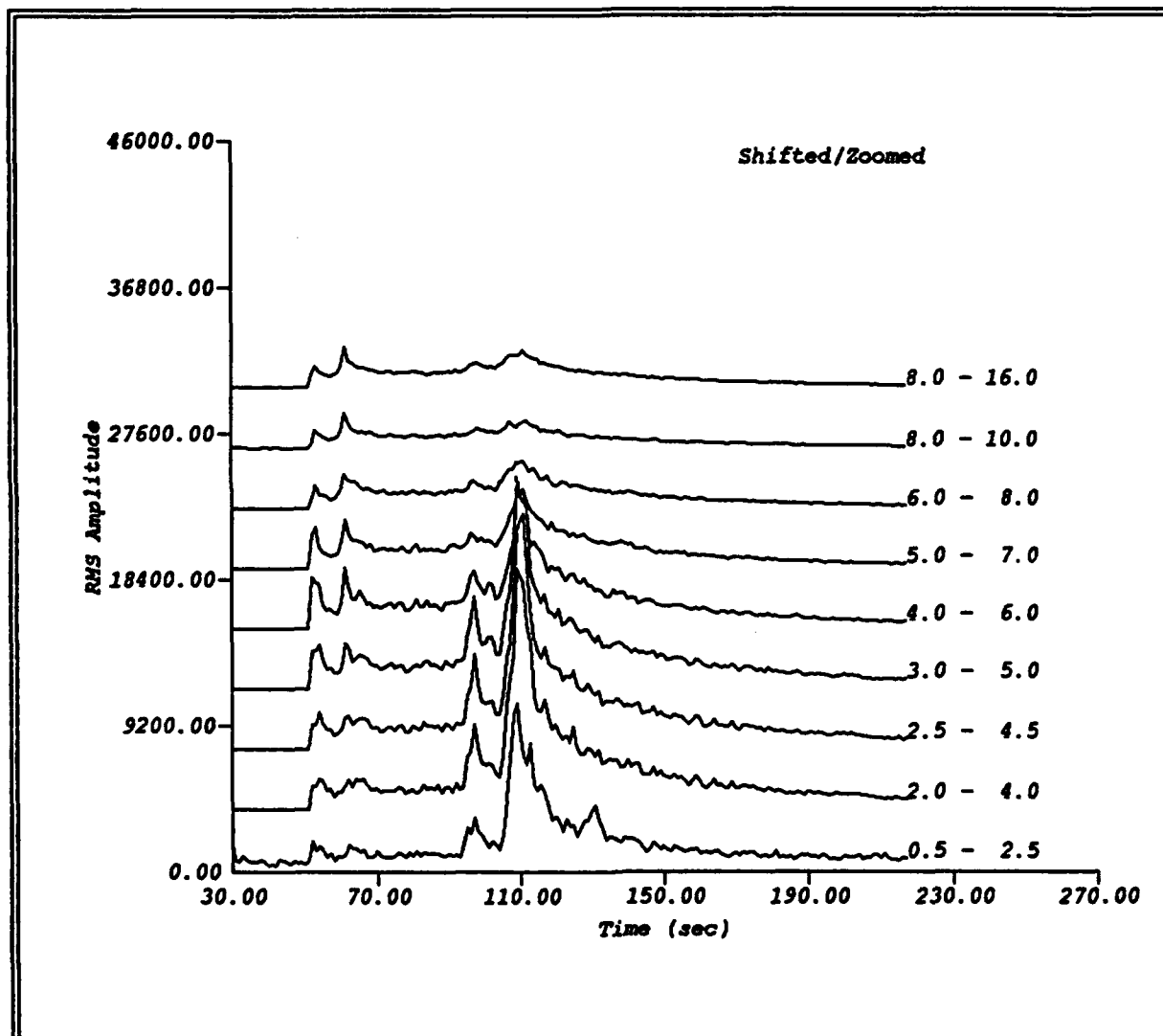


FIGURE 7(c): Same plot as Figure 7b after Unlog Beams button is selected.

VIEW TIME SERIES for orid 198225

Use drag, then press button for Zoom

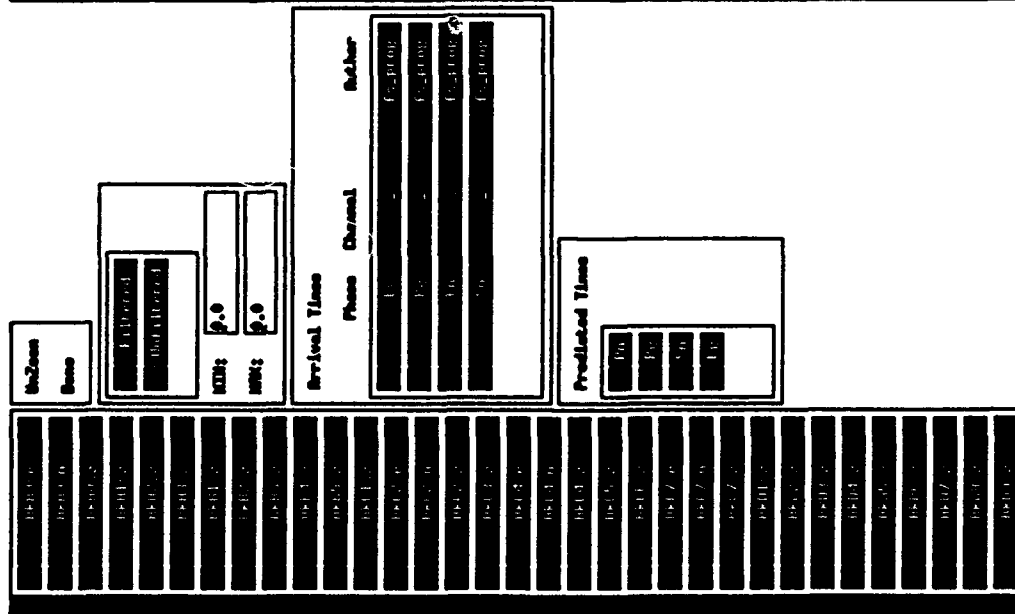
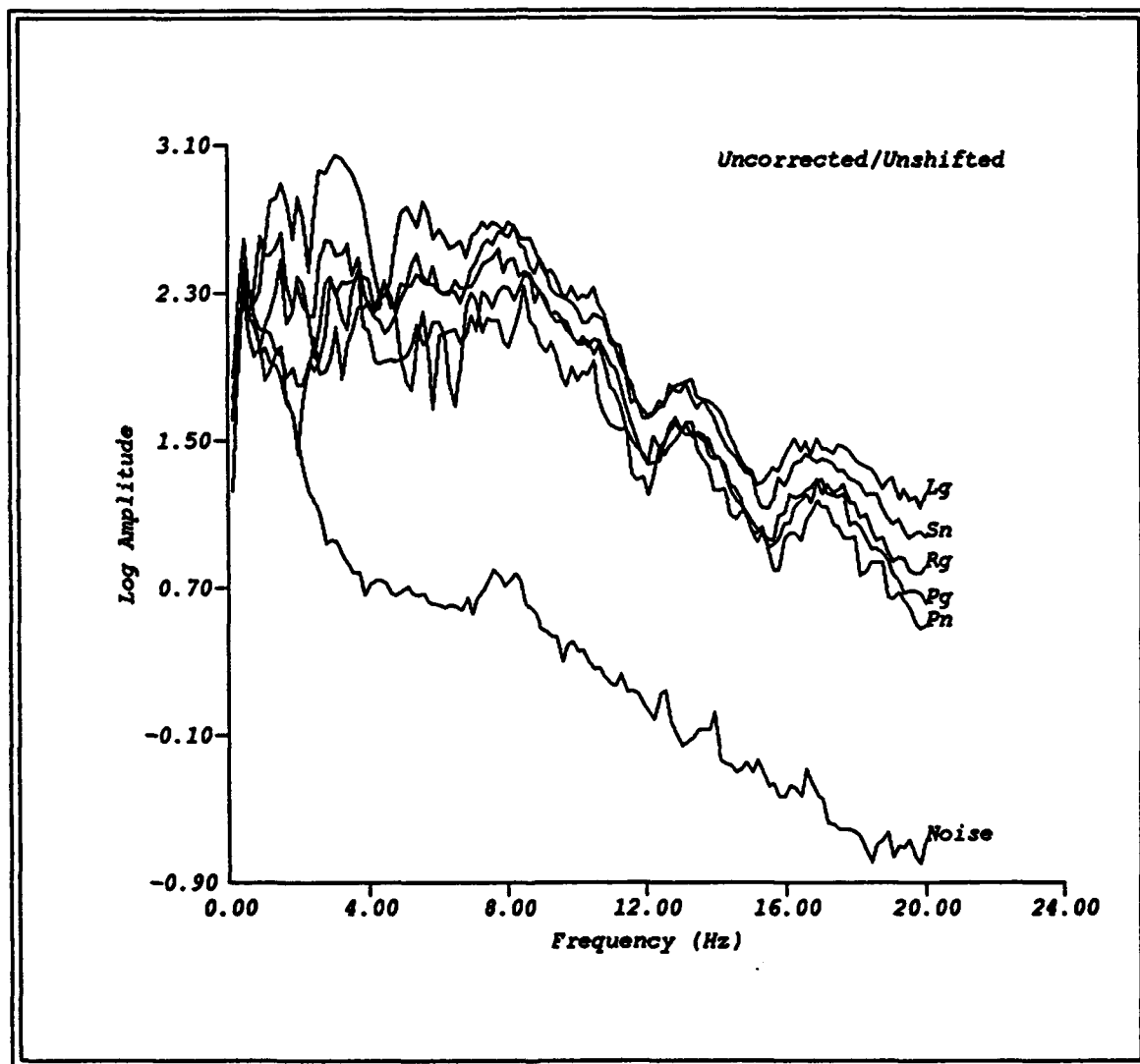


FIGURE 8: Plot of single channel waveforms for selected orid=198225 which appears when *TIME SERIES* under the *VIEW* menu is selected in the *ViewEvs* interface.

Correct Spectra
Shift Plot
Base

VIBR FOURIER SPECTRA for erid 200000, station 0000



**FIGURE 9(a):** Plot of array-stacked spectra for the four phases picked in Figure 8.

Correct Spectra
Unshift Plot
Done

VIBR FOURIER SPECTRA for grid 200050, station 0000

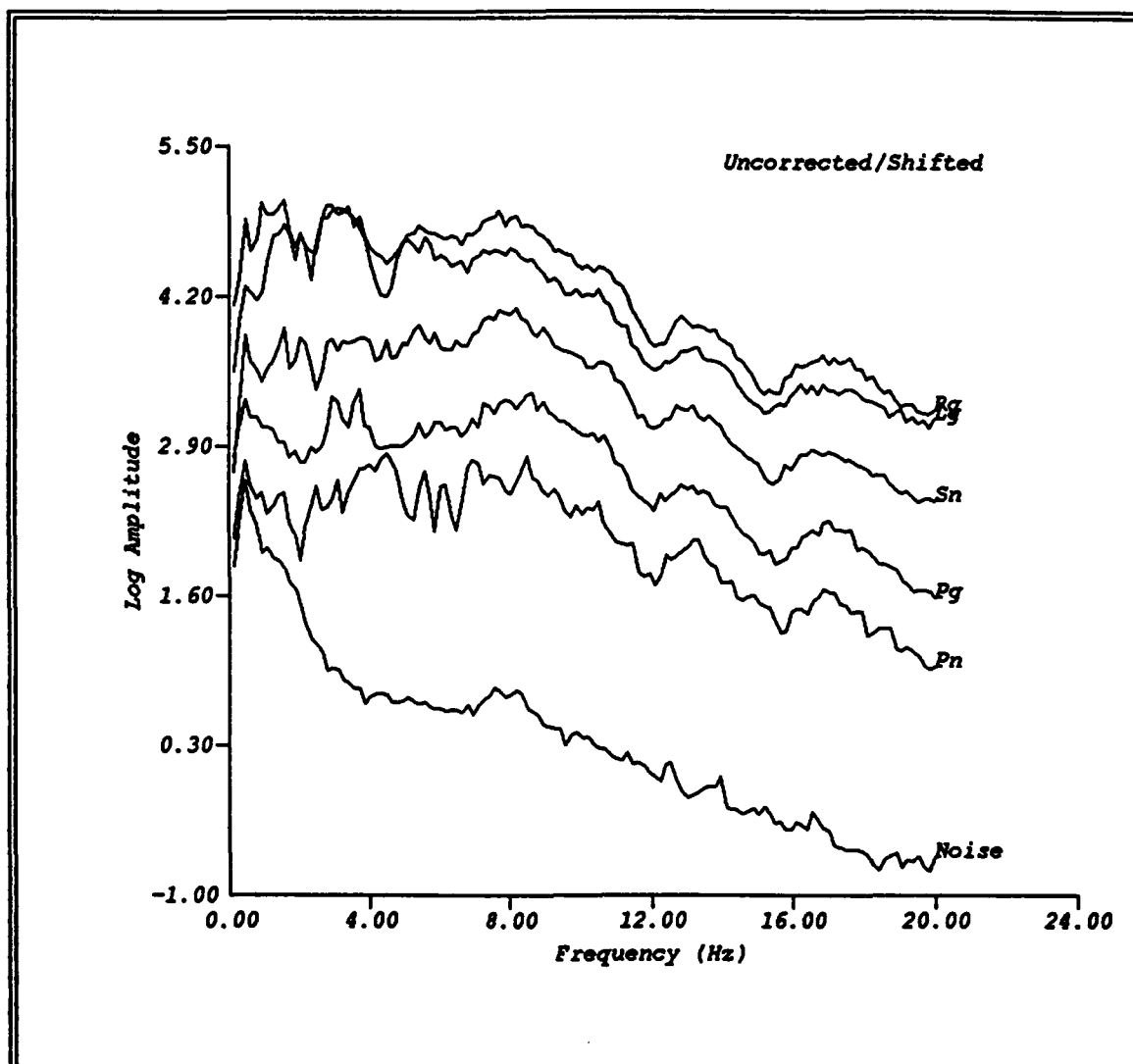


**FIGURE 9(b):** Plot of the array-stacked spectra in (a), except that they have been shifted by 1/8 of the difference between the maximum and minimum amplitudes. This display results from mousing on the Shift Plot button. Selecting Unshift Plot reverts the display back to that shown in Figure 9a.

### 2.3.3 Top Level Summary (TLS) Interface

The original ISEIS system has a top level interface, called the *Spreadsheet*, which provides a color-coded display of all the results of ISEIS processing. However, this display attempts to include a great deal of information and could sometimes be confusing. For this reason, another top level interface was developed which was simpler but which also provides some additional, important capabilities which were not available in the *Spreadsheet*.

An example of the *ISEIS Top Level Summary Display (TLS)* is shown in Figure 10, which is a table of the results of ISEIS processing of a group of events in the Steigen earthquake swarm in northern Norway (See Section 3.0). Columns under label **EVENT DESCRIPTION** give event parameter information for the event listed, which includes **DATE**, **TIME** (origin time), **ORID** (origin id), **LAT** (latitude), **LONG** (longitude), **DEPTH**, **MAG** (magnitude) and **ETYPE**. Under **ETYPE** is the true event identification, or the one assigned by the analyst. The column **REF-REG** refers to the reference region to which the event is assigned.

All the columns under the label **DISCRIMINANT STATUS** are the results of ISEIS processing. Mouse-selecting the **HELP** button on the upper left of the *TLS* display brings up a window with an explanation of these columns, which is shown in Figure 11. Each column has three labels, representing *Event Status*, *Model-Based Event Id*, and *Case-Based Event Id*. Event status can be either C (complete), I (incomplete), or N (no data). *Model-Based Event Id* can be Q (earthquake), X (explosion), or U (unidentified) and *Case-Based Event Id* can be either S (similar to reference events), D (dissimilar), or U (unidentified). N means the discriminant has not been run. The **ICOMP** lists the overall ISEIS event identification based on the combination of all the individual discriminant results.

The three pull-down menus in Figure 10, **FILE**, **EDIT**, and **VIEW**, provide most of the same functionality as those in the *Spreadsheet* (see Baumgardt, 1991a) and will not be further discussed in this section. The new functionality in *TLS* is invoked from the **PROCESS** pull-down menu, which provides numerous functions for accessing the database, entering or modifying event identifications.

The *TLS* interface was designed to also allow the analyst to enter event identifications, based on the review of the ISEIS analysis and/or the availability of independent "ground truth." The "ground truth" or analyst's decision about the identification of the event appears under the **ETYPE** column. The analyst should be sure that this will be the final event identification before

# ISEIS Top Level Summary

FILE EDIT VIEW PROCESS

EVENT DESCRIPTION										DISCREPANT STATUS							
DATE	TIME	QKID	LAT	LONG	DEPTH	PAGE	TYPE	REF-REG	ICOMP	1	PAPPS	HPS	HOT	APPLIC	DEPTH	SHLG	SHEN
01-JAN-1992	03:01:56	31265	67.7	15.3	0.2	3.2	eq	Steigen	CQN	I	CQN	CQN	CQN	CQN	NNN	NNN	CQN
01-JAN-1992	03:18:07	31291	67.4	16.6	7.3	-999.0	eq	Steigen	CQN	I	CQN	CQN	CQN	CQN	NNN	NNN	CQN
01-JAN-1992	08:39:04	31251	67.5	15.9	9.3	2.0	eq	Steigen	CQN	I	CQN	CQN	CQN	CQN	NNN	NNN	CQN
01-JAN-1992	08:57:09	31292	67.5	16.1	1.8	-999.0	eq	Steigen	CQN	I	CQN	CQN	CQN	CQN	NNN	NNN	CQN
01-JAN-1992	10:15:08	31295	67.0	16.0	8.1	1.0	eq	Steigen	CQN	I	CQN	CQN	CQN	CQN	NNN	NNN	CQN
01-JAN-1992	14:46:10	31296	66.9	16.7	7.5	1.4	eq	Steigen	CQN	I	CQN	CQN	CQN	CQN	NNN	NNN	CQN
01-JAN-1992	03:43:44	31347	67.5	15.6	0.0	1.9	eq	Steigen	CQN	I	CQN	CQN	CQN	CQN	NNN	NNN	CQN
01-JAN-1992	04:15:04	31294	67.6	15.5	0.2	-999.0	eq	Steigen	CQN	I	CQN	CQN	CQN	CQN	NNN	NNN	CQN
01-JAN-1992	05:33:23	31343	66.9	16.5	0.0	1.0	eq	Steigen	CQN	I	CQN	CQN	CQN	CQN	NNN	NNN	CQN
01-JAN-1992	05:00:51	31293	67.8	15.1	10.0	-999.0	eq	Steigen	CQN	I	CQN	CQN	CQN	CQN	NNN	NNN	CQN
01-JAN-1992	09:06:29	31256	67.7	15.2	2.3	2.2	eq	Steigen	CQN	I	CQN	CQN	CQN	CQN	NNN	NNN	CQN
05-JAN-1992	01:20:49	31395	67.3	16.1	0.0	1.7	eq	Steigen	CQN	I	CQN	CQN	CQN	CQN	NNN	NNN	CQN
05-JAN-1992	02:11:19	31328	67.6	17.2	0.0	1.2	eq	Steigen	CQN	I	CQN	CQN	CQN	CQN	NNN	NNN	CQN
05-JAN-1992	05:11:56	31343	67.6	15.4	0.0	1.6	eq	Steigen	CQN	I	CQN	CQN	CQN	CQN	NNN	NNN	CQN
05-JAN-1992	07:57:10	31325	67.3	17.4	0.0	1.0	eq	Steigen	CQN	I	CQN	CQN	CQN	CQN	NNN	NNN	CQN
05-JAN-1992	08:26:23	31349	67.2	16.4	0.0	1.6	eq	Steigen	CQN	I	CQN	CQN	CQN	CQN	NNN	NNN	CQN
10-JAN-1992	22:07:14	31380	67.8	17.3	0.0	1.1	eq	Steigen	CQN	I	CQN	CQN	CQN	CQN	NNN	NNN	CQN
10-JAN-1992	22:25:42	31301	67.6	15.5	0.0	2.1	eq	Steigen	CQN	I	CQN	CQN	CQN	CQN	NNN	NNN	CQN
11-JAN-1992	01:17:29	31310	67.0	16.3	11.7	1.5	eq	Steigen	CQN	I	CQN	CQN	CQN	CQN	NNN	NNN	CQN
11-JAN-1992	01:45:34	31300	67.1	16.1	9.9	1.5	eq	Steigen	CQN	I	CQN	CQN	CQN	CQN	NNN	NNN	CQN
13-JAN-1992	12:51:43	31347	67.5	16.2	4.0	-999.0	eq	Steigen	CQN	I	CQN	CQN	CQN	CQN	NNN	NNN	CQN
22-JAN-1992	21:39:00	31250	67.8	16.1	0.0	1.0	eq	Steigen	CQN	I	CQN	CQN	CQN	CQN	NNN	NNN	CQN
25-JAN-1992	11:57:35	31391	67.6	15.5	7.8	1.9	eq	Steigen	CQN	I	CQN	CQN	CQN	CQN	NNN	NNN	CQN
25-JAN-1992	12:16:46	31394	67.7	15.3	0.0	2.7	eq	Steigen	CQN	I	CQN	CQN	CQN	CQN	NNN	NNN	CQN
25-JAN-1992	12:26:30	31399	67.6	15.6	2.2	1.8	eq	Steigen	CQN	I	CQN	CQN	CQN	CQN	NNN	NNN	CQN
25-JAN-1992 19:18:53										CQN	I	CQN	CQN	CQN	CQN	NNN	CQN
										CQN	I	CQN	CQN	CQN	CQN	NNN	CQN



Event Comment:

Steigen Earthquake Swarm, Tornod Kvætna and Lora Grant

ARCSES, FIDES, HORESS

ARCSES Sn repicked not to overlap Eg. Multiple Sn onset(?)

Author: Doug Baumgardt

CONTINUE

FIGURE 10: Example of the *Top Level Summary (TLS)* display for the event in the Steigen region of northern Norway, discussed in Section 3.0.

## Top Level Summary - Help

The abbreviations for the Discriminant status are interpreted as follows:

### Column 1 - Status:

C: Data is complete (green on spreadsheet)  
I: Data is incomplete (yellow on spreadsheet)  
N: No data is available (red on spreadsheet)  
-: Event has not been processed (white on spreadsheet)

### Column 2 - Model Based:

Q: Event is earthquake (green on spreadsheet)  
U: Event is unknown (yellow on spreadsheet)  
B: Event is quarry blast (orange on spreadsheet)  
X: Event is explosion (red on spreadsheet)  
-: Event has not been processed (white on spreadsheet)

### Column 3 - Case Based:

S: Event is similar to reference events (green on spreadsheet)  
U: Event is similarity is indeterminate (yellow on spreadsheet)  
D: Event is dissimilar to reference events (red on spreadsheet)  
-: Event has not been processed (white on spreadsheet)

DONE

FIGURE 11: Window, produced by mouse-selecting the HELP button in the upper right of the TLS display in Figure 10, containing explanations of the DISCRIMINANT STATUS columns in the TLS display.

entering it. However, it is important that the analyst provide an explanation of why the event was identified as shown under **ETYPE**. At the bottom of the table in Figure 10 is shown an example of an explanation window invoked from the **READ COMMENT** option under the **PROCESS** pull-down. This explanation is for event with **orid=313112** selected at the bottom of the table. The explanation indicates that the event was identified independently as part of an earthquake swarm in the Steigen region.

Figure 12 shows how this information is entered. First, the event to be identified is selected from the **TLS** display. When **SET EVENT ID** is selected under **PROCESS**, the table shown in Figure 12a appears, which has radial buttons for event types that can be selected by the analyst as the identification of the selected event. These are the **etype** attributes in the *origin* relation from the CSS 3.0 database schema (Anderson et al, 1990). The abbreviations are **eq** - earthquake, **ex** - generic explosion, **me** - marine explosion, **qb** - quarry (or mine) explosion, **o** - other unknown, **l** - local unknown, **r** - regional unknown, and **t** - teleseismic unknown. After selecting one of the options (**eq** in Figure 12a) and then selecting **DONE**, the display shown in Figure 12b appears, which consists of two writeable windows. In the first one to the right of the word **Comment**, the analyst can enter a description of the event. Below that window, to the right of **Author**, the analyst's name can be entered. When the **DONE** button is selected, the **etype** attribute in the *origin* relation is updated and the comment is entered into the database tagged to the origin id of the event. Also, the entry will also be updated in under the **ETYPE** column in the **TLS** table in Figure 10.

#### 2.3.4 ISEIS Interface to the NMRD Map Process

The *Spreadsheet* display can send events to the NMRD Map process in addition to the ISEIS map process. The user selects events in the spreadsheet in the usual way and then he/she selects **ARS Map** under the **PROCESS** menu. The Map process must be already active and the *Spreadsheet* assumes that it is. It is started by running 'runmap' using an X window display other than the one that the *Spreadsheet* is currently using. Events on the NMRD map are colored the same as colors on the **COMBINED ID MODEL** button on the spreadsheet. It is important to note that these colors do NOT reflect final event classification in the *ORIGIN* relation. The sizes of the events on the NMRD map directly correlate to the confidence of classification in the **COMBINED ID MODEL** button. Events will appear smaller if we are not as sure about their classification. In cases where events are the same size, solid circles indicate more confidence than outline symbols.

Please enter a comment and author ( 10 Lines max )

Comment: Event believed to be part of an earthquake swarm in the Steigen region of Northern Norway. References: Tormod Kvaerna, HORSAR; Lori Grant, CSS.

Author: Doug Baumgardt

DONE CANCEL

**FIGURE 12(a):** Display of selection table which is displayed when SET EVENT ID under the VIEW pull-down menu is selected. The analyst can select one of the available event types defined for the ETYPE attribute.

☒ eq

☐ ex

☐ me

☐ qb

☐ o

☐ l

☐ r

☐ t

☐ umm

☐ unk

☐ unc

☐ -

DONE

CANCEL

HELP

**FIGURE 12(b):** When the DONE button is selected by the mouse in the SET EVENT ID window in Figure 12(a), this window appears for the analyst to enter a comment under Comment describing the reason for the event identification and the analyst's name under Author.

### 2.3.5 Coherence, Deconvolution, and Neural Networks

For completeness, we also mention three additional processes which have been added to ISEIS during the past reporting period but which we will not describe in detail in this report. These include *Coherence*, *Deconvolution*, and *Neural Networks*. Two of these, *Coherence* and *Deconvolution*, are shown in Figure 1 in the Interactive Processing box available for research purposes. These interfaces are described briefly below. However, evaluation of these processes has begun and will be described in subsequent reports.

*Coherence* is an interface which implements the multichannel processing methods described by Der et al (1990, 1992), which Der et al (1992) points out is the frequency domain equivalent to the time-domain correlation method of Harris (1992). In brief, the process determines the multichannel spectral coherences, defined as transfer functions, to produce a seismogram for an event from one or more master-event seismograms in the same region. The values of coherence estimates, averaged over a specified frequency band, provide a measure of the similarity of a regional event to reference events in a particular region. Moreover, the method can also be applied to mine explosions, as has been done by Riviere-Barbier and Grant (1992), to determine how well events in the same mine cluster in terms of their intercorrelations. Hopefully, if it can be shown that mine blasts in the same mine have high multichannel coherences, precise relative location, on the order of seismic wavelengths, can be accomplished by analysis of coherences. Moreover, anomalous events in mines, such as clandestine, possibly decoupled nuclear tests, may be detectable using multichannel coherences. This interface, which enables the analyst to set up, run, and analyze the results of this processing, has just been completed and a subsequent report will describe the processing and interface in more detail, as well as the results of the evaluation of the process on IMS data.

The *Deconvolution* process and interface implements the algorithm described by Der et al (1987) for the large-array deconvolution of teleseismic data. This process takes as input array recordings of multiple explosions at a particular test site and applies a spectral factoring algorithm to separate the waveforms into a source term waveform for each event and receiver term waveform for each array sensor. The source and receiver terms can be recombined to reproduce the original waveforms; the similarity of the original waveforms to the reconstructed waveforms is a measure of the validity of the factorization assumptions. If valid, the source term can be analyzed to find evidence of near source effects, such as *P-pP* effects. The receiver terms contain all the effects of site-scattering. Part of the interface itself was developed under an earlier contract and is described in detail in Appendix B of the report by Der et al (1991). This interface was

implemented using the ISEIS style pull-down menus and can be invoked from the spreadsheet display under the EXECUTE menu. Additional improvements were also made in some of the setup and results displays.

In our view, we believe that *Deconvolution* will have more utility in nuclear weapons proliferation monitoring than in the context of regional discrimination with small regional arrays. The regional arrays like NORESS are probably too small to allow effective factorization of source and receiver effects. The method was designed primarily to be applied to large arrays, like the UK or NORSAR arrays. Second, it is likely that regional seismic phases, like  $P_n$ , will not be factorable, like teleseismic  $P$  waves, because the former is composed of many compressional phases propagating over a number of ray parameters. The assumption for factorability is that the phases propagate along nearly the same ray parameter. In spite of these limitations for regional processing, *Deconvolution* was still implemented in ISEIS because of its potential for processing teleseismic recordings from possible proliferating countries for which there may be limited regional data. Moreover, since there has to-date been limited evidence of depth phases in regional seismograms, such phases may only be detectable on teleseismic recordings. Moreover, we also believe that deconvolution algorithms may still provide useful analysis of regional recordings, even if the factorability assumptions are not validated. We plan to evaluate *Deconvolution* at some level in the next reporting period to test its possible utility for the processing of regional seismic events.

Finally, an interface which implements a simulation of a neural network on a serial computer for event identification using multivariate data is now being developed and will be evaluated and discussed in a subsequent report. *Neural Network* has been implemented because of our need for a process which can be trained to identify events based on the myriad of observations that ISEIS currently makes. The simulation algorithm, which trains a three-layer perceptron model using a backpropagation algorithm, has been discussed in detail by Der and Baumgardt (1992). This study and that of Baumgardt (1992) showed that such a network could be trained to identify mine blasts and explosions using multiple frequency measurements of  $P_n/S_n$  and  $P_n/L_g$  ratios. The interface will provide the user with tools to access features from the ISEIS database for training of the neural network and for recognition of events using a variety of feature measurements, as well as visualization displays for analyzing the network interconnections and recognition results. This process and the results of its application to the IMS database will be also be the subject of a later report.

### **3.0 COMPARATIVE STUDY OF DISCRIMINATION OF MINE EXPLOSIONS AND EARTHQUAKES IN THREE DIFFERENT GEOGRAPHIC REGIONS**

Douglas R. Baumgardt

#### **3.1 BACKGROUND AND OBJECTIVES**

In this section, we discuss a preliminary study of selected features for seismic events in three distinct geographic areas: southern Germany and southern and northern Norway. These events were studied because independent information, i.e., "ground truth," was available about the true identity of the events. The first objective of this study is to investigate the performance of certain key waveform discriminants in the discrimination of mine blasts and earthquakes. The second objective is to investigate the performance of the ISEIS discriminant rules for the identification of these events. Specifically, we wish to address the question of the "portability" of discriminant rules from one geographic region to another. In our case, the discriminant rules were developed to identify seismic events in Norway recorded at the NORESS array. We are interested in knowing how well these rules perform in identifying other known events in other regions and for feature data extracted from other arrays besides NORESS.

Significant success has been reported in the use of certain waveform features for the discrimination of nuclear explosions, mine blasts, and earthquakes (e.g., Murphy and Bennett, 1982; Bennett and Murphy, 1986; Taylor et al, 1989; Bennett et al, 1988, 1989; Baumgardt and Young, 1991; Wuster, 1992). The best discriminant appears to be some form of the regional  $P/S$  ratio, where earthquakes excite more shear wave energy relative to compressional wave energy than earthquakes. A major concern addressed by Baumgardt and Young (1991), in the case of Scandinavian data recorded at NORESS, Lynnes and Baumstark (1991) for earthquakes and explosions the U.S. and Canada, and Bennett et al (1991) for earthquakes and explosions in Eurasia, is that propagation path effects may affect the discriminant. In most discrimination studies, the earthquakes and explosions are not in the same place so that it is possible that differences in propagation path may cause variations in relative  $P$  and  $S$  excitation. Lynnes and Baumstark (1991) have argued that such effects possibly obscure any discriminant capability. Although propagation path corrections, such as those for differential  $Q$  effects, may be made to try to remove propagation path effects, we believe that such corrections are too uncertain. The approach suggested by Baumgardt and Young (1990) and adopted in the ISEIS system is to regionalize reference events and define discriminants for earthquakes and explosions on a regionalized basis. Thus, if earthquakes and explosions are in different regions, we try to

determine if the propagation paths from the two regions are similar enough that we can assume that the propagation effects on the discriminants are the same.

Murphy and Bennett (1982) and Bennett and Murphy (1986) also found that earthquakes and explosions in the same region and magnitude range had *Lg* spectral ratios which were different. Earthquake *Lg* waves appeared to be enriched in high frequencies compared to explosions. Taylor et al (1988) confirmed this result for the western U.S. explosions and earthquakes and also found the same spectral differences in other regional phases besides *Lg*. Taylor and Denny (1991) presented an explosion source model which explained this difference in terms of possible differences in depth of explosions and earthquakes, with earthquakes usually being deeper than explosions.

Other discrimination studies outside of the western U.S. have generally not found spectral differences between explosions and earthquakes in *Lg* or any other phases. These include the eastern U.S. and Canada (Lynnes and Baumstark, 1991), Scandinavia (Dysart and Pulli, 1990; Baumgardt and Young, 1990), and Eurasia (Bennett et al, 1989). This raises the question of why the discriminant seems to work well in the western U.S., which is a tectonically active region, but not so well in more stable platform and shield regions. In other words, does the performance of this discriminant depend on the tectonic or geologic conditions of the source region, and why?

In this study, we have chosen to study in detail the events in the known-events database being generated at the CSS (Grant and Coyne, 1992) in order to investigate the regional performance of these waveform discriminants which are minimally affected of propagation-path differences. Specifically, we focus on the regional amplitude ratio discriminant,  $Pn/Sn$  and  $Pn/Lg$  ratios in multiple frequency bands, and the ratio of low-to-high frequency content in the *Lg* phase. For the former discriminant, we also investigate further the use of multivariate analysis and visualization techniques proposed by Baumgardt (1992b), including face and star plots. We believe these techniques provide unique insights into the overall patterns of multivariate feature space which are harder to discern with single component scatterplots.

The second objective of this study, the portability of regional discriminant rules, is still being pursued and will be discussed in a later report.

### **3.2 DATA AND ANALYSIS PROCEDURES**

The events which we have studied include: (1) western and southern Norway events, mine blasts and earthquakes, recorded at NORESS; (2) known mine explosions and earthquakes

recorded at the GERESS array; and (3) events from a known earthquake swarm in northern Norway and presumed mine explosions recorded at the NORESS.

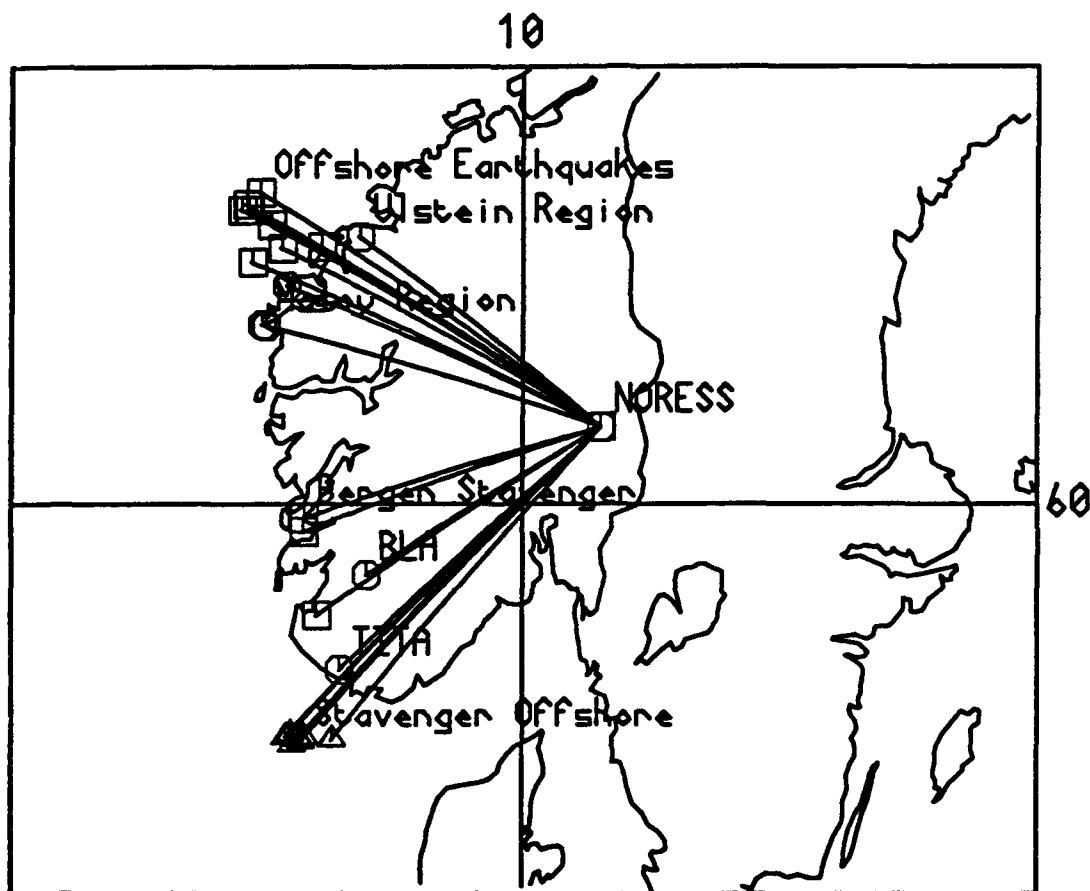
#### *Western and Southern Norway - Recorded at NORESS*

Figure 13 shows a map with the locations and propagation paths for known seismic events recorded at NORESS, originally studied by Baumgardt and Young (1990) and Baumgardt (1992). The events consist of earthquakes and explosions which are in the same or similar regions, and propagate across similar distance range (300 to 400 km). Events included an earthquake swarm in the Maloy region (offshore earthquakes), felt earthquakes near Bergen, known blasts at the Blasto and Titania sites, and a group of events in the Stavenger region which are likely underwater blasts, originally identified by Baumgardt and Young (1990).

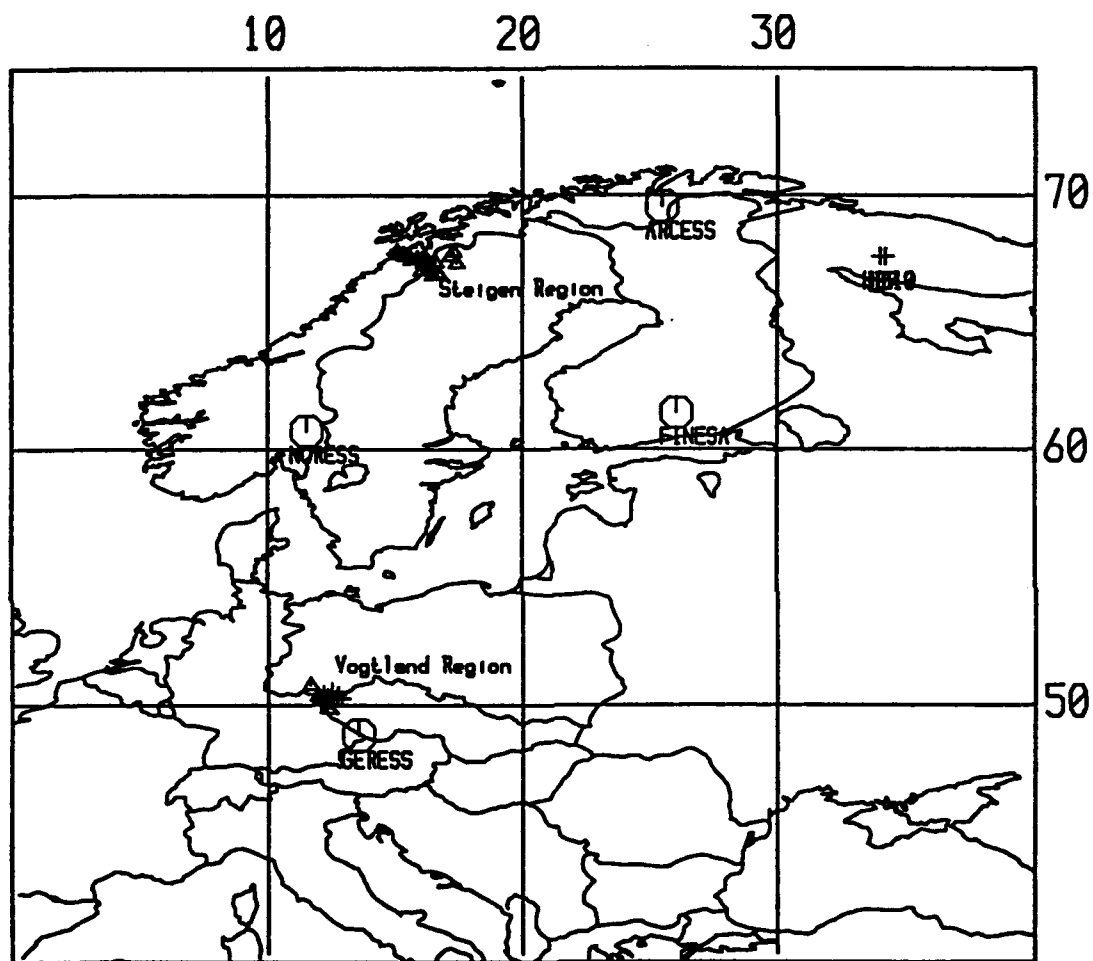
#### *Vogtland and Steigen Events - Recorded at ARCESS*

Figure 14a shows IMS locations of events in the Steigen region of northern Norway and the Vogtland region in Germany. These locations are shown on expanded scale in Figures 14b and 14c. The triangles indicate earthquakes and the plus signs are blasts. The Steigen events were detected at ARCESS, FINESA, and NORESS, and the Vogtland region. The Steigen events are strongly believed to be earthquakes in a swarm. The Vogtland events have been studied by Jan Wuster (Wuster, 1992); mine blasts have been confirmed by mines and the earthquakes have been well located in regional earthquake bulletins. As mentioned above, these data are part of a "known-events" database currently being assembled at the CSS (Grant and Coyne, 1992). However, although the mine blasts have been confirmed by the mines, the locations in Grant and Coyne (1992) come from a small regional seismic networks in the mining district.

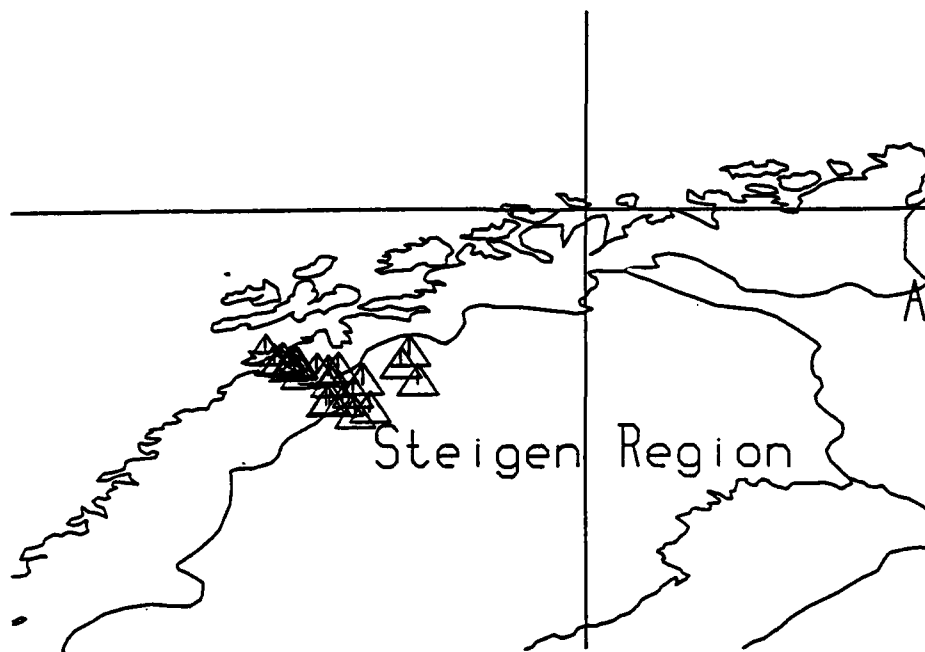
Notice that in the case of the Vogtland data, the earthquakes and blasts occur in nearly the same region. Thus, we expect propagation paths for the earthquake and explosion classes to be identical. Because we have no data for known mine explosions in the same region as the Steigen swarm, we will compare the features of these earthquakes with presumed mine explosions on the Kola Peninsula, which are at comparable distance from ARCESS. In Figure 14a, we show the locations of the HD9 (K2) and HD10 (K5) mines, which are at about the same distance from ARCESS as the Steigen events. We have also studied events from other events on the Kola, although we will focus primarily on these two regions. Although these mine blasts do not occur in the same region as the earthquake swarm, we expect that the paths are very similar, since both groups of events occur in the same shield-type region. Thus, for comparable distances, we expect that the propagation path effects should be nearly the same.



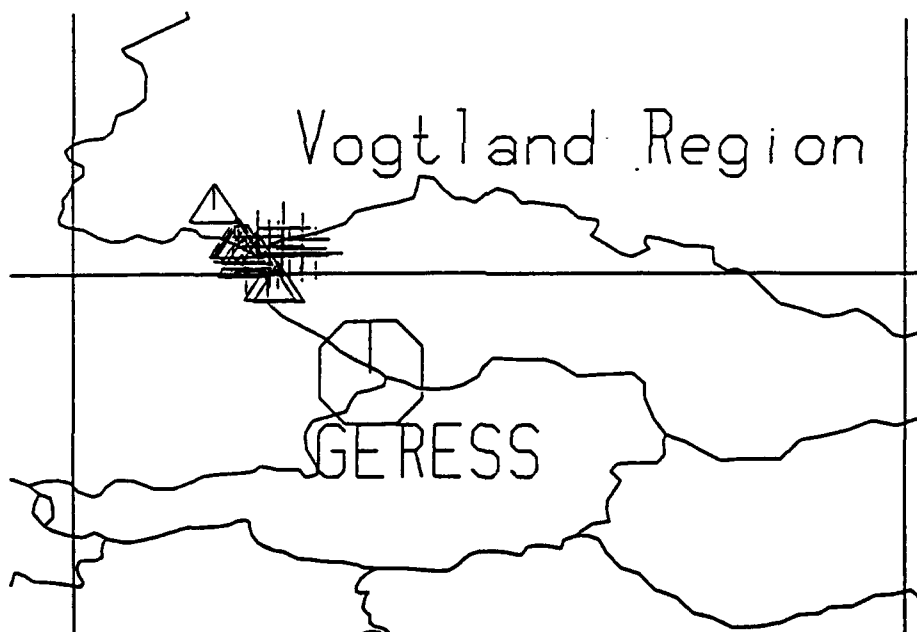
**FIGURE 13: Map showing location and propagation paths of southern Norway seismic events studied at NORESS (from Baumgardt, 1992).**



**FIGURE 14(a):** Map showing IMS locations of events in the Steigen region (upper right) of northern Norway and the Vogtland region (lower right) in Germany. The triangles indicate earthquakes and the plus signs are blasts. Also shown above are the locations of the HD9 and HD10 mines, which are at about the same distance from ARCESS as the Steigen events.



(b)



(c)

**FIGURE 14(b):** The Steigen events were detected at ARCESS, FINESA, and NORESS, and the Vogtland region. The Steigen events are strongly believed to be earthquakes in a swarm. (c) The Vogtland events have been studied by Jan Wuster (Wuster, 1992); mine blasts have been confirmed by mines and the earthquakes have been well located in regional earthquake bulletins.

### 3.3 DATA ANALYSIS RESULTS

In this section, we discuss the results of the analysis of these events, with primary focus on the amplitude ratio and spectral ratio discriminants. ISEIS was used for all the feature extraction processing, which is discussed in the next section, and the generation of scatterplots. In addition, various multivariate visualization display methods proposed by Baumgardt (1992b) were also applied to the data for comparison purposes.

#### 3.3.1 Phase Selections and Incoherent Beams

Figure 2b shows typical ISEIS phase selection windows on a suite of log-RMS incoherent beams in nine-filter frequency bands (0.5-2.5 Hz., 2.0-4.0 Hz., 2.5-4.5 Hz., 3.0-4.0 Hz., 4.0-5.0 Hz., 5.0-7.0 Hz., 7.0-8.0 Hz., 8.0-10.0 Hz., and 6.0-16.0 Hz) for an earthquake in the Maloy earthquake swarm (offshore earthquakes) shown in the map. Phases selected in this case include *Pn*, *Pg*, *Sn*, *Lg*, and *Rg*. The darkened regions show the phase selections, obtained either automatically relative to phase picks provided by the IMS/analyst, or interactively in ISEIS by mouse drag. When these selections are selected and entered by the analyst in ISEIS, the maximum RMS amplitude in the window, the average RMS amplitude in the window, the start time, and duration of the windows in each of the frequency bands are stored in the database.

In our earlier studies of these events (Baumgardt and Young, 1990; Baumgardt, 1992b), we generally found all four of these phases to be well recorded across the entire frequency band from 2 to 16 Hz, both for explosions and for earthquakes. No strong *Rg* wave was actually recorded for most of these events, although enhancements in the *Lg* coda were evident at the expected *Rg* time on the low-frequency (0.5 to 2.5 Hz) band. Baumgardt (1992b) found that the ratio of the rms maximum in the *Rg* window to that in the *Lg* discriminated the earthquake population from the explosions, with earthquakes having more apparent *Rg* energy relative to the *Lg*.

ISEIS *PhaseSelect* screendump displays of the phase selections for a typical Vogtland earthquake, recorded at GERESS, are shown in Figure 15. The white lines indicate the analyst picks from the ARS and the darkened regions are the ISEIS phase selections. In this case, the ARS analyst picks were altered, because of the apparent double-peak feature in the *P* and *S* wave trains, which we have interpreted to be *Pn*, *Pg* and *Sn*, *Lg*. This distinction between two different *P* and *S* waves is problematic because these events are very near the crossover distance (about 150 to 190 km) between *Pn* and *Pg* and *Sn* and *Lg*, and the double-peak character in the incoherent beams is not always obvious. This distinction is generally clearer in the earthquake than in the

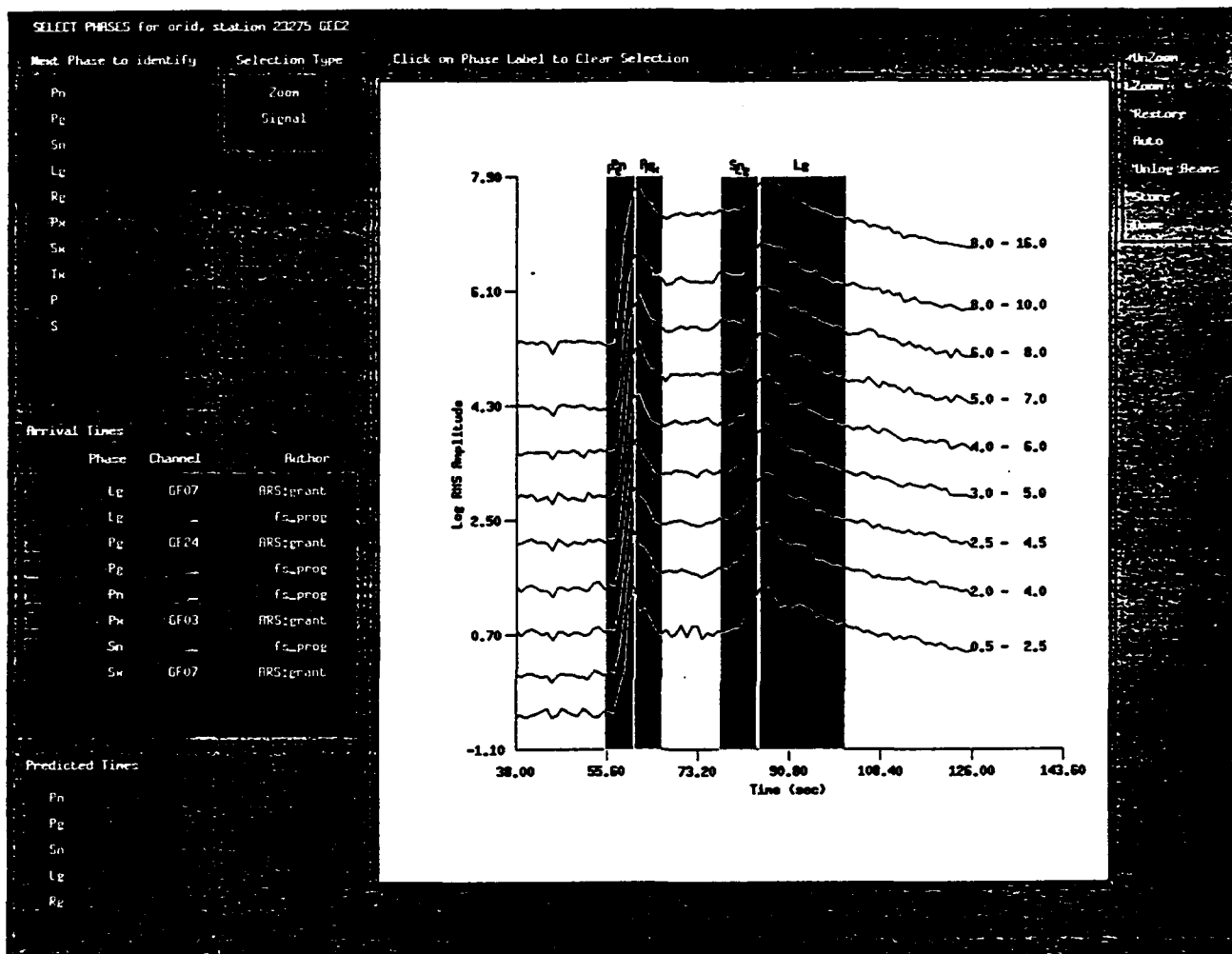


**FIGURE 15:** ISEIS displays of the phase selections for a typical Vogtland event, recorded at GERESS. The white lines indicate the analyst picks from the ARS and the darkened regions are the ISEIS phase selections. In this case, the ARS analyst picks were altered, because of the apparent double-peak feature in the *P* and *S* wave trains, which we have interpreted to be *Pn*, *Pg* and *Sn*, *Lg*. Maximum RMS amplitudes in the phase-select window were used in the amplitude ratio calculations.

explosion incoherent beams. We decided to focus on a general *P*-to-*S* type ratio, defined to be a *Pn/Lg*, which gives the ratio between the maximum *P* energy to the maximum *S* energy. Also, a clear *Rg* phase is also clearly visible on most of the explosion signals, as was first observed by Wuster (1992) and these phases were picked when visible.

ISEIS *PhaseSelect* displays of the phase selections for a typical Steigen event, recorded at ARCESS, are shown in Figure 16. Again, the vertical, white lines indicate the analyst picks from the ARS and the darkened regions are the ISEIS phase selections. Generally, the four phase types, *Pn*, *Pg*, *Sn*, and *Lg* are easy to discern on the incoherent beam plots because these events were at a greater distance from ARCESS (about 400 km) than the Vogtland events were from GERESS. However, it is interesting to notice that the *Sn* phase appears to commence ahead of the time picked by the analyst, which is especially obvious on the 2.0-4.0 to 3.0-5.0 Hz bands. The amplitudes on the incoherent beams appear to "ramp up" before the maximum amplitude in the *Sn*, and thus, the ISEIS phase selections begin before the IMS analyst phase picks. This ramp-like onset for *Sn* was observed on every incoherent beam which had high enough signal-to-noise ratio indicating that the feature is a propagation effect, not a source effect. Its exact cause is currently unknown.

### **3.3.2 Visualization Methods - Southern Norway Events**

Baumgardt (1992b) investigated in detail a number of discriminants applied to the set of events located in southern Norway and a variety of multivariate analysis and visualization methods. As this report has not been generally circulated, we briefly review these techniques as applied to the southern Norway events recorded at NORESS before discussing in more detail the results of their application to the new data from GERESS and ARCESS arrays.

#### **3.3.2.1 Scatterplot and Boxplot Visualizations**

The primary visualization tool presently built into ISEIS is the scatterplot. Specifically, options are provided to plot amplitude ratio features versus frequency, distance, region, local magnitude, and signal-to-noise. Distinct symbols are assigned to distinct source types, including squares for earthquakes, circles for mine explosions, plus signs for nuclear explosions, triangles for underwater explosions, and x symbols for unknown events. Also, ISEIS makes use of color graphics with a consistent color coding pattern for different source types. In this report, of course, these plots have been rendered in black-and-white which unfortunately reduces the distinctiveness of the different source types.

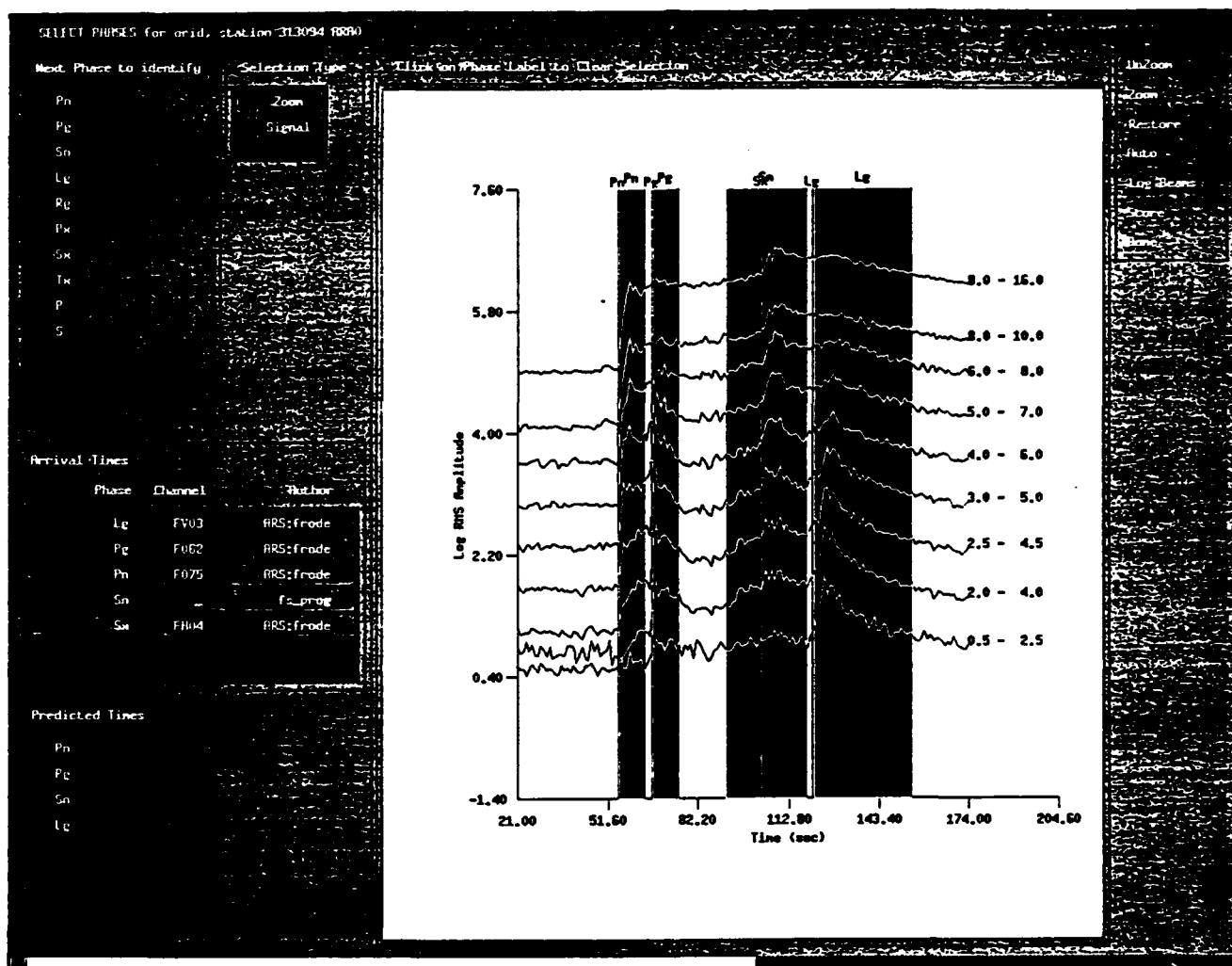


**FIGURE 16:** ISEIS displays of the phase selections for a typical Steigen event, recorded at ARCESS. The white lines indicate the analyst picks from the ARS and the darkened regions are the ISEIS phase selections. Notice that the  $S_n$  phase appears to commence ahead of the time picked by the analyst, which is especially obvious on the 2.0-4.0 to 3.0-5.0 Hz bands. Maximum RMS amplitudes in the phase-select window were used in the amplitude ratio calculations.

The events shown on the map in Figure 13 included earthquakes in a swarm, felt earthquakes near Bergen, reported mine explosions, and presumed underwater explosions. See Baumgardt and Young (1990) for more detailed descriptions of these events. Figure 17 shows ISEIS scatterplots of  $Pn/Lg$  ratio in two frequency bands, 4-6 Hz (left) and 8-10 Hz (right) as a function of distance (from Baumgardt, 1992). This plot shows that generally earthquakes have the lowest values and blasts have the highest values, indicating that earthquakes excite more shear wave energy, relative to  $Pn$ , than do the blasts. The greatest separation is in the higher frequency bands.

Figure 18 shows boxplots of spectral ratio (2.5-4.5 Hz/5.0-7.0 Hz) in  $Lg$ , computed from the log RMS maximum amplitude ratios. These ratios have not been corrected for distance attenuation or instrument. The plot shows complete overlap in these ratios between the mine explosions and earthquakes. However, the presumed underwater blasts have higher spectral ratios than either the mine explosions or earthquakes. In general, we have found that the spectral ratio discriminant (Murphy and Bennett, 1982; Bennett and Murphy, 1986) does not discriminate mine explosions and earthquakes in this region.

### 3.3.2.2 Multivariate Visualizations

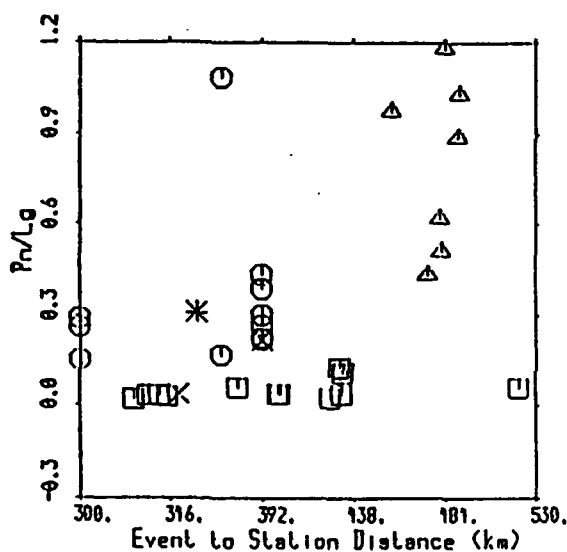
Discrimination analysis has always involved multidimensional features. This is especially true of regional data because of the broad bandwidths involved. Scatterplots can provide only partial views of this multidimensional space and quite often multiple scatterplots have to be studied. An alternative approach would be to use a multivariate visualization approach. Two techniques investigated in the earlier study (Baumgardt, 1992b) are *Chernov faces* and *stars*.

The Chernov face approach to visualizing amplitude ratio features is illustrated in Figure 19. First proposed by Chernov (1973), this method provides anthropomorphic visualizations of multivariate feature vectors by assigning the values of the vector components to the features of a cartoon face. Usually, humans are very good at recognizing faces and thus, may be able to visually cluster multivariate data more effectively by looking at the similarities and differences in the faces than with the actual numerical values. The implementation of the Chernov faces which we use comes from the SPLUS statistics package and allows the representation of up to 15 features. In this example, since only nine filters are used, there is redundancy in the frequency band assignments to face features.

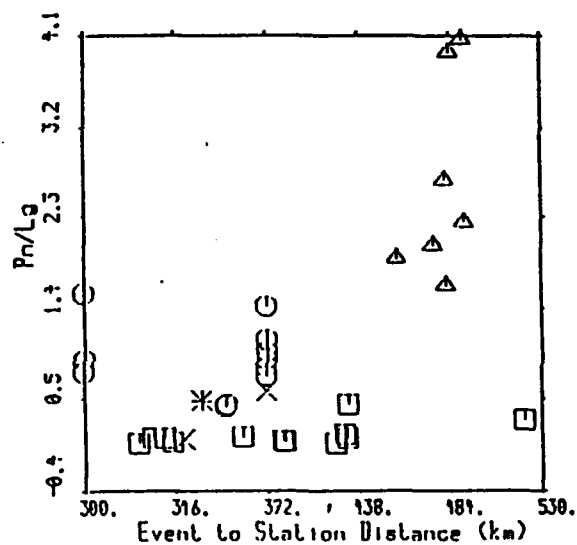
Figure 20 shows Chernov face plots of the  $Pn/Sn$  ratios (top) and  $Pn/Lg$  ratios (bottom) for 13 earthquakes and 13 mine explosions in southwestern Norway, recorded at NORESS. The

□ : Earthquake  
 ○ : Quarry Blast  
 ▲ : Marine Explosion  
 X : Unknown

# **Pn / Lg Amplitude Ratio Discriminants** **NORESS Incoherent Beam Maximums** **300 to 530 Km**



**Incoherent Beam Filter**  
**4 - 6 Hz**



**Incoherent Beam Filter**  
**8 - 10 Hz**

**FIGURE 17:** Above are shown ISEIS scatterplots of  $Pn/Lg$  ratio in two frequency bands, 4-6 Hz (left) and 8-10 Hz (right) as a function of distance (from Baumgardt, 1992b).

## Boxplot Comparison of Spectral Ratios For Explosions, Earthquakes, and Underwater Explosions NORESS Recordings

2.5-4.5Hz/5.0-7.0 Spectral Ratios: Max Log RMS; NORESS Recordings

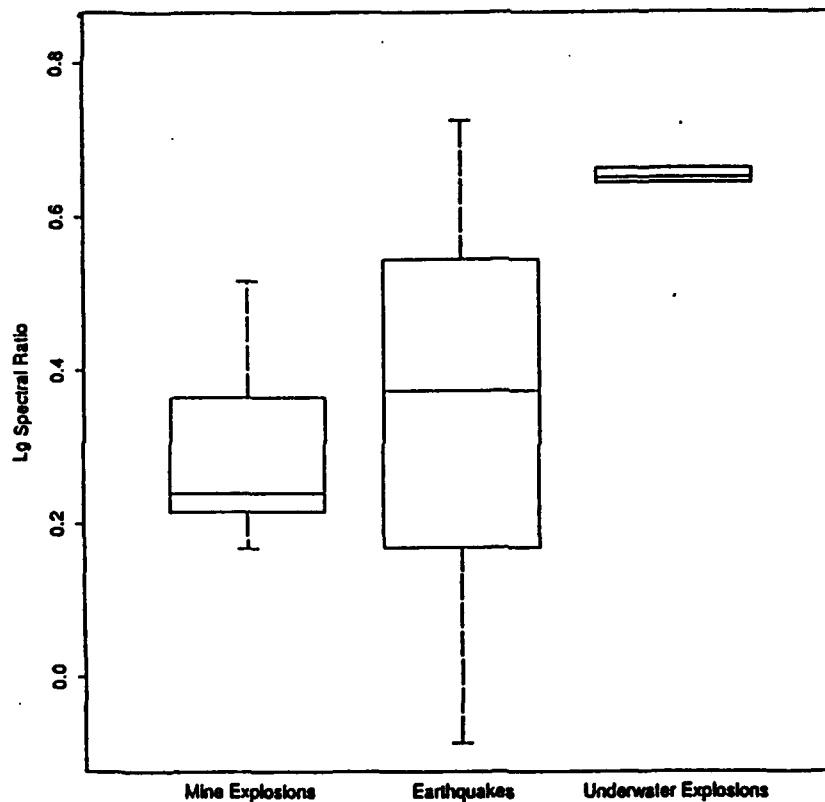


**FIGURE 18:** This figure compares boxplots of spectral ratio (2.5-4.5 Hz/5.0-7.0 Hz) in  $L_g$ , computed from the log RMS maximum amplitudes. These ratios have not been corrected for distance attenuation. The plot shows complete overlap in these ratios between the mine explosions and earthquakes. However, the presumed underwater blasts have higher spectral ratios than either the mine explosions or earthquakes.

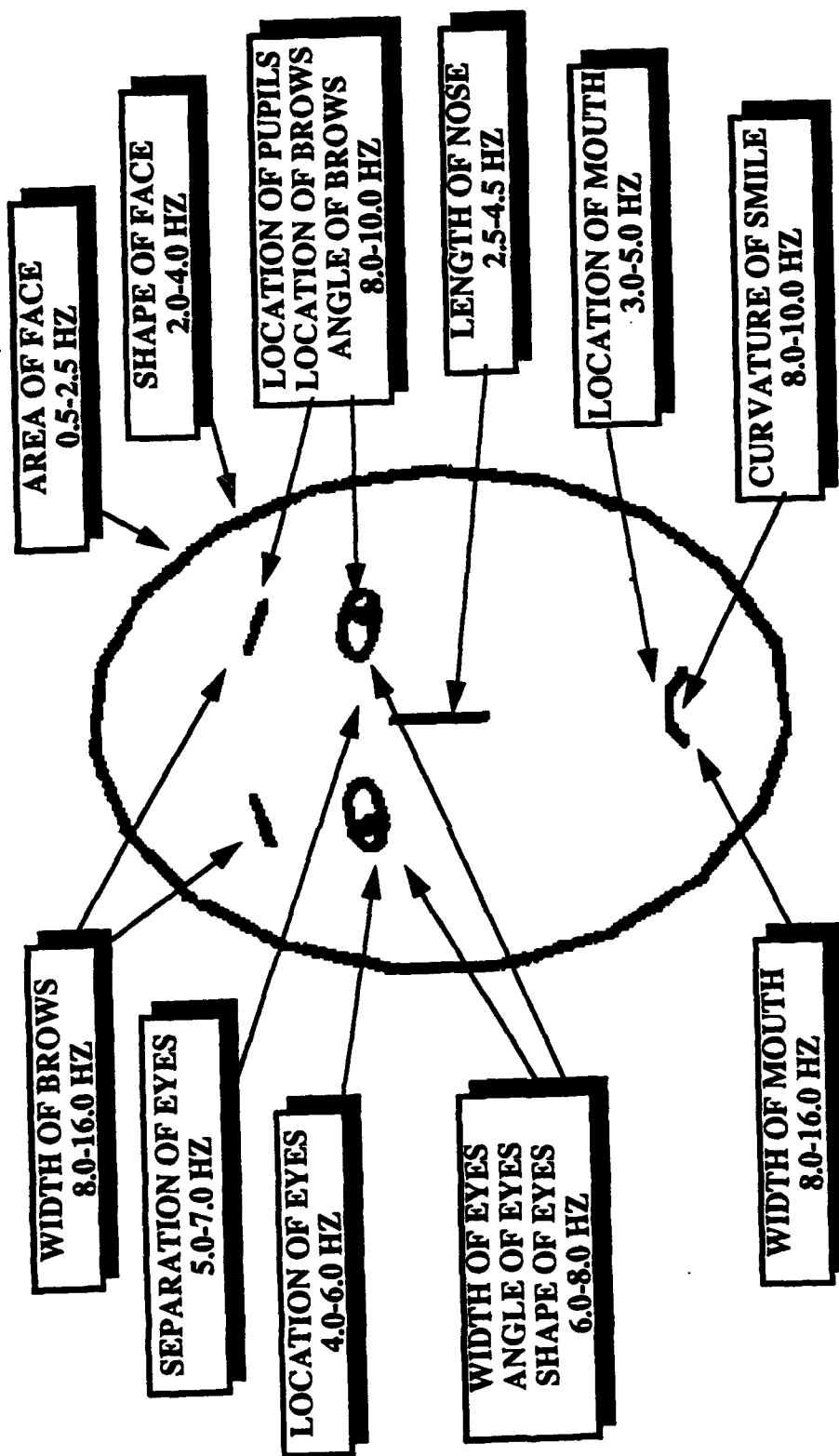
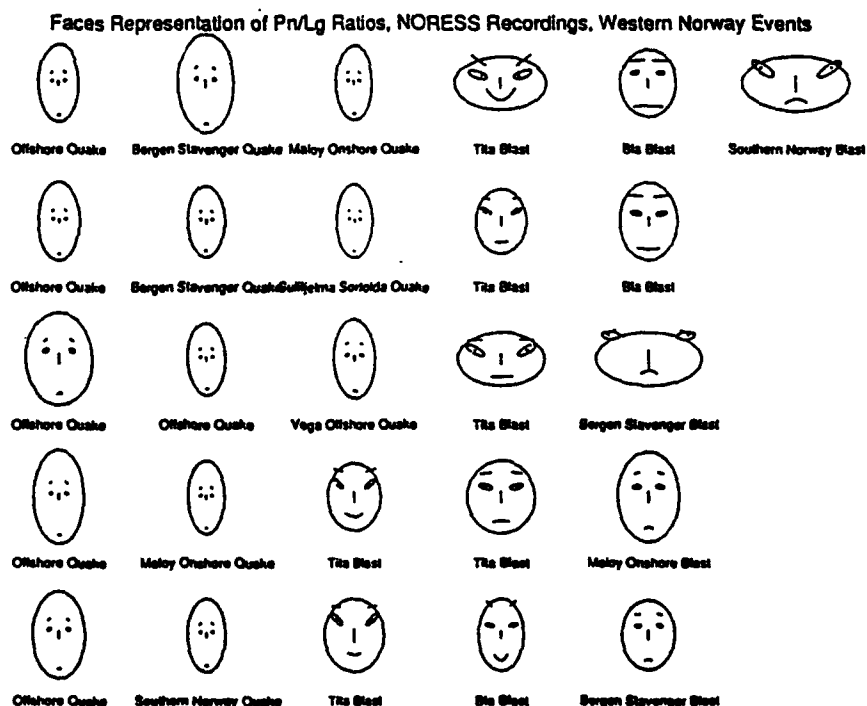
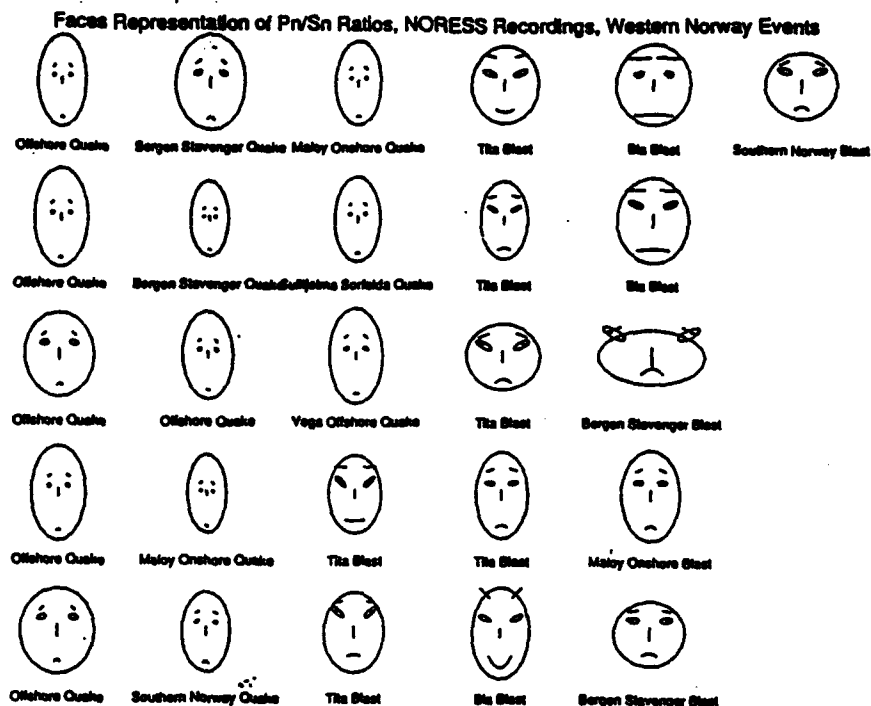


FIGURE 19: Chernov face feature assignments to bandpass filter bands used in  $Pn/Sn$  and  $Pn/Lg$  ratios. All features normalized to combined earthquake explosion training sets.



**FIGURE 20:** Chernov face plots of the  $Pn/Sn$  ratios (top) and  $Pn/Lg$  ratios (bottom) for 13 earthquakes and 13 mine explosions in southwestern Norway, recorded at NORESS, using the face feature assignments shown in Figure 19.

face assignments were made so as to make the earthquake face features smaller than those for the blasts and frowning, whereas the blasts should be larger and smiling. In general, the assignments in Figure 19 do make the earthquakes and explosions distinctive. The eye and mouth features of the earthquakes are smaller than those of the mine blasts because the features assigned to them (i.e., amplitude ratios) are small for earthquakes. However, we were not successful in making all earthquakes frown and blasts smile.

The important thing to note in this display, however, is that the earthquake features are very similar to each other in that they all have frowning faces with small features. Mine blast faces, on the other hand, exhibit a much greater degree of variability. Not all mine blasts smile, and some are very similar to the earthquakes. We have found this to be a universal observation in the IMS data and we will discuss its significance below.

Baumgardt (1992) also studied a method for automatically finding similarities between different features, or clustering. Figure 21 shows the results of clustering of the  $Pn/Sn$  ratios (top) and  $Pn/Lg$  ratios (bottom), using the method of minimal spanning trees (MST) and multivariate planing (Friedman and Rafsky, 1981). The method uses an agglomerative clustering method to connect nearest neighbors in nine-dimensional hyperspace for the nine frequency filter bands used in computing the amplitude ratios. Multivariate planing is a graph theoretic method for showing the proximity of nearest neighbors in two dimensions. (See Baumgardt (1992) for details of algorithm.) The triangles refer to the blasts and the squares to earthquakes.

We find, however, that the multivariate planing display has limited utility in actually studying how the different events cluster. We have found another useful method is to show the trees on the face plots. Figure 22 shows how the minimal spanning tree connects the different faces, i.e., faces connected by arrows are those judged to be the closest by the MST method. These plots show the equivalency of automatic machine learning methods, like MST clustering, to human visual clustering with Chernov faces. Other methods include multivariate discrimination methods and neural networks, which were also discussed by Baumgardt (1992).

Finally, Figure 23 shows the method of *stars*. Stars are made by constructing a reference circle with nine equally-spaced rays extending from the center of the circle. The rays are drawn proportional to the size of the  $Pn/Lg$  and  $Pn/Sn$  amplitude ratios. In the examples shown above, the  $Pn/Lg$  ratios are plotted on the top half of the stars and the  $Pn/Sn$  ratios on the bottom half. The example in this figure is for an earthquake in the Maloy offshore swarm and the top right is for a blast at the Titania mine site, both recorded at the NORESS array.

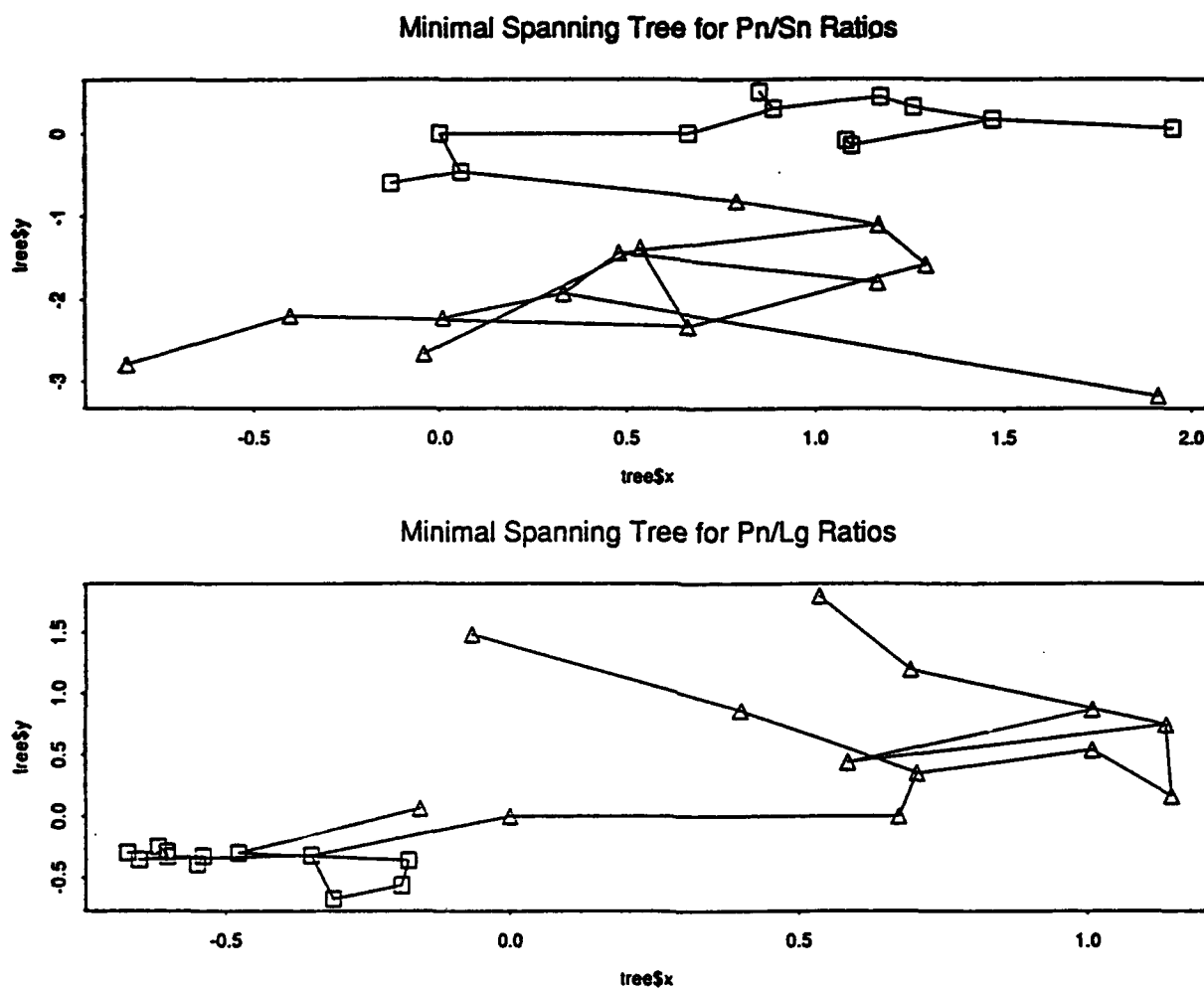


**FIGURE 21:** The plot above shows the results of clustering of the  $Pn/Sn$  ratios (top) and  $Pn/Lg$  ratios (bottom), using the method of minimal spanning trees (MST) and multivariate planing (Friedman and Rafsky, 1981). The triangles refer to the blasts and the squares to earthquakes.

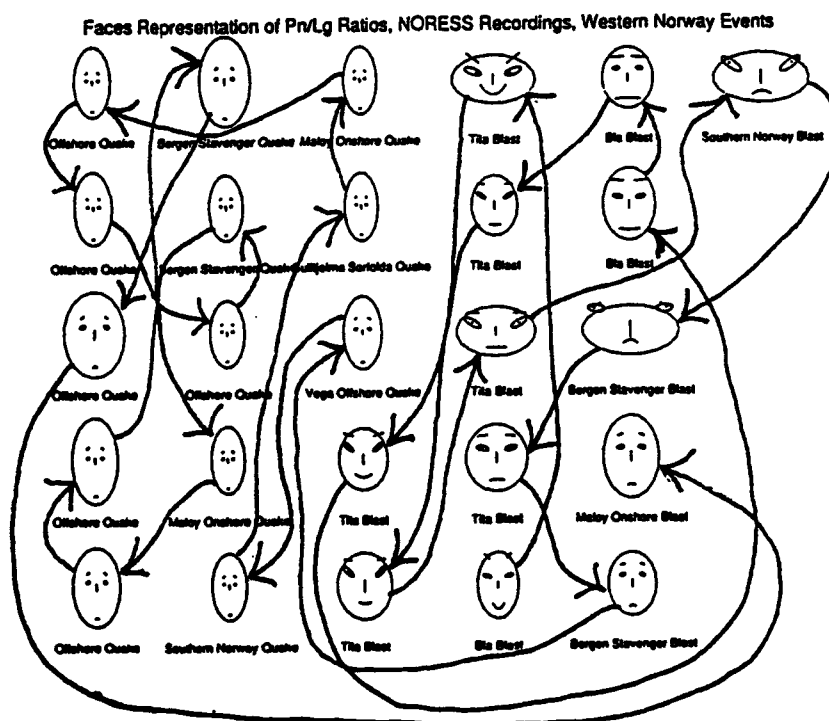
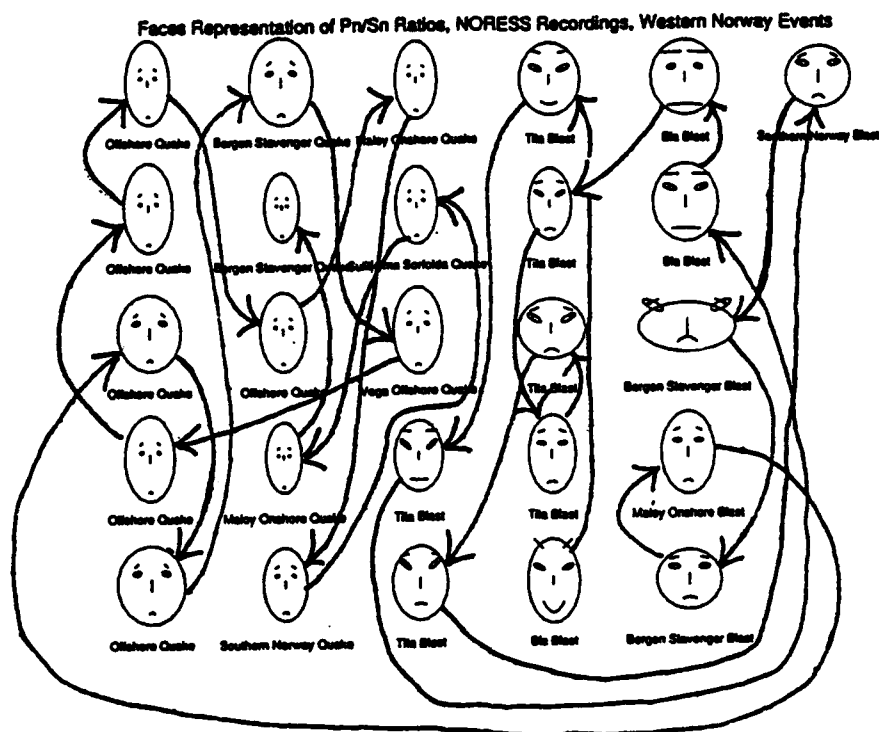
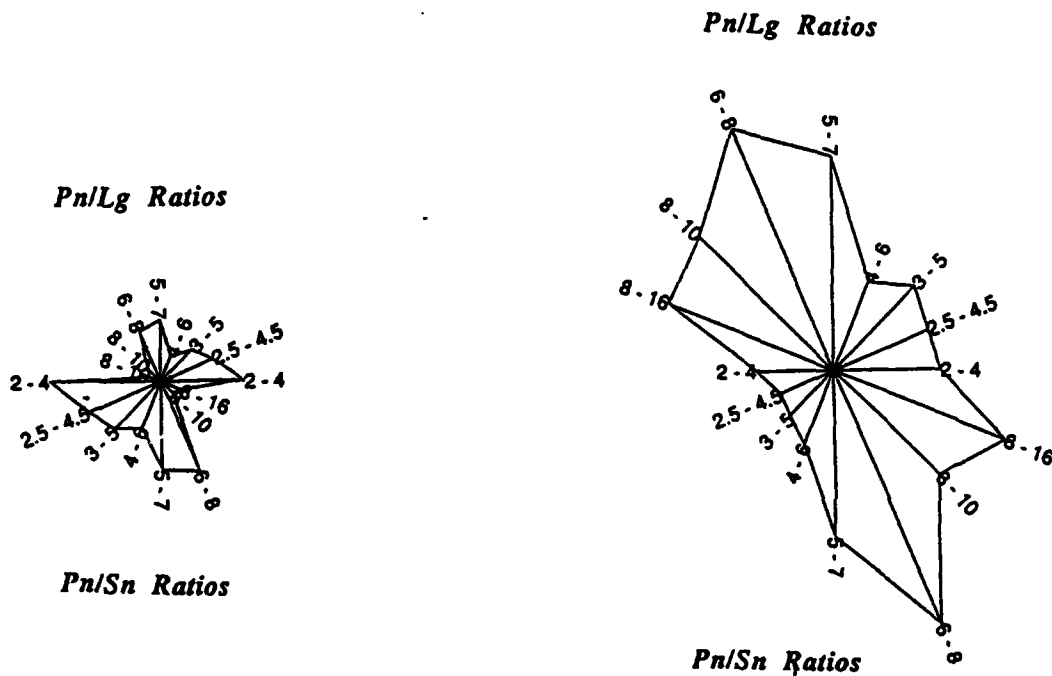


**FIGURE 22:** The figures above are the same as in Figure 20 but show how the minimal spanning tree in Figure 21 connects the different faces, i.e., faces connected by arrows are those judged to be the closest by the MST method. These plots show the equivalency of automatic machine learning methods, like MST clustering, to human visual clustering with Chernov faces.

Western Norway Earthquake - NORESS

Western Norway Blast (TITA) - NORESS



*Ratios computed from maximum RMS amplitudes in phase selection window for phases.*

**FIGURE 23:  $Pn/Lg$  ratio star plots computed from maximum RMS amplitudes in phase selection windows for  $Pn$  and  $Lg$ . The left plot shows  $Pn/Lg$  ratio assignments for an earthquake in Norway, the right plot shows the same for an explosion at Titania (TITA). The plots show the ratio values normalized to the entire set of 13 earthquakes and 13 explosions studied at NORESS (Baumgardt, 1992).**

Figure 24 shows star plots of the combined  $Pn/Sn$  and  $Pn/Lg$  ratios for the 13 explosions and 13 earthquakes recorded at NORESS, corresponding to the faces plots in Figure 20. These plots show that the stars are in general much smaller for the earthquakes relative to the explosions, indicating that the former have smaller values of ratios than the latter across the entire frequency band. It is notable that this discrimination appears to be broad band and not limited only to the high frequencies.

### 3.3.3 Discrimination of Steigen Earthquakes and Kola Blasts - ARCESS

We now compare waveform feature data for the Steigen events with those of the Kola Peninsula blasts.

Figure 25 shows the ISEIS scatterplot of the  $Pn/Lg$  ratio as a function of frequency. Figure 25a shows all the points; in black and white, this plot does not clearly show the distinction between explosions and earthquakes although it is clearer on color plots. However, Figure 25b shows the averages of all the points in the explosion and earthquake classes and their standard deviations. Also in Figure 25b, a test event has been plotted, a mine explosion, which is the circle with the overlaid star and falls close to the earthquake group at high frequencies. From this plot, we infer the best separation between blasts and earthquakes to be in the 5-7 and 6-8 Hz bands. The largest overlap is in the low frequencies, particularly in the 0.5-2.5 Hz bands. Also, note that the error bars on the explosion group are larger than those for the earthquake group.

Figure 26a shows ISEIS scatter plot of  $Pn/Lg$  ratios, recorded in the 6-8 Hz band, versus distance. The Steigen events are the cluster of squares near 440 km. Notice that the blasts vary in amplitude ratio on the order of a factor of three or more, whereas the earthquake distribution is much less variable, even for earthquakes outside the Steigen region and closer to ARCESS. Many of the blasts have similar ratios as the earthquakes, indicating that they excite much shear wave energy. Figure 26b shows the same ratios plotted versus local magnitude. There is no apparent dependence of these ratios on magnitude. However, it can again be noted that the blast points are much more scattered than the earthquakes at all magnitudes.

Figure 27a shows a plot of the  $Lg$  spectral ratio (2-4 Hz/4-6 Hz) as a function of distance. With the exception of some outlier explosion points, which have high ratios, we find almost complete overlap between the earthquakes and blasts. Note that the only correction that has been made to the spectra prior to computing the ratios is instrument. The lack of dependence of spectral ratio on distance indicates that it would probably be fruitless to try to correct the spectra for

# Star Representation of Combined $Pn/Sn$ , $Pn/Lg$ Ratios, NORESS Recordings, Western Norway Events

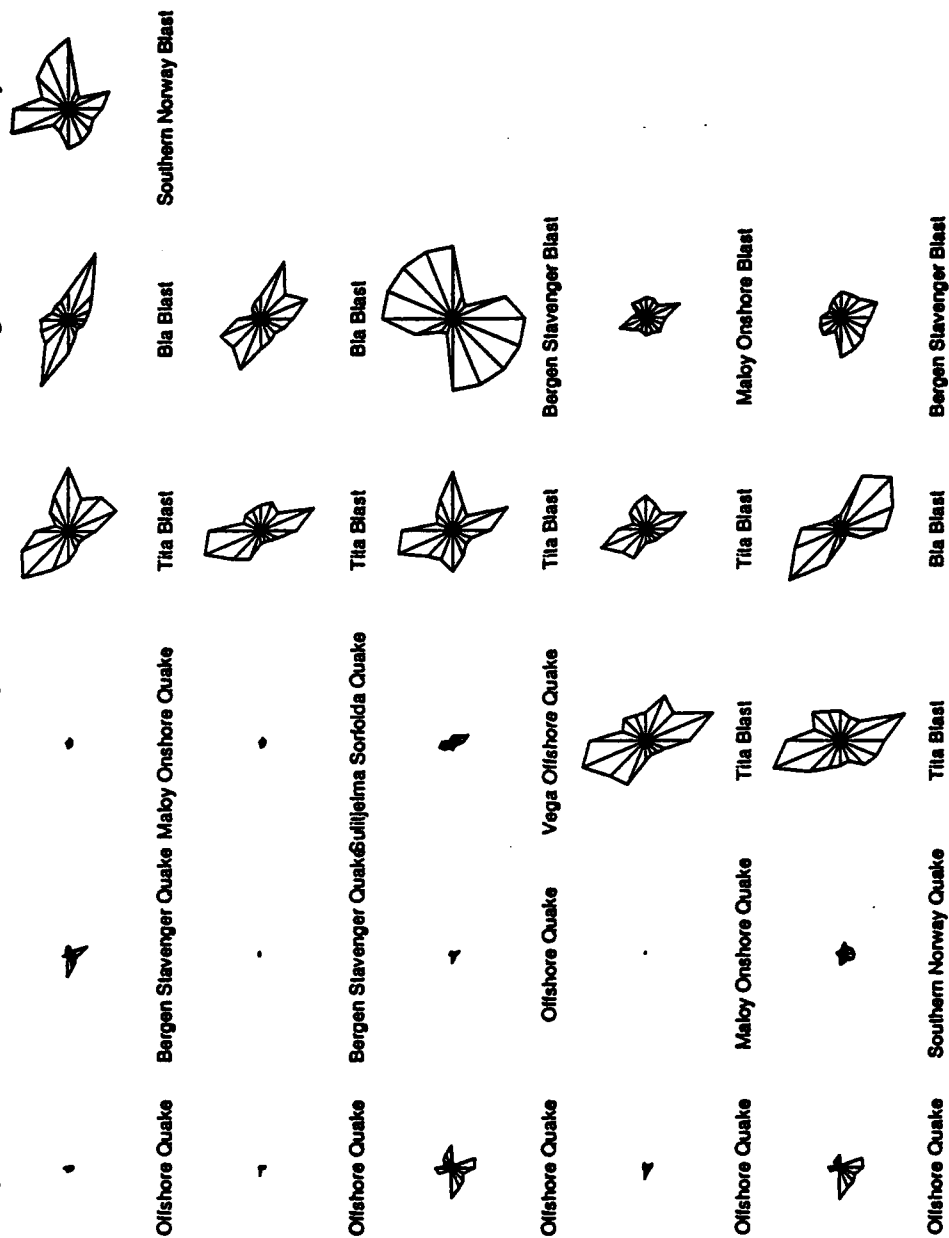


FIGURE 24: Star plots of the combined  $Pn/Sn$  and  $Pn/Lg$  ratios for the 13 explosions and 13 earthquakes recorded at NORESS, corresponding to the faces plots in Figure 20.

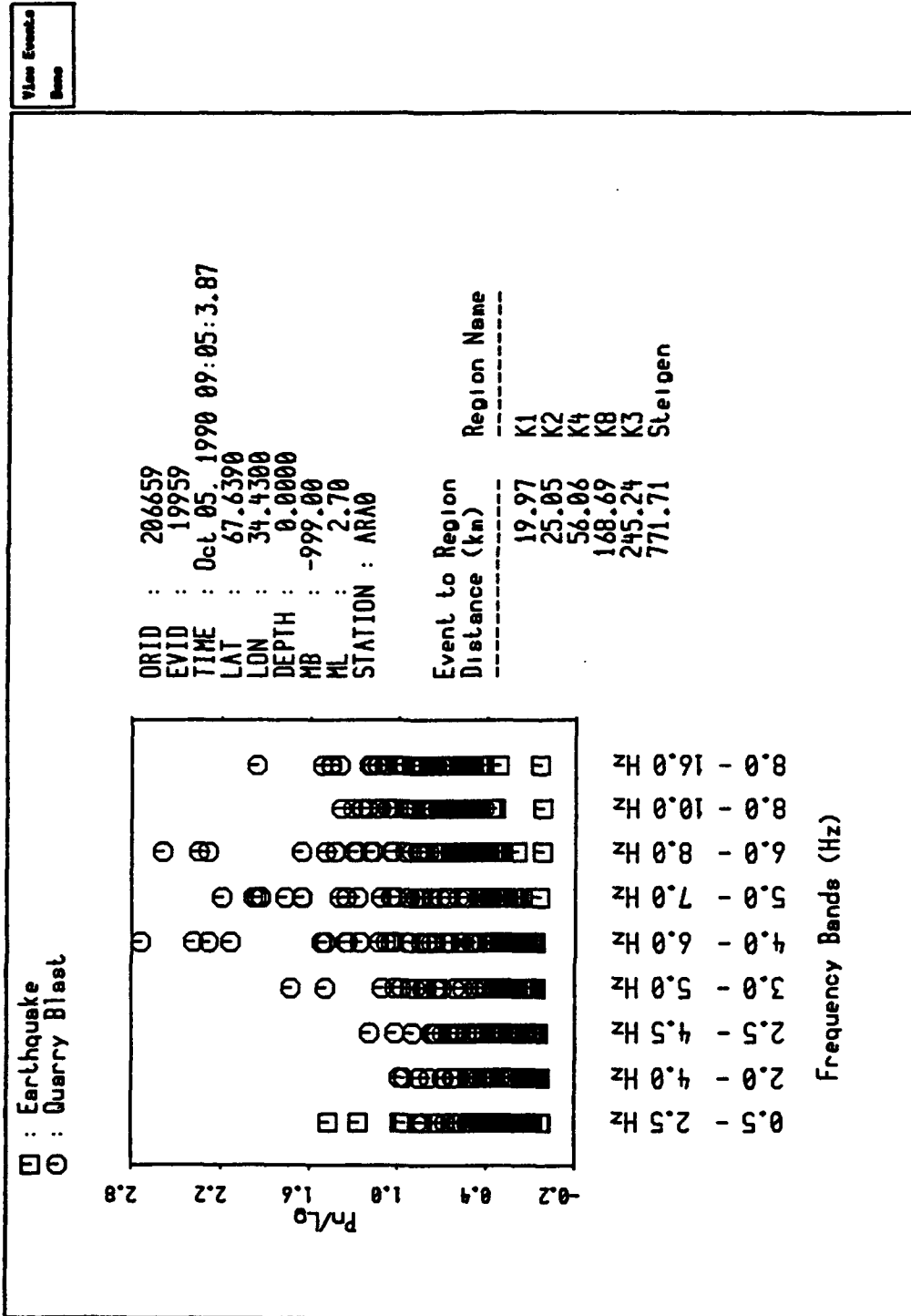


FIGURE 25(a): ISEIS scatterplot as a function of frequency band of the  $Pn/Lg$  ratios for five Kola Mine blasts regions and the Steigen earthquakes recorded at ARCESS.

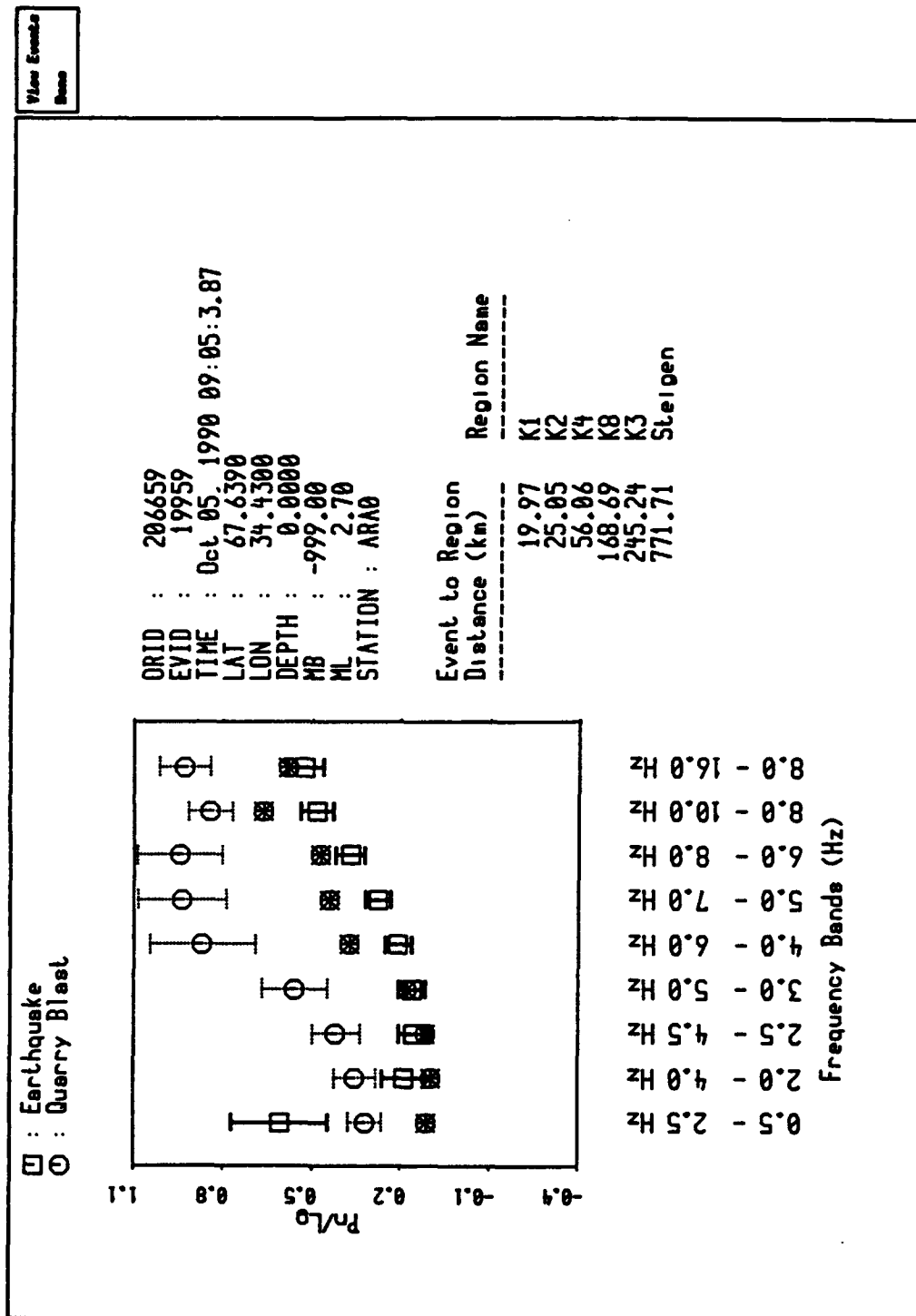


FIGURE 25(b): ISEIS scatterplot as a function of frequency band of the averages for the explosion and earthquakes groups of the ARCESS  $Pn/Lg$  ratios from the Steigen earthquakes and Kola explosions. The error bars indicate the standard deviations of the groups. The "test event" is a blast indicated by the circle with the star on top of it and its source parameters are given to the right of the plot.

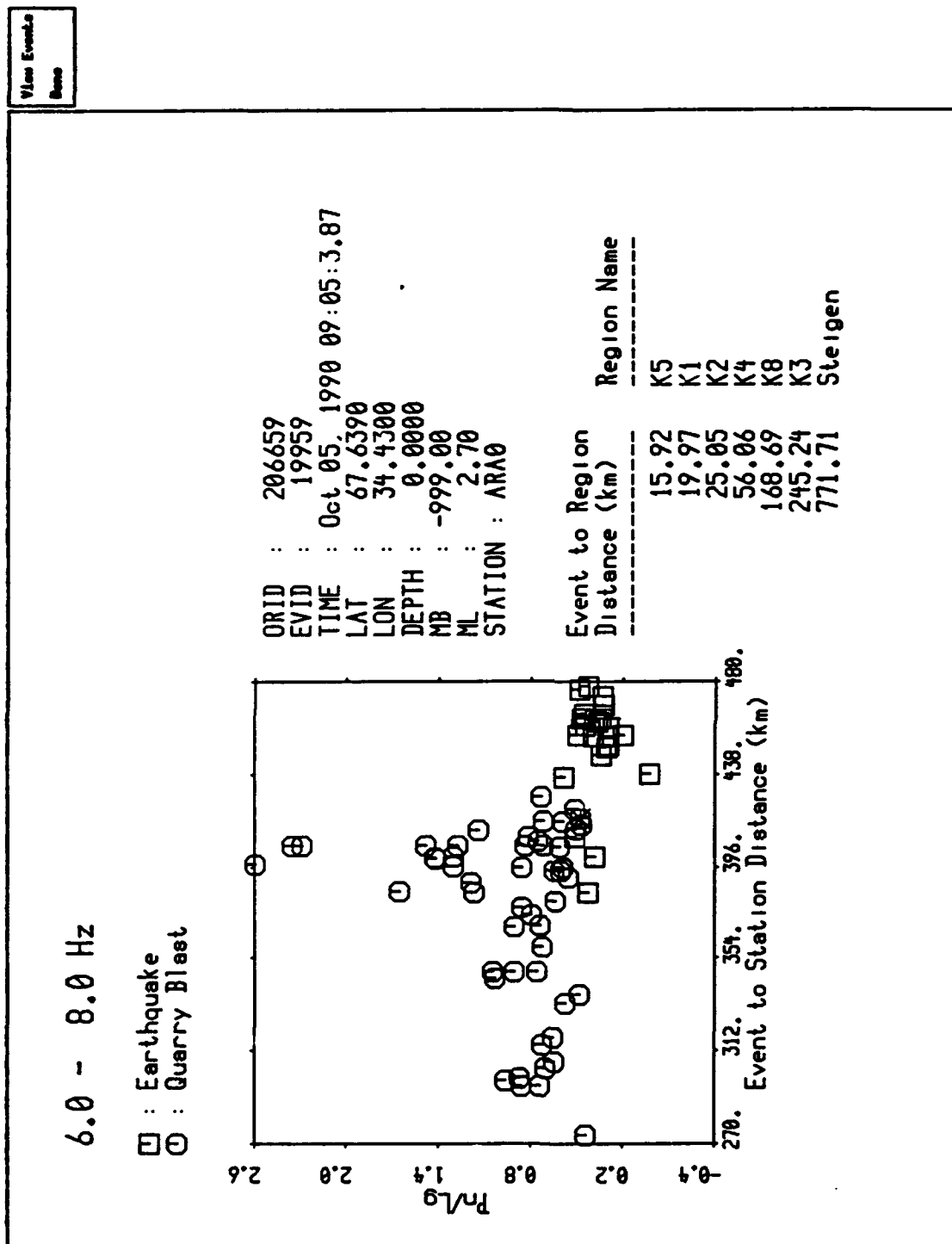


FIGURE 26(a): Plot of the  $Pn/Lg$  ratio in the 6-8 Hz band as function of distance of the event from ARCESS for the Steigen earthquakes and Kola explosions.

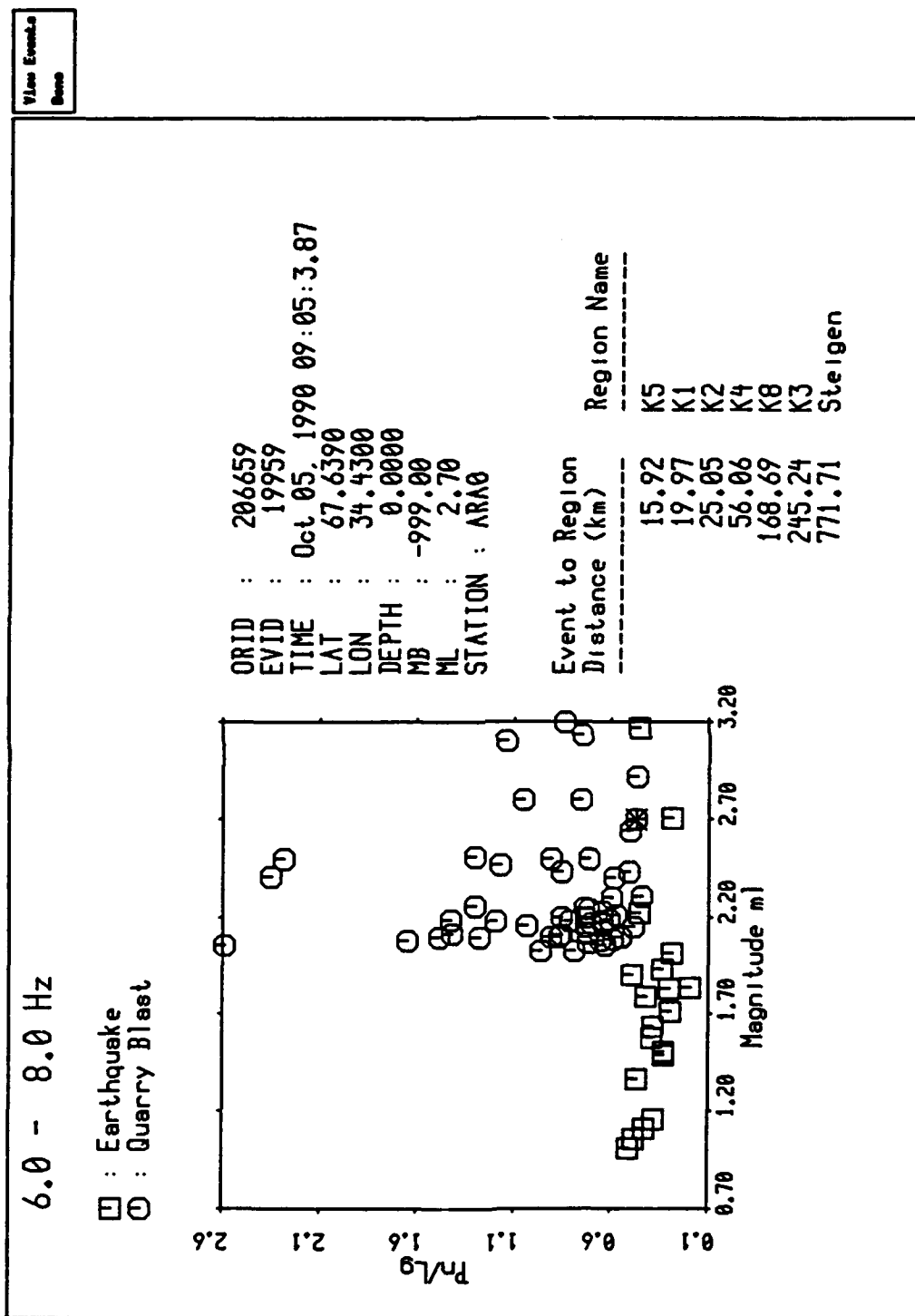


FIGURE 26(b): Plot of the  $P_n/L_g$  ratio in the 6-8 Hz band as a function of local magnitude (ml) for ARCESS recordings of the Steigen earthquakes and Kola explosions.

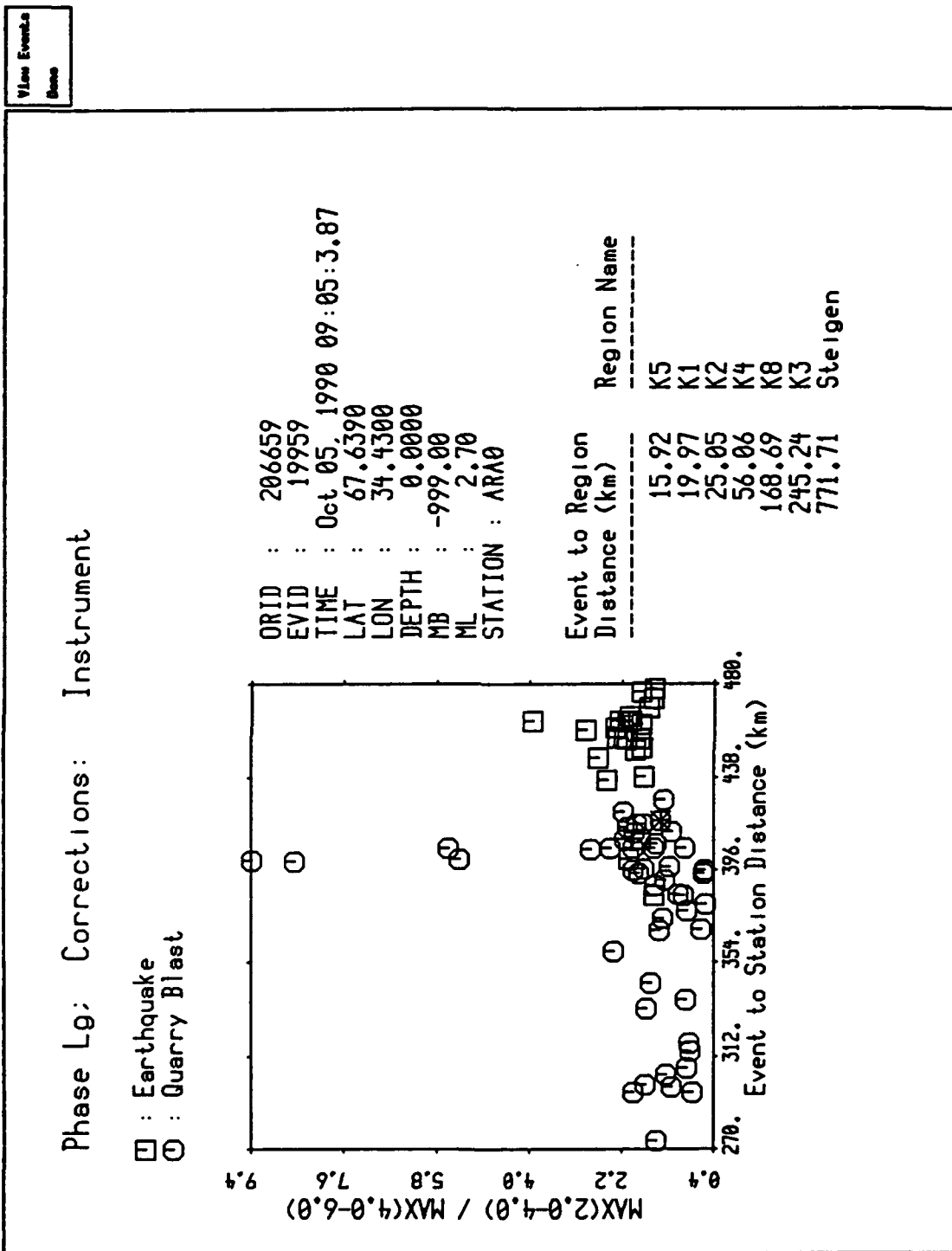


FIGURE 27(a): Plot of the Lg spectral ratio (2-4 Hz/4-6 Hz) as a function of distance for the Steigen earthquakes and Kola explosions recorded at ARCESS.

distance. The large scatter and overlap does not seem to be due to distance-dependent attenuation affects. Figure 27b shows the same ratios plotted against local magnitude. In general, there does not appear to be any dependence of the spectral ratio on magnitude, although there may be a slight trend in the earthquakes of spectral ratio increasing with magnitude. The blasts, on the other hand, are entirely scattered.

Figure 28 shows the Chernov faces for  $Pn/Sn$  ratios (top) and  $Pn/Lg$  ratios (bottom) for the Steigen earthquakes recorded at ARCESS and comparable distance Kola blasts at the HD9 and HD10 sites. Notice the similarity of the Steigen faces, which are uniformly small and sad, compared with the larger but more variable faces for the blasts. As in the case of the NORESS data discussed above, this reflects the greater variation in these ratios, evident in the scatter plots.

The star plots for the combined  $Pn/Sn$  and  $Pn/Lg$  ratios corresponding to the faces displays are shown in Figure 29. The larger sized blasts' stars compared to the earthquakes are evident. Also apparent is that the earthquakes have a trend from the upper left to lower right, indicating that the ratios are peaked in the mid-frequency bands (5 to 8 Hz), a trend also apparent in some blasts. Again, the blasts have a greater variety of shape and size compared to the earthquakes.

In summary, we find that Steigen-swarm earthquakes and Kola blasts can be separated on the basis of  $Pn/Lg$  ratios but not  $Lg$  spectral ratios. However, the faces and star plots reveal that although the multifrequency amplitude ratios are distinctive between blasts and earthquakes, the blast faces and stars exhibit much greater variability than the earthquakes. This is noted also in the scatterplots for single frequency features, where the scatter in blasts is much greater than that of the earthquakes.

### **3.3.4 Discrimination of Vogtland Earthquakes and Blasts - GERESS**

The events in the Vogtland region, recorded at GERESS, were first studied in detail in a discrimination context by Wuster, 1992 (also see Harjes et al, 1992). Wuster applied six discriminations, including an  $S/P$  amplitude ratio, an  $S/Rg$  amplitude ratio, and three spectral discriminants sensitive to spectral shape and spectral modulations, due to ripple fire. Ripple fire was studied using the sonogram methods of Hedlin et al (1990) applied to a single broad-band, three-component sensor. In this study, we processed through ISEIS a subset of these events available through the IMS, which are shown in the map in Figure 14. The ISEIS approach to discrimination differs in some significant ways from that of Wuster (1992), which we discuss below in terms of the successes and failures of both approaches.

# Phase Lg: Corrections: Instrument

□ : Earthquake  
 ○ : Quarry Blast

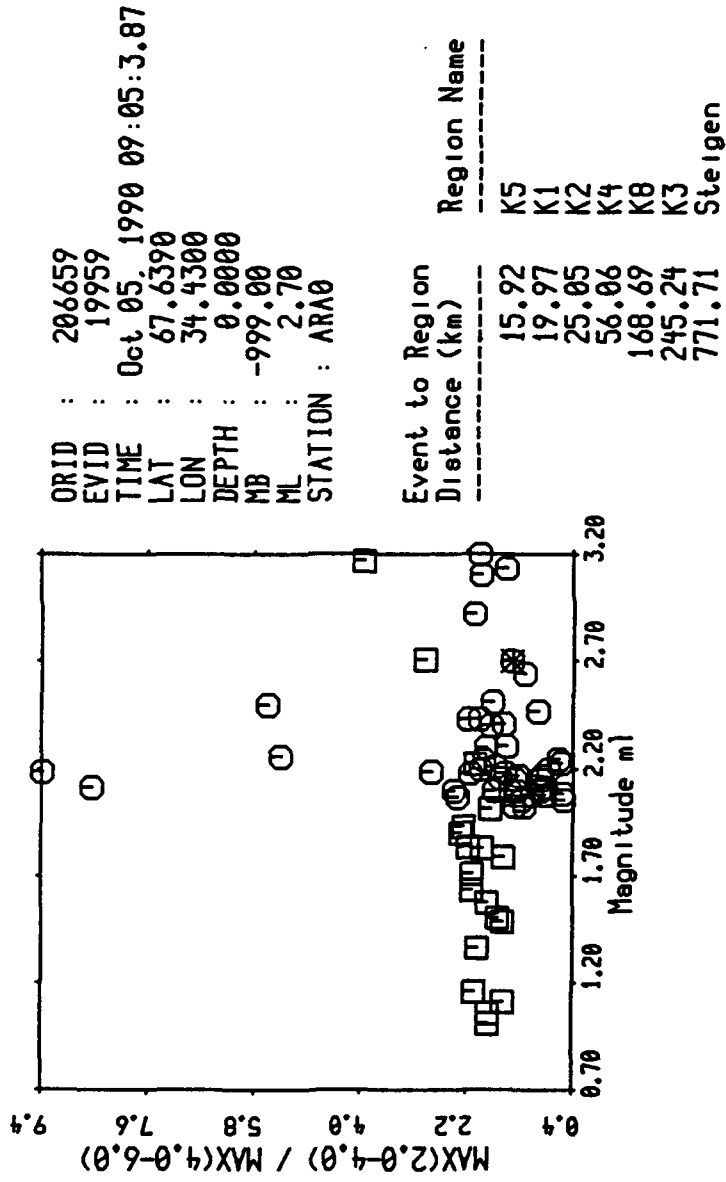
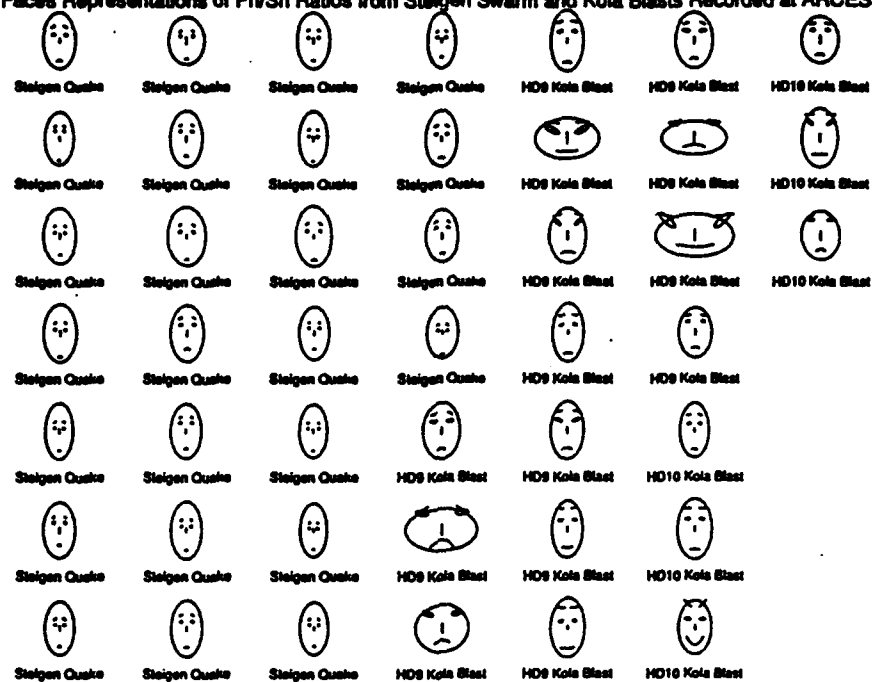
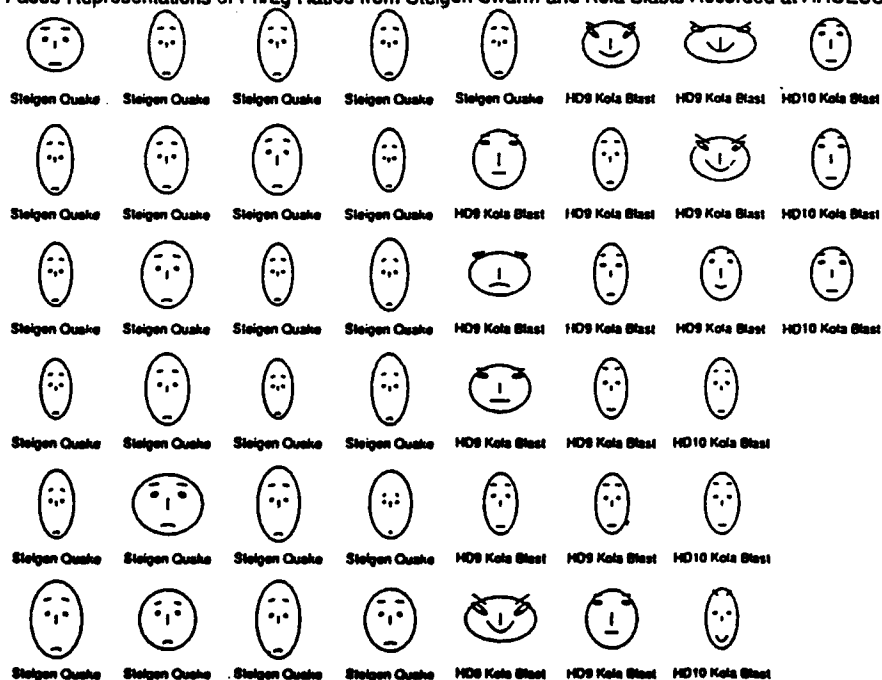


FIGURE 27(b): Plot of the  $L_g$  spectral ratio (2-4 Hz/4-6 Hz) as a function of local magnitude (ml) for the Steigen earthquakes and Kola explosions recorded at ARCESS.

Faces Representations of  $P_n/S_n$  Ratios from Steigen Swarm and Kola Blasts Recorded at ARCESS



Faces Representations of  $P_n/L_g$  Ratios from Steigen Swarm and Kola Blasts Recorded at ARCESS



**FIGURE 28:** Chernov faces for  $P_n/S_n$  ratios (top) and  $P_n/L_g$  ratios (bottom) for the Steigen earthquakes recorded at ARCESS and comparable distance Kola blasts at the HD9 and HD10 sites.

# Star Representations of $Pn/Lg, Pn/Sn$ Ratios from Steigen Swarm and Kola Blasts Recorded at ARCESS

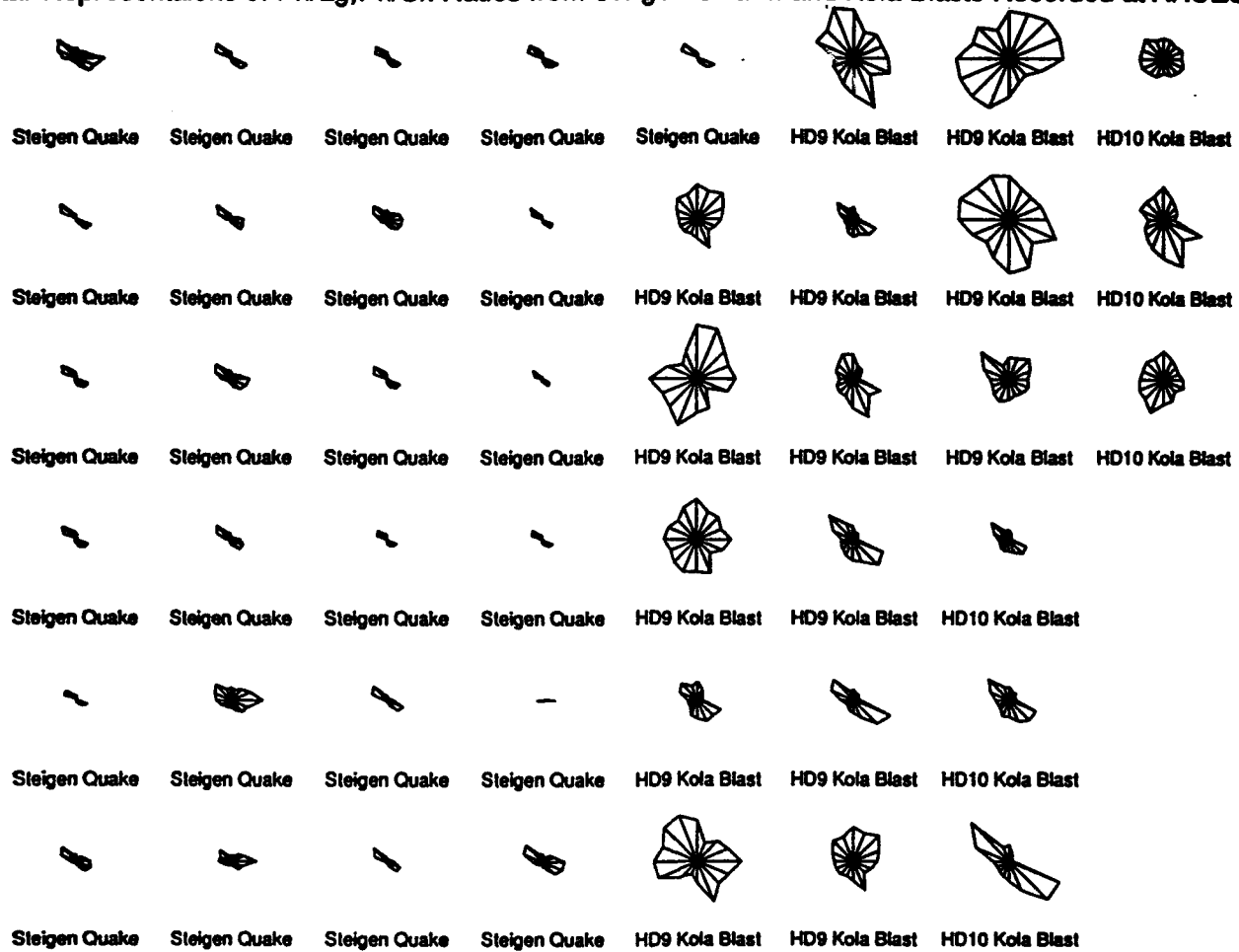


**FIGURE 29: Star plots for the combined  $Pn/Sn$  and  $Pn/Lg$  ratios corresponding to the faces displays shown in Figure 28.**

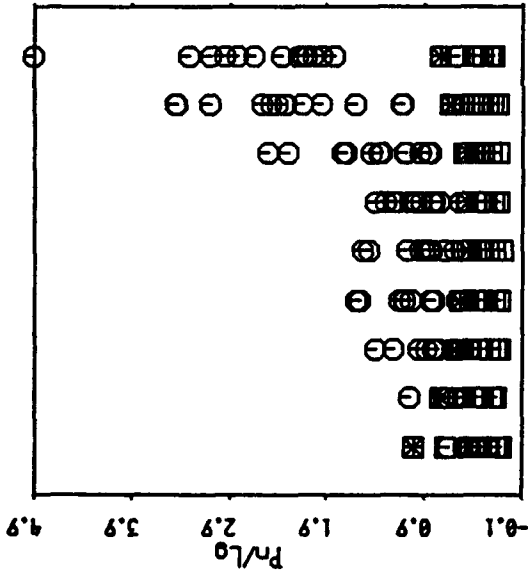
Figure 30 shows plots of the  $Pn/Lg$  ratios as a function of frequency. Figure 30a shows all the points and 30b the means and standard deviations of the earthquake and explosion groups. As in most of the cases we have seen at NORESS and ARCESS, the explosion and earthquake groups separate well on the basis of this discriminant, with this separation being greater at high frequency. As in the case of the Kola events recorded at ARCESS when compared to the Steigen earthquakes, the explosion group has much greater variability, particularly at high frequency, than the explosions, which vary little as a function of frequency. Note that in Figure 30b, the test event, represented by the square with a star on top of it, has a high ratio at low frequency and a low ratio at high frequency. We shall examine this event in more detail below.

Figure 31 shows a plot of the  $Pn/Lg$  ratios in the 8 to 10 Hz band as a function of local magnitude. (Note: We do not show scatterplots as a function of distance since all these events are at almost the same distance from GERESS.) The lack of dependence of this ratio on local magnitude is evident. The explosion and earthquake groups are cleanly separated. However, the explosion points exhibit much greater variation, greater than a factor of three, than the earthquakes, which are very stable.

Figure 32 shows a scatterplot of  $Lg$  spectral ratio (2-4 Hz/4-6 Hz) as a function of local magnitude, which shows that most of the earthquakes separate the explosions, with the earthquakes having apparently enriched high frequencies compared to the explosions. This is consistent with the results found for earthquakes and explosions in the western U.S. Thus, we are faced with the interesting dilemma that spectral ratio works in this region in Germany, as in the western U.S., but not in Scandinavia and other shield regions. Also note in Figure 33 that one explosion falls in the earthquake category. We shall discuss this anomalous event later.

Figure 33 shows the multivariate visualizations of faces plots (top) and stars (bottom) for the  $Pn/Lg$  ratios for the Vogtland events recorded at GERESS. Notice that the stars include the 0.5 to 2.5 Hz band, which is the ray pointing to the right on each star. The earthquake faces, as in the case of the southern Norway and Steigen earthquakes, are again uniformly sad and have small features, whereas most of the blast faces smile, indicating large ratios at high frequency, and are much more variable. Notice how the "anomalous earthquake" face, which is the first face in the third column, has an earthquake-like shape, but its eye and mouth signatures are more explosion-like. This reflects the larger low frequency ratios for this event. The stars for the earthquakes are smaller than the blasts. Also, the blast stars are much smaller for the earthquakes than for the blasts.

□ : Earthquake  
⊙ : Quarry Blast



ORID : 23275  
EVID : -1  
TIME : May 19, 1991 03:22:10.52  
LAT : 50.2776  
LON : 12.0905  
DEPTH : 0.0000  
MB : -999.00  
ML : 2.44  
STATION : GEC2

Event to Region  
Distance (km) -----  
15.22  
Region Name -----  
Vogtland

8.0 - 16.0 Hz  
8.0 - 10.0 Hz  
6.0 - 8.0 Hz  
5.0 - 7.0 Hz  
4.0 - 6.0 Hz  
3.0 - 5.0 Hz  
2.5 - 4.5 Hz  
2.0 - 4.0 Hz  
0.5 - 2.5 Hz

Frequency Bands (Hz)

FIGURE 30(a): ISEIS scatterplot of the  $P_n/L_g$  ratios for five Vogtland explosions and earthquakes, recorded at GERESS, as a function of frequency.

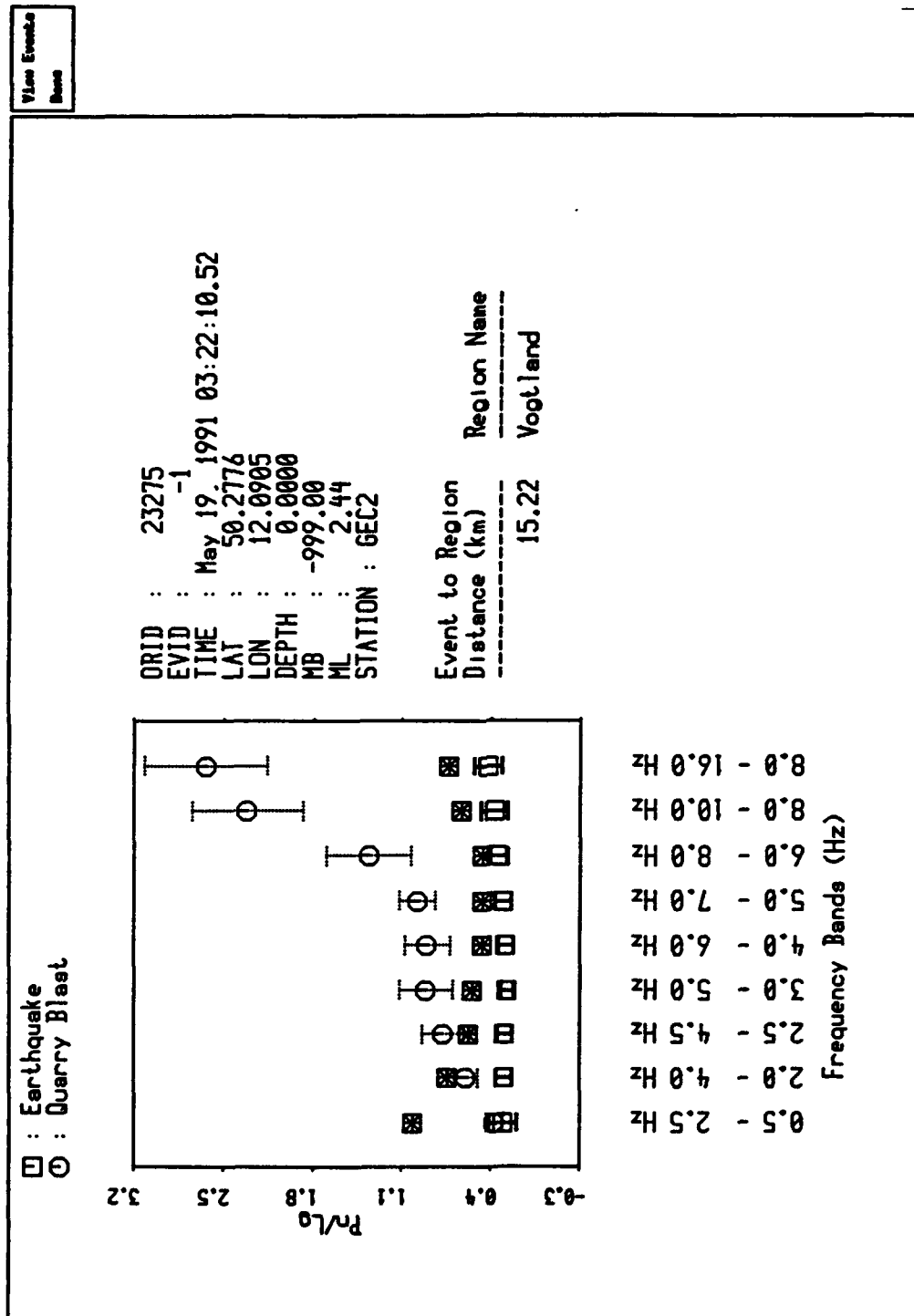


FIGURE 30(b): ISEIS scatterplot plot of the averages for the explosion and earthquakes groups of the GERESS  $Pn/Lg$  ratios from the Vogtland region. The error bars indicate the standard deviations of the groups. The "test event" is a blast indicated by the circle with the star on top of it and its source parameters are given to the right of the plot.

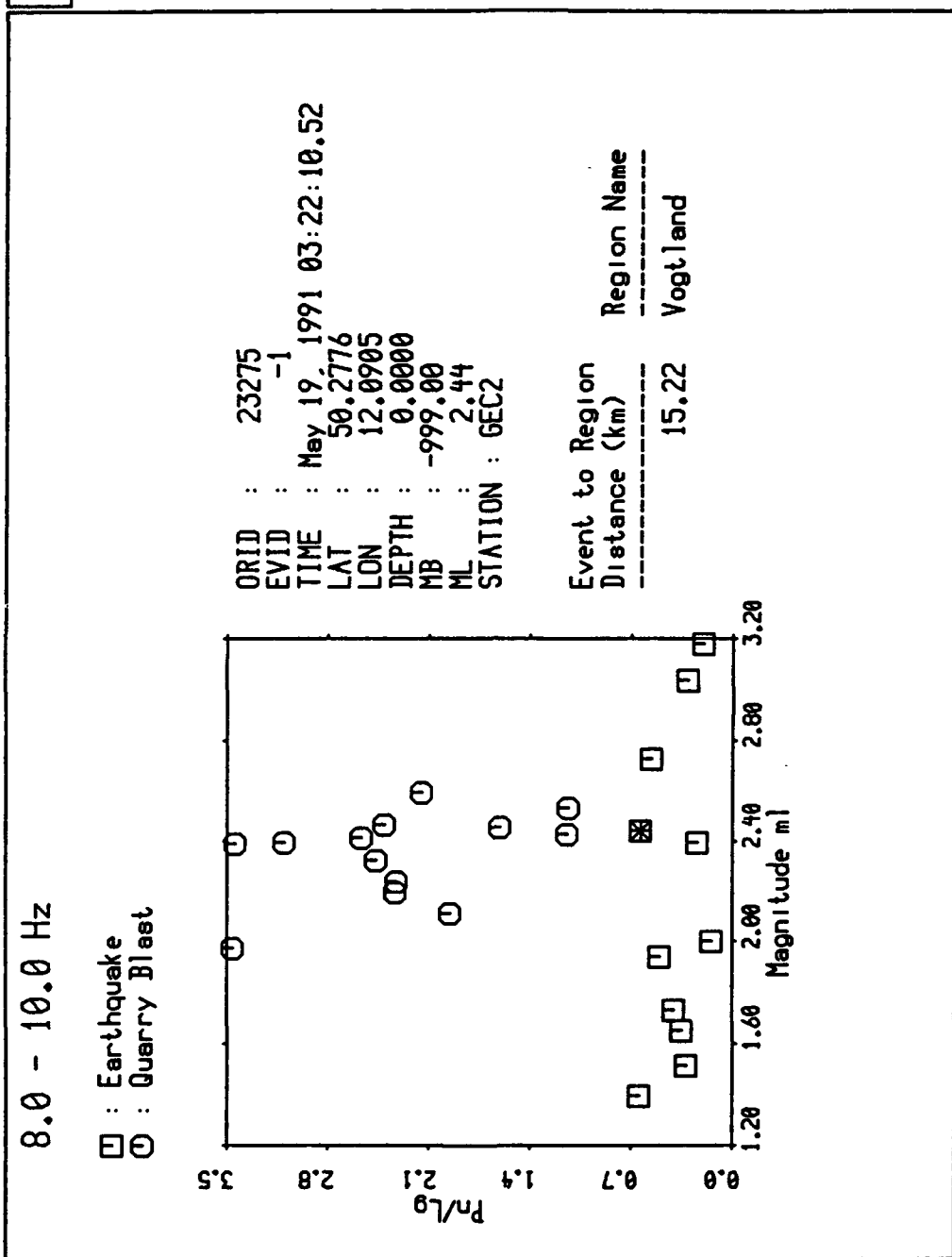
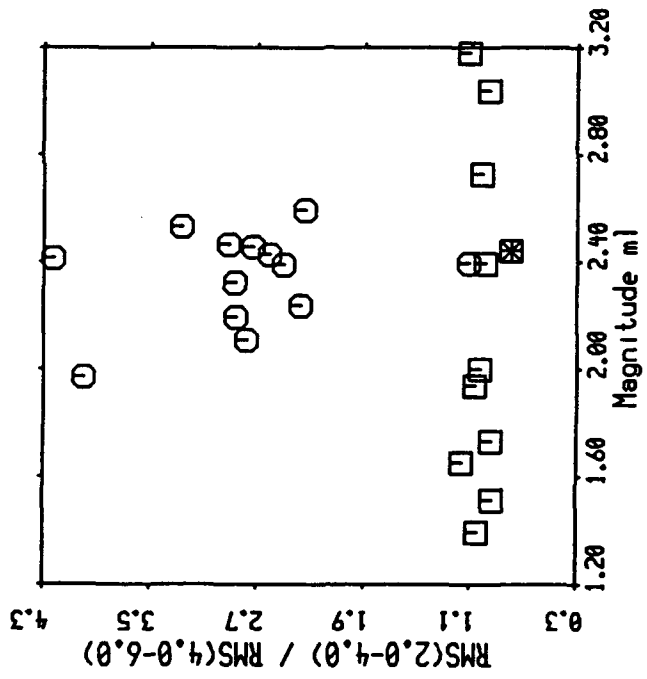


FIGURE 31: ISEIS scatterplot as a function of local magnitude (ml) of the  $P_n/L_g$  ratios in the 8-10 Hz band measured at GERES for earthquakes and explosions in the Vogtland region.

Phase Lg: Corrections: Instrument

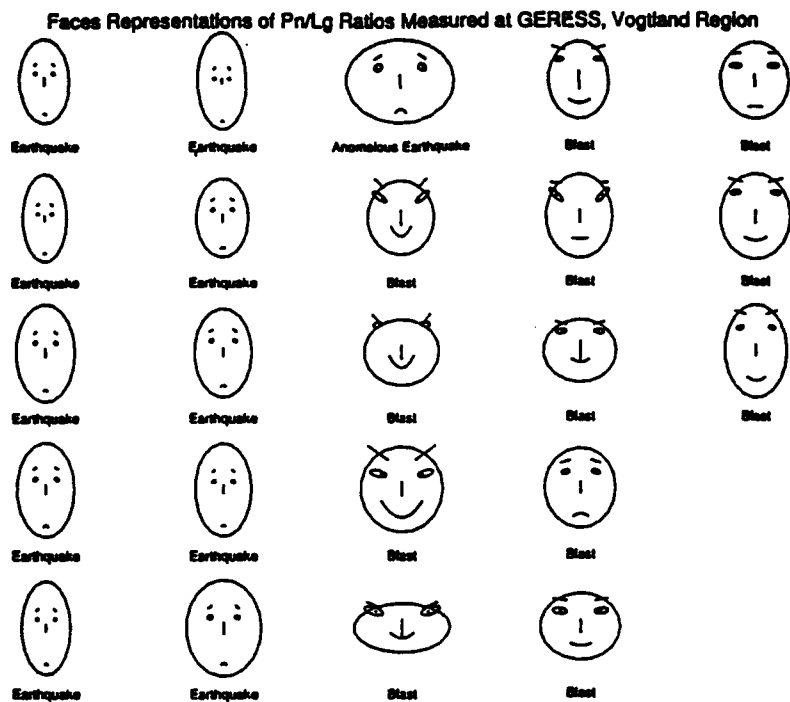
- : Earthquake
- : Quarry Blast



ORID : 23275  
 EVID : -1  
 TIME : May 19, 1991 03:22:10.52  
 LAT : 50.2776  
 LON : 12.0905  
 DEPTH : 0.0000  
 MB : -999.00  
 ML : 2.44  
 STATION : GEC2

Event to Region	Region Name
Distance (km)	
15.22	Vogtland

FIGURE 32: ISEIS scatterplot as a function of local magnitude (ml) of the Lg spectral ratio (2-5 Hz/4-6 Hz) measured at GERES for earthquakes and explosions in the Vogtland region.



**Star Representations of  $Pn/Lg$  Ratios, GERESS Recordings, Vogtland Events - 0.5-2.5 Hz Filter Included**

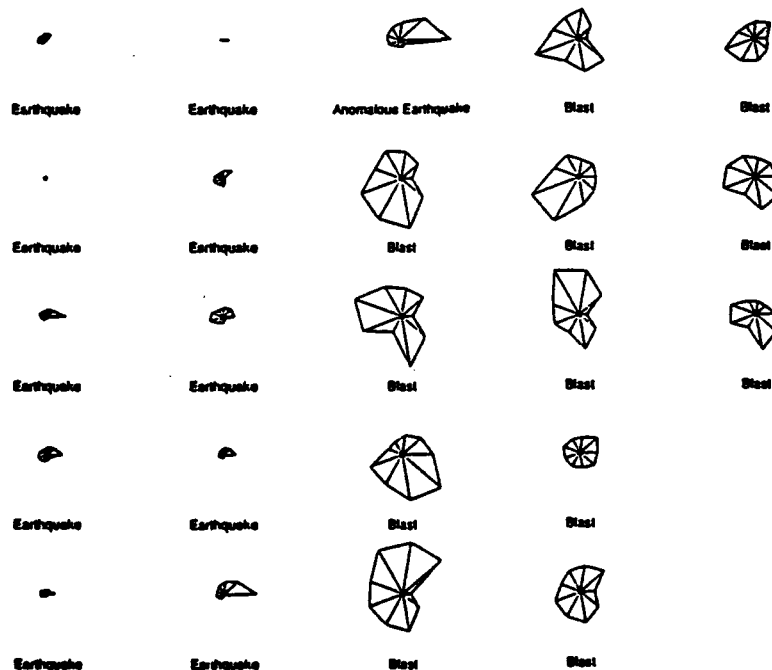


**FIGURE 33: Faces plots (top) and stars (bottom) for the  $Pn/Lg$  ratios for the Vogtland events recorded at GERESS. Notice that the stars include the 0.5 to 2.5 Hz band, which is the ray pointing to the right on each star.**

In summary, with regard to amplitude ratios, the Vogtland events show a very similar picture as those in the other two regions, with the earthquakes being very consistent and the explosions displaying much larger variances in these ratios. However, for the first time in our studies of the IMS data, we have found a set of events for which the  $Lg$  spectral ratio discriminant works.

### 3.4 DISCUSSION

This study has highlighted two interesting dilemmas regarding the discrimination of mine explosions and earthquakes using data from the IMS:

- (1) The variance of  $Pn/Lg$  amplitude ratios at high frequencies is much greater for blasts than for earthquakes. Sometimes this variance can be on the order of a factor of four or greater, even for blasts in the same mine.
- (2) The  $Lg$  spectral-ratio discriminant, which performed so well for discriminating explosions and earthquakes in the western U.S., fails for events in the IMS which occur in Norway. However, the discriminant does work for earthquakes and explosions in Germany.

In this section, we explore these dilemmas in more detail and offer some explanations.

#### 3.4.1 High Amplitude Ratio Variance in Blasts

Figure 34 shows a scatterplot of the  $Pn/Lg$  ratios in the 4 to 6 Hz band, measured at the ARCESS array, as a function of local magnitude for a set of events which we assume to be in the same Kola Peninsula mine, designated K2 in the Helsinki bulletin, and HD9 at the CSS. The integers plotted to the right of each of the points are the origin ids (orids) assigned by the IMS for each of the events. The designation of mine types by analysts at the University of Helsinki, which they call "Manual Locations" in their bulletin, is based on a visual pattern recognition approach. The analysts assign the mine types partly on the basis of a rough location estimate, based on a standard triaxial location (trix), and by visually comparing the waveforms with historical examples. The precise method for assigning these mines has never been described, and it may be uncertain. However, we are reasonably confident that manual locations in the same mine are probably good to a few tens of kilometers. Given that most of the events in Figure 34 may be in the same mine, it is surprising to observe the large variance in the observed amplitude ratios. It might be assumed that events in the same location should have very similar waveforms. This, in fact, was the assumption made in the "script-match" approach that had first been proposed by Kandt et al (1987). However, the results of this study refutes this assumption and makes problematic the script-match approach to locating blasts to specific mines on the basis of waveform features alone.

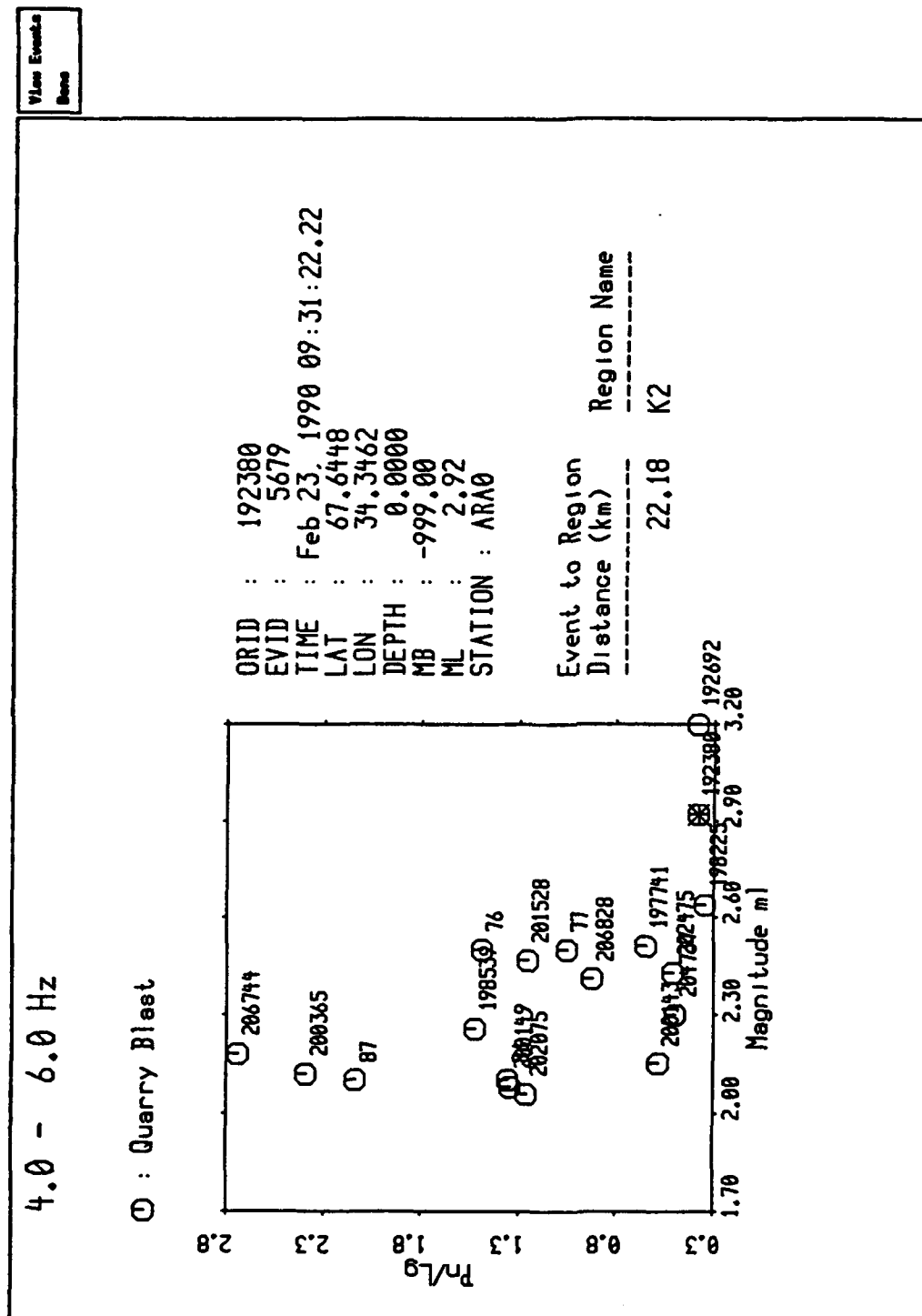


FIGURE 34: ISEIS scatterplot as a function of local magnitude (ml) of the  $P_n/L_g$  ratio measured at ARCESS for mine blasts in the K2 (HD9) mine region on the Kola Peninsula. The numbers to the right of each point is the origin id (orid) of each event.

Figure 35a shows a plot of the vertical component waveform at ARA0 for an event, *orid*=206744, on the high-*Pn/Lg* ratio part of the plot in Figure 34. This waveform has been filtered in the 4 to 6 Hz band corresponding to the filter band used in the scatter plot in Figure 34. The picks *Pn* and *Lg* mark the start points of the *PhaseSelect* windows used to make the amplitude-ratio measurements. Clearly, the *Pn* wave has a higher amplitude in this band than the *Lg* wave. Figure 35b shows all the filtered, shifted/unlogged rms incoherent beams corresponding to this part of the waveform. Clearly, these plots show that the *Pn*-wave amplitude always exceeds the *Lg* wave at all frequencies.

Figure 36a shows the ARA0 sz waveform plot for an event, *orid*=192380, on the low end of the amplitude-ratio plot. In this case, it is clear that the *Lg* amplitude exceeds that of the *Pn* in the 4 to 6 Hz band. The corresponding incoherent beam plots are shown in Figure 36b, which show that *Lg* exceeds the *Pn* wave across most of the frequency band. It is also interesting to note that an apparent *Rg* arrival can be discerned on the 0.5 to 2.5 Hz incoherent beam. Figure 35 shows that there is little dependence of amplitude ratio on local magnitude and these two events have nearly the same local magnitude (2.3 for 206744 and 2.92 for 192380).

Because these variations in *Pn/Lg* are so large, as reflected in these two events, and the fact that we do not observe such variations in earthquakes, measurement errors cannot be the cause of these variations. If these mine blasts are in the same mine, or close to being in the same location, we must rule out propagation effects as the cause of this difference in the relative excitation of *Pn* and *Lg*. Near source effects or variations in the source itself must be the cause. We have generally explained the success of the *Pn/Lg* ratio discriminant to be due to the fact that earthquakes generate more shear than explosions at the same magnitude. However, we have observed that many of the mine blasts on the Kola generate nearly as much shear wave energy as earthquakes.

We believe that the best explanation for this variation is that all mine blasts generate some amount of shear energy, perhaps produced by the fracturing and spalling of rock caused by the blasting. In other words, the large shear waves for the blasts may not come from the explosions but from the secondary fracturing produced by the explosion. It is well known that mine explosions are ripple-fired in order to increase the fracture efficiency of the blasting and to reduce the degree of ground motion produced by the blasts. The ripple-fire detection program in ISEIS, called Multiple Event Recognition System (MERSY), which applies the cepstral methods of Baumgardt and Ziegler (1988), has shown that most of these events are ripple-fired. Since it is the intent of ripple-firing in fracture rock, it would be expected that there should be significant shear associated with many of the explosions.

VIEW TIME SERIES for orid 206744  
 Use drag, then press button for Zoom

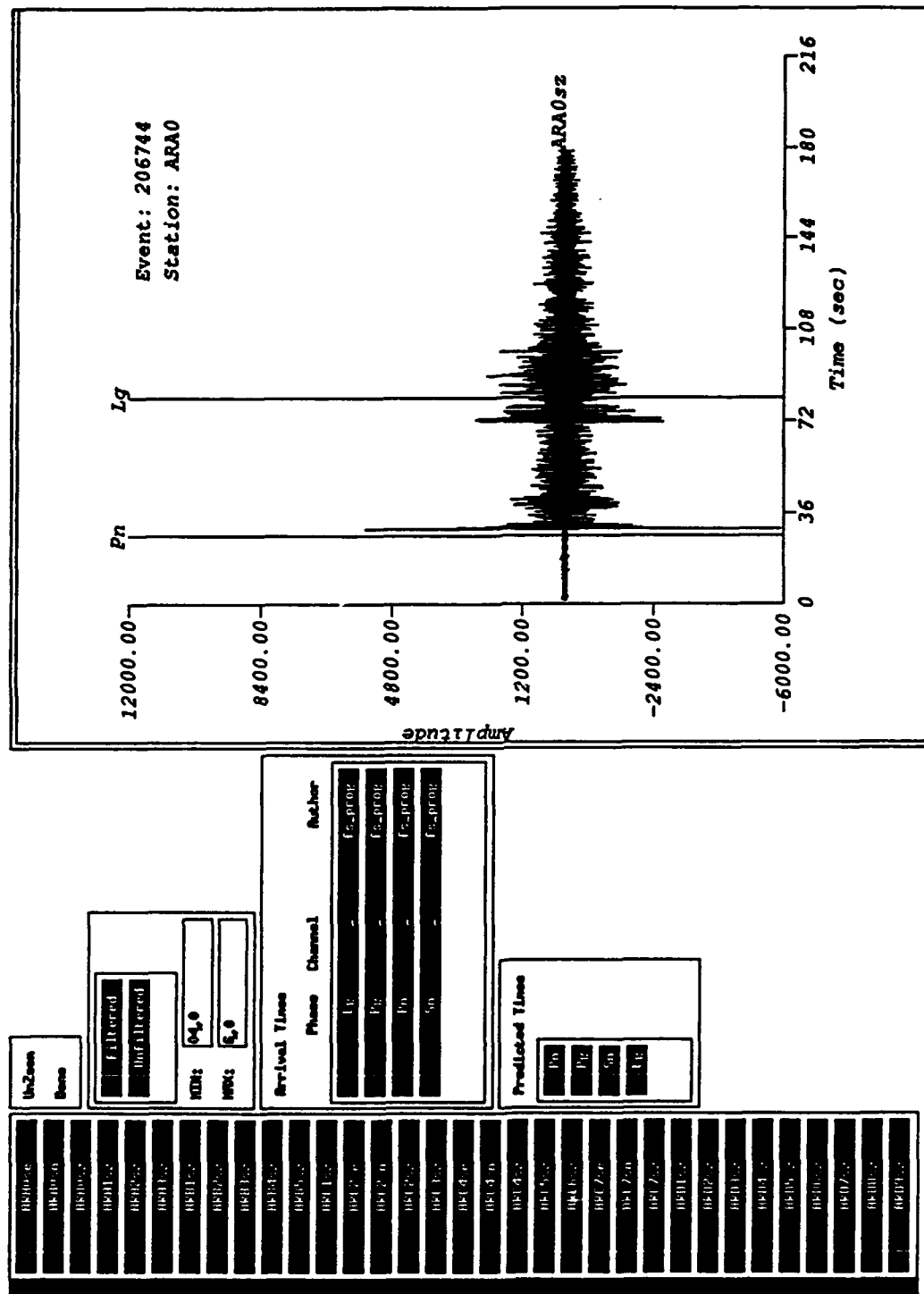
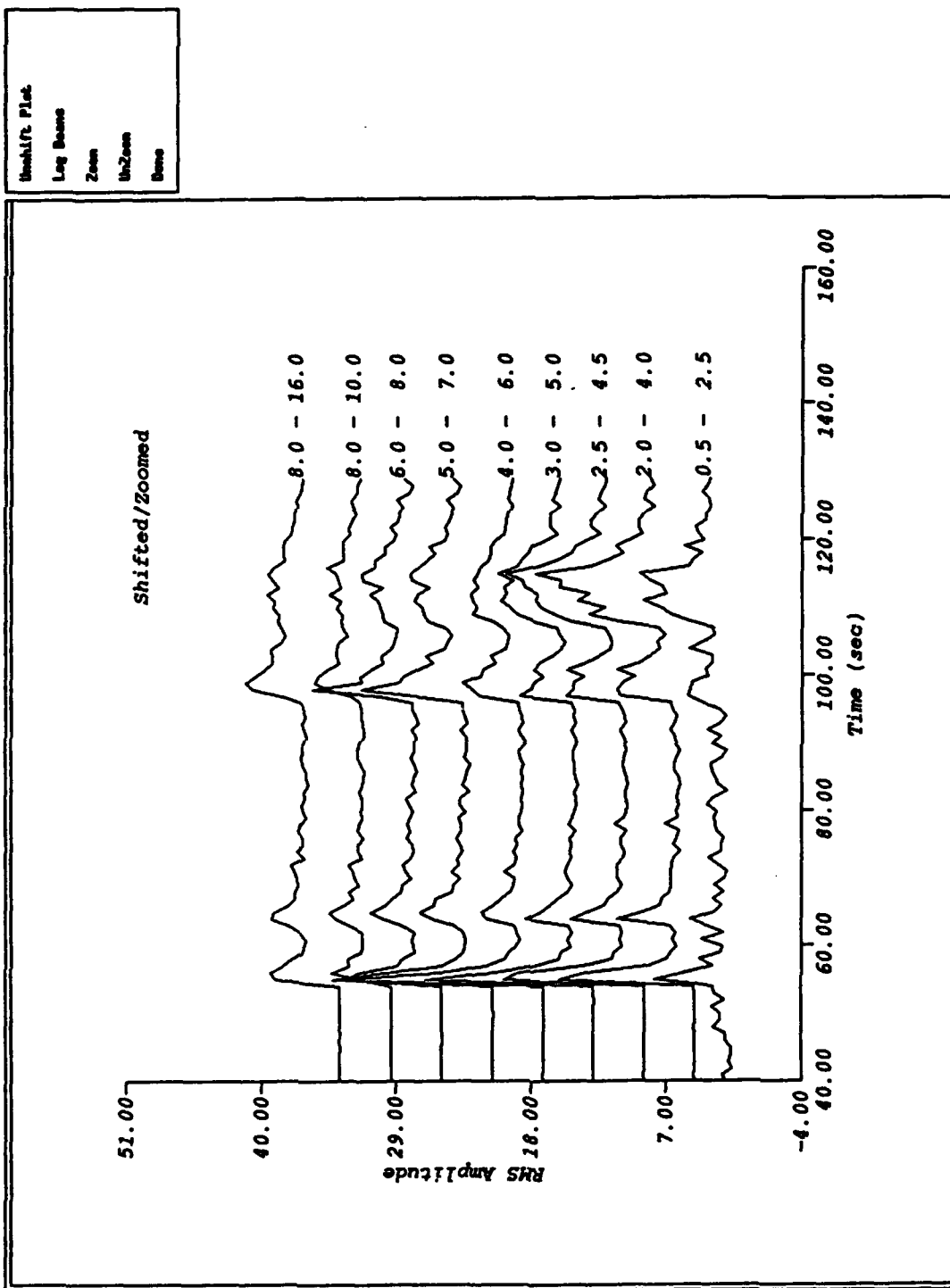


FIGURE 35(a): Waveform plot of the ARA0 sz component at ARCESS for one of the Kola explosions (orid=206744) which had a high  $Pn/Lg$  ratio. This waveform has been filtered in the 4 to 6 Hz band, corresponding to the scatterplot in Figure 34.



**FIGURE 35(b):** Incoherent beam plot of the ARCESS vertical components in all nine frequency bands. Each beam has been shifted for display purposes.



VIEW BEAMS for arid 182300, aka 8800

Unshift Plot  
Log Beam  
Zoom  
UnZoom  
None

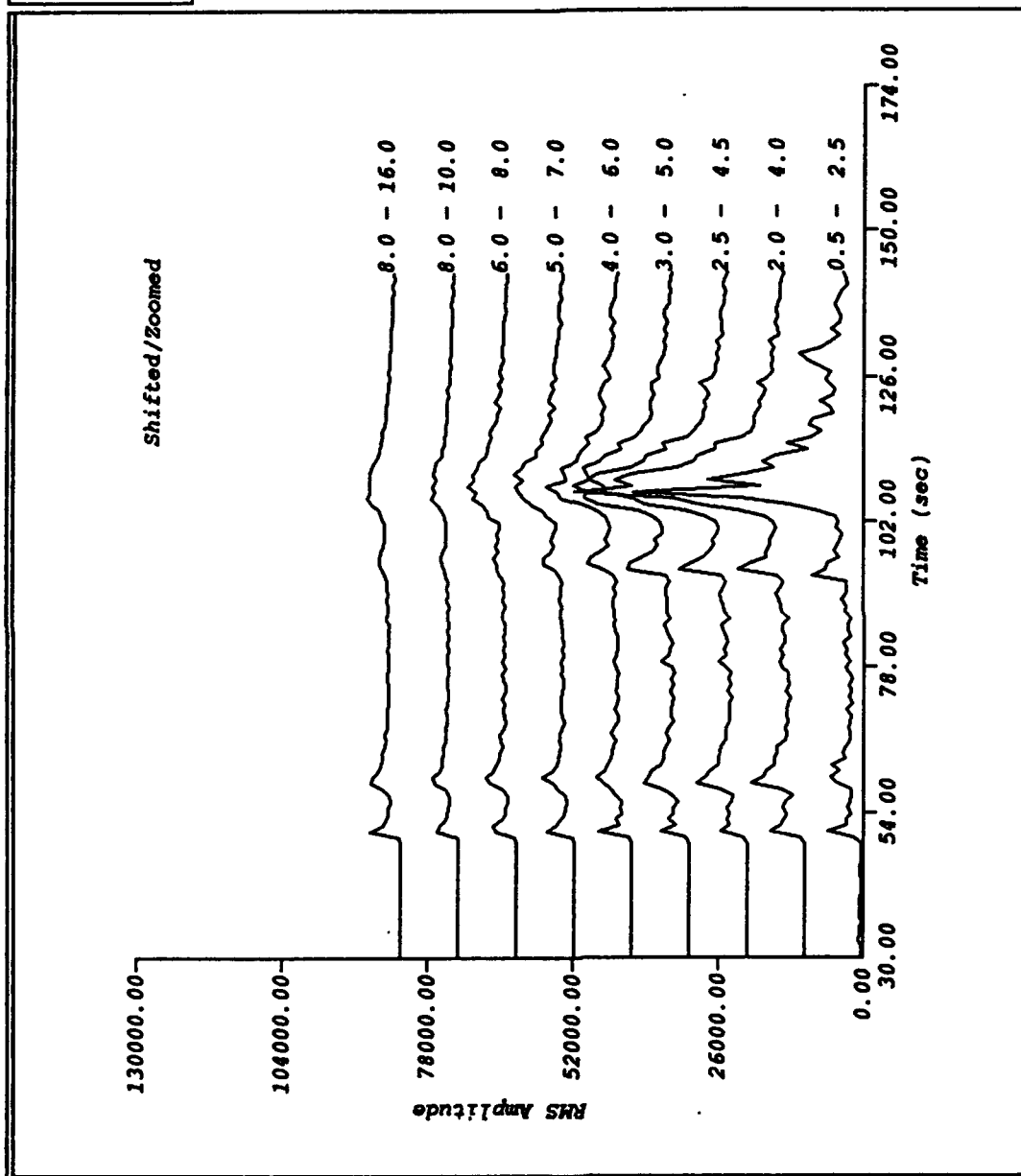


**FIGURE 36(b):** Incoherent beam plot of the ARCESS vertical components in all nine frequency bands. Each beam has been shifted for display purposes.

Also, the fact the amplitude ratios for blasts appear to be uniformly distributed from low to high values, and are not strongly clustered, supports the idea that the large variations are caused by ripple-fire induced shear. If the ratios were clumped or clustered, differences in location or shot media might explain the differences. However, the fact that the variations are not discrete but vary continuously could be a reflection of the fact that the ripple-firing would produce varying degrees of shear that would depend on many factors (e.g., number of shots, shot placement, pre-shot stress patterns). We expect this variation in shear excitation to be continuously variable and not discrete.

Yet another possibility is that many of the events we are assuming to be mine blasts may, in fact, actually be mine tremors or rock bursts. Such events are known to generate significant shear waves (e.g., Bennett et al, 1992). Perhaps these events occur at the same time as a mine blast or are even induced by the blast itself.

We also showed that the same variability occurred in the Vogtland mine blasts. In this case, the mine blasts are known to be in the same mine. However, there was one event, an earthquake, which had anomalous  $Pn/Lg$  ratios at low frequency. Figures 37a and 37b show region plots of the anomalous event (CURRENT EVENT in the plots) compared with all the other Vogtland events in the 0.5-2.5 Hz and 8-10 Hz bands, respectively. In the low frequency band, the ratio is very high, indicative of a mine explosion. However, the event is known to be an earthquake. This event corresponds to event VB538 in Wuster (1992), which he classified as a blast on the basis of the his  $S/P$  ratio, although other spectral discriminants classified the event correctly as earthquake. Figure 38b shows the same comparison in the high frequency band, where clearly this event would be correctly classified in the earthquake category. The reason Wuster (1992) misclassified this event as an explosion on the basis of  $S/P$  ratio is that his discriminant is broad-band, high-passed filtered from 0.5 Hz. The large enhancement of  $Pn$  in the low frequency band caused this discriminant to fail. However, we find that the explosion and earthquake groups are not as well separated at low frequency and we have frequently seen an enhancement like this in other regions. In one example, Baumgardt (1991a), in a study of a presumed underwater submarine explosion, found such an enhancement for an earthquake offshore of northern Norway. Also, notice in Figure 25b that the average  $Pn/Lg$  ratio for the Steigen earthquakes exceeds that of the blasts in the 0.5 to 2.5 Hz band. This may be due to noise contamination of the  $Pn$  at low frequency in the case of the Steigen events, i.e., the  $Pn$  waves may drop below the noise level in the 0.5 to 2.5 Hz band but the  $Lg$  wave is still above the noise. However, this is clearly not the case for the anomalous earthquake in the Vogtland region. The enhancement of  $Pn$  waves at low frequency may be caused by earthquake source radiation pattern

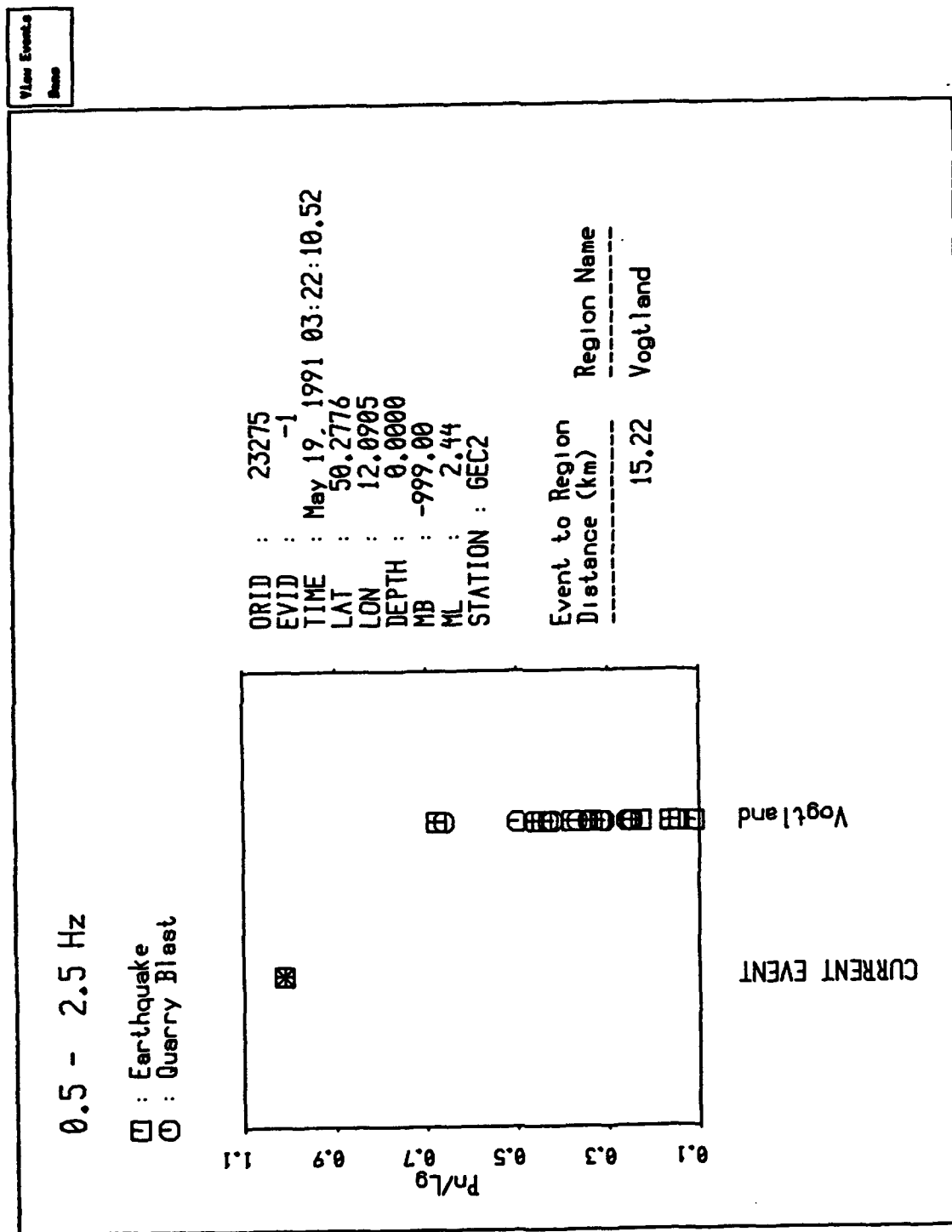


FIGURE 37(a): ISEIS plot of the anomalous earthquake (CURRENT) event in the 0.5 to 2.5 Hz band compared to the other events in the Vogtland region recorded at GERESS.

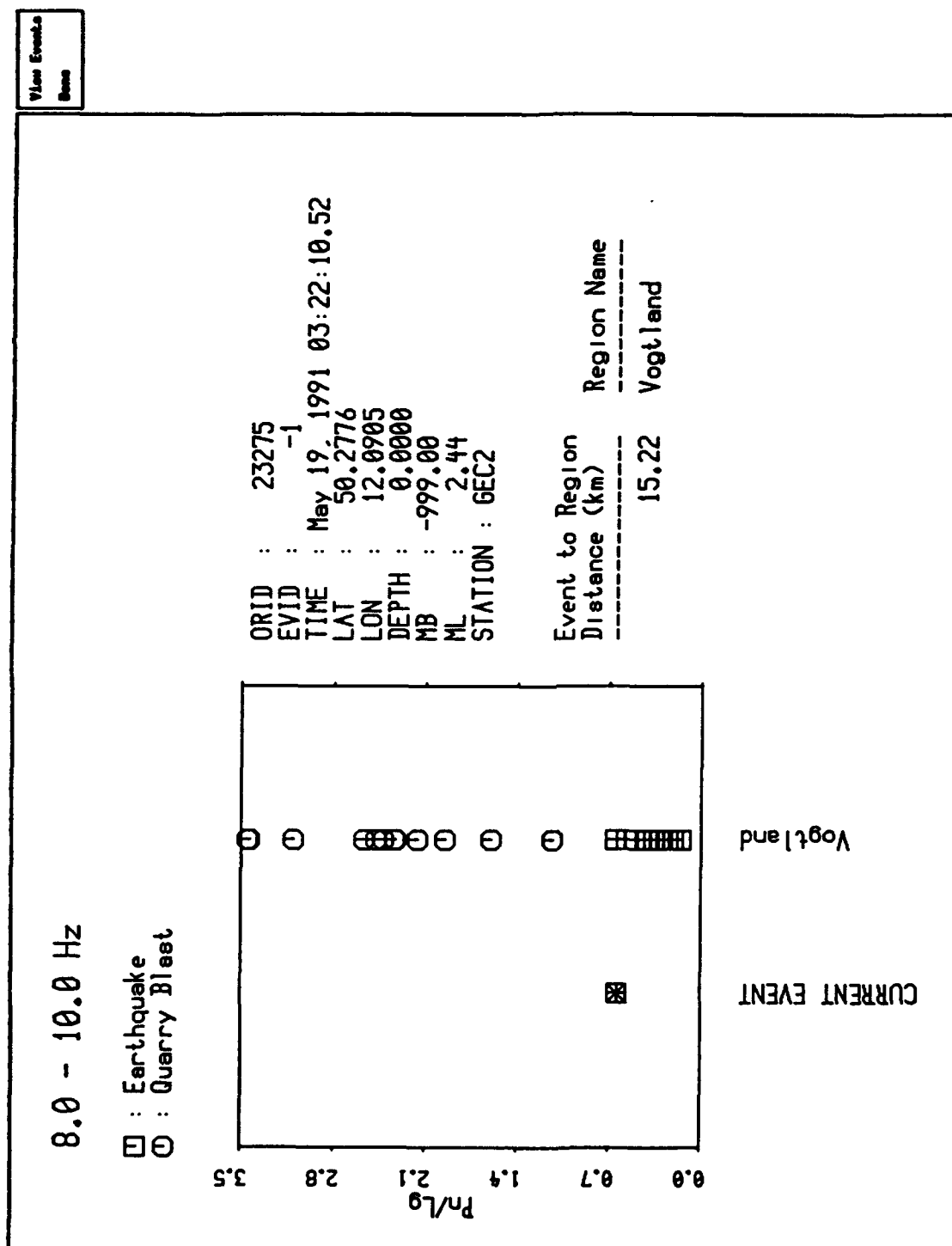


FIGURE 37(b): ISEIS plot of the anomalous earthquake (CURRENT) event in the 8 to 10 Hz band compared to the other events in the Vogtland region recorded at GERESE.

effects on either  $Pn$  and/or  $Lg$ , which may be more important at low frequency than at high frequency.

This observed variation in  $Pn/Lg$  ratios for blasts has great significance for discrimination. It shows that mine blasts can be made to look like earthquakes and raises the question of whether a nuclear explosion could also be made to resemble an earthquake. Perhaps by combining a nuclear explosion with a set of ripple-fired mine explosions, significant shear waves can be produced which might cause confusion in discrimination. Such scenarios need to be addressed in modeling studies and further observations in other mines.

### 3.4.2 Variability in Performance of the $Lg$ Spectral Ratio Discriminant

Figure 38 shows another example of a scatterplot of the spectral ratio versus local magnitude with the orids plotted to the right of each point. We now examine the spectra to find out why this discriminant works.

First, examine the spectra for two earthquakes with nearly the same magnitude (about 2.4), orid=16618 and orid=23275, in Figures 39a and 39b, respectively. Note that the latter are the spectra for the event that had the anomalously high  $Pn/Lg$  ratio at low frequency. The spectra for all the picked phases and the  $Pn$  background noise are plotted, unshifted. Comparison of these two plots shows that the 23275 event has higher signal-to-noise across the entire band, even though these two events have nearly the same estimated magnitude. However, both spectra are nearly flat throughout the band to about 17 Hz, where the anti-alias filter cuts off the high frequencies.

Figures 40a and 40b show two explosion spectra, orid=16310 and orid=26911, respectively. Comparison of these two plots clearly shows that there is less high frequency in the explosions compared to the earthquakes. Ripple-fire effects are apparent in these two sets of spectra, although they do not appear to have much effect on the overall shape of the spectra. In both cases, there appears to be a sharp peak in the spectra at about 2 Hz and then a rapid falloff to about 5 Hz, where modulations can be seen at the higher frequencies.

Figure 41 shows the data point for one Vogtland mine explosion which was classified as an earthquake on the basis of spectral ratio. Clearly, this event, orid=26825 (CURRENT EVENT in Figure 41) has a very low spectral ratio which places it well in the earthquake category, but it is known to be a blast. The spectra for this event are plotted in Figure 42 which shows why this discriminant failed. The peaking of the spectra is still apparent at about 2 to 4 Hz. However, this

# Phase Lg: Corrections: Instrument

- : Earthquake
- : Quarry Blast

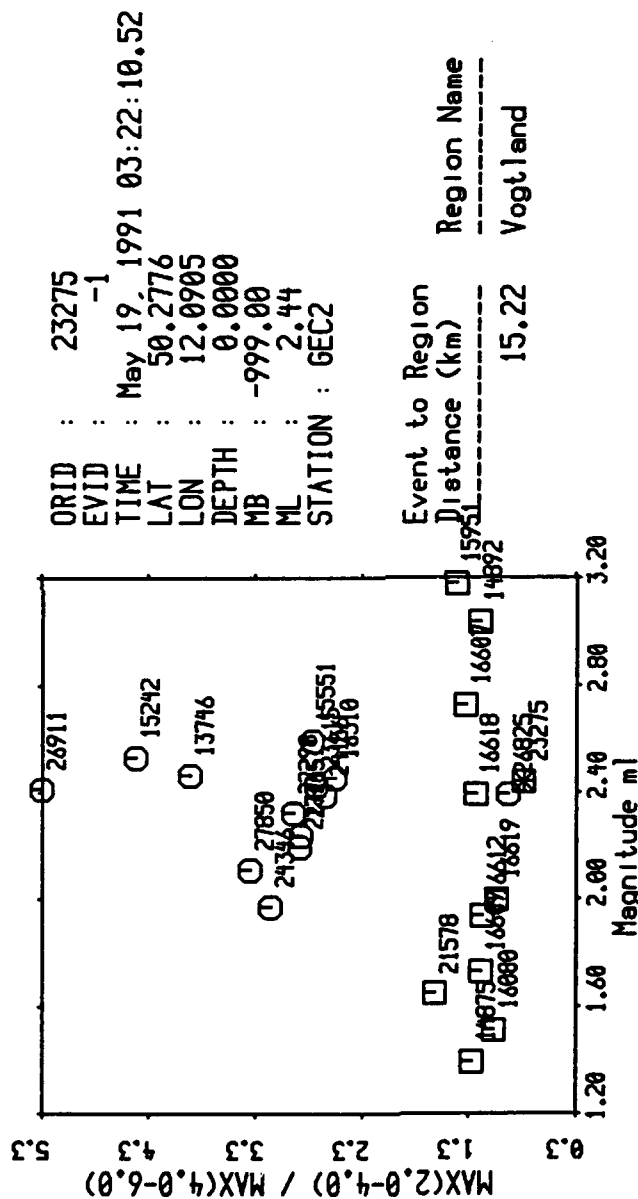


FIGURE 38: Scatterplot of the  $L_g$  spectral ratio (2-4 Hz/4-6 Hz) for the Vogtland events recorded at GERESS. The numbers to the right of each point are the IMS origin ids for the events.

VTEH FOURIER SPECTRUM for orid 16618, station GEC2

Correct Spectrum  
Shift Plot  
None

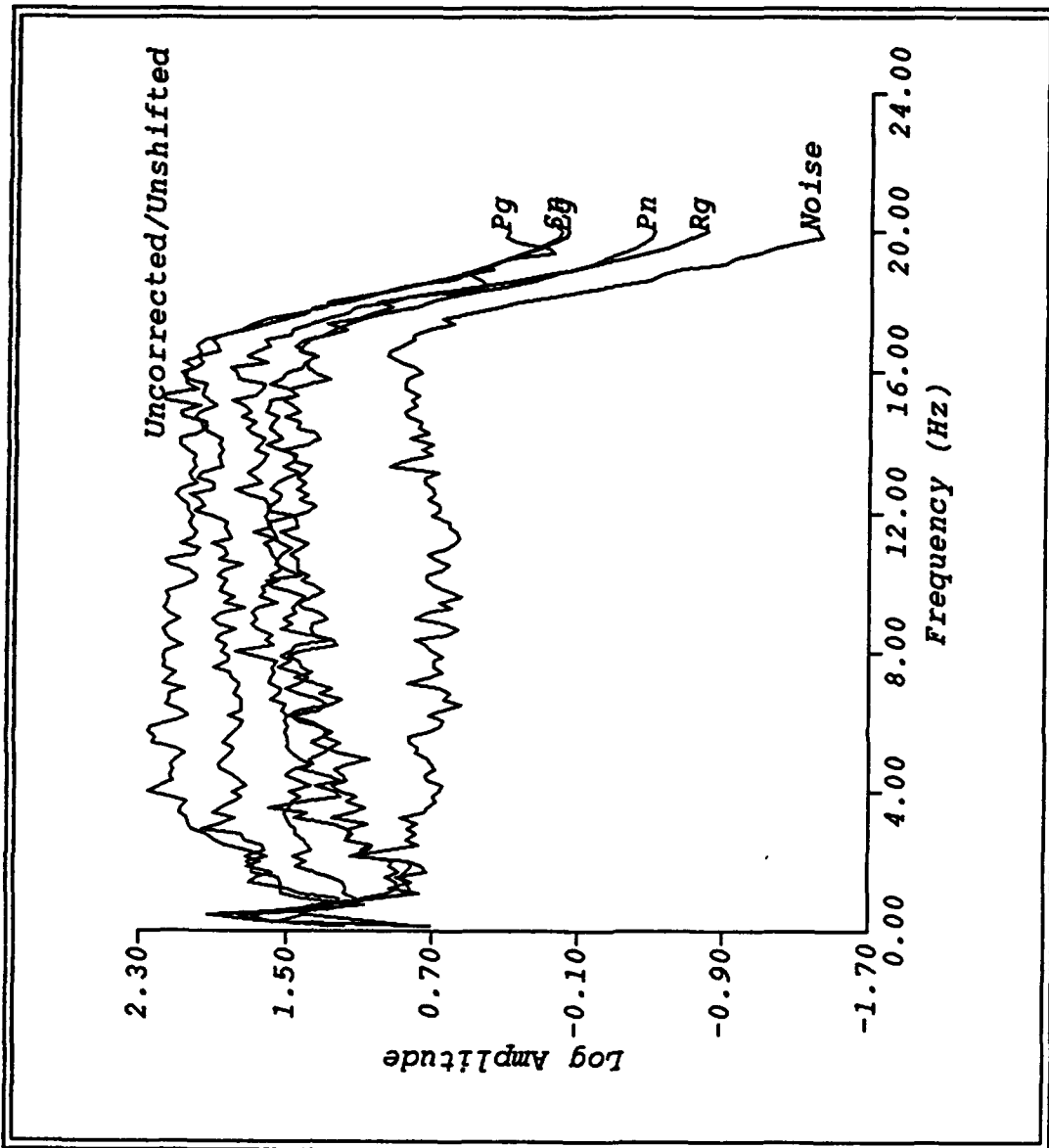


FIGURE 39(a): Plot of the spectra for the four phases and noise for a Vogtland earthquake (orid=16618) recorded at GEREES.

VIGOR FAULT SPECTRUM for orid 23276, station GE12

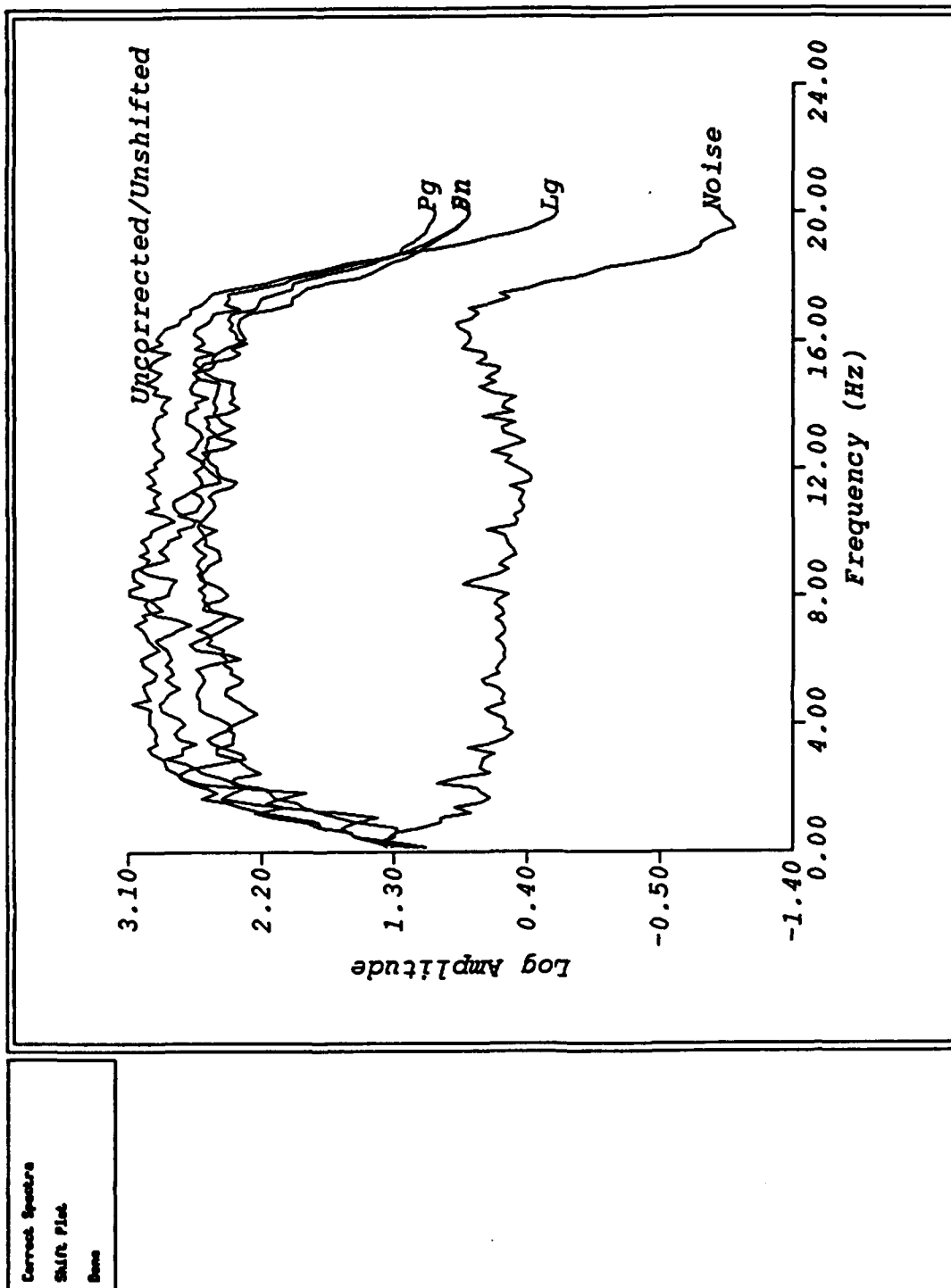


FIGURE 39(b): Plot of the spectra for the four phases and noise for a Vogtland earthquake (orid=23265) recorded at GERES.

VIEW FOURIER SPECTRA for orid 16310, station GESS

Correct Spectra  
Shift Plot  
Done

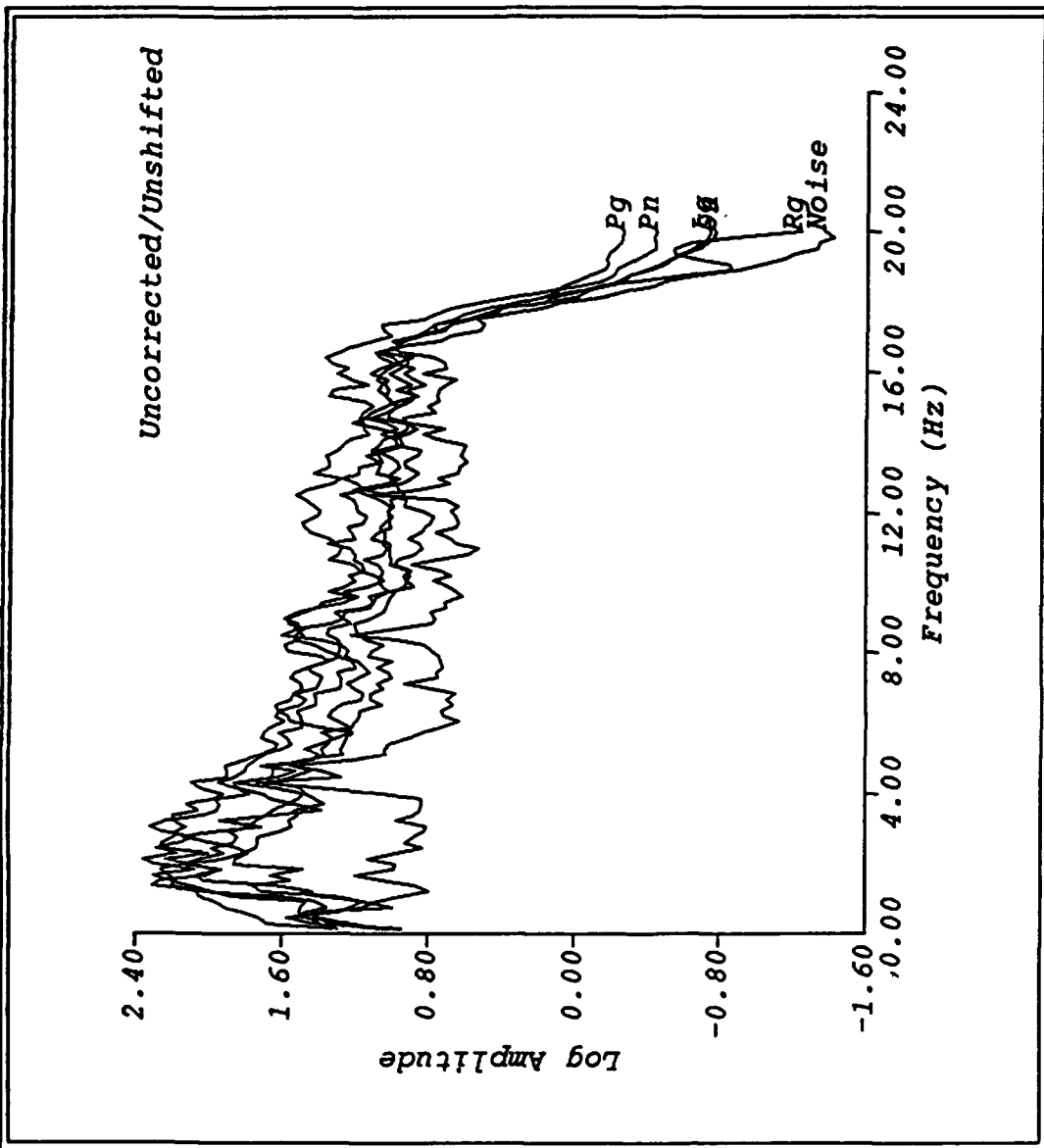


FIGURE 40(a): Plot of the spectra for the five phases and noise for a Vogtland explosion (orid=16310) recorded at GESS.

VIEW FOURIER SPECTRUM for orid 26911, station 002

Current Spectra  
Shift Plot  
None

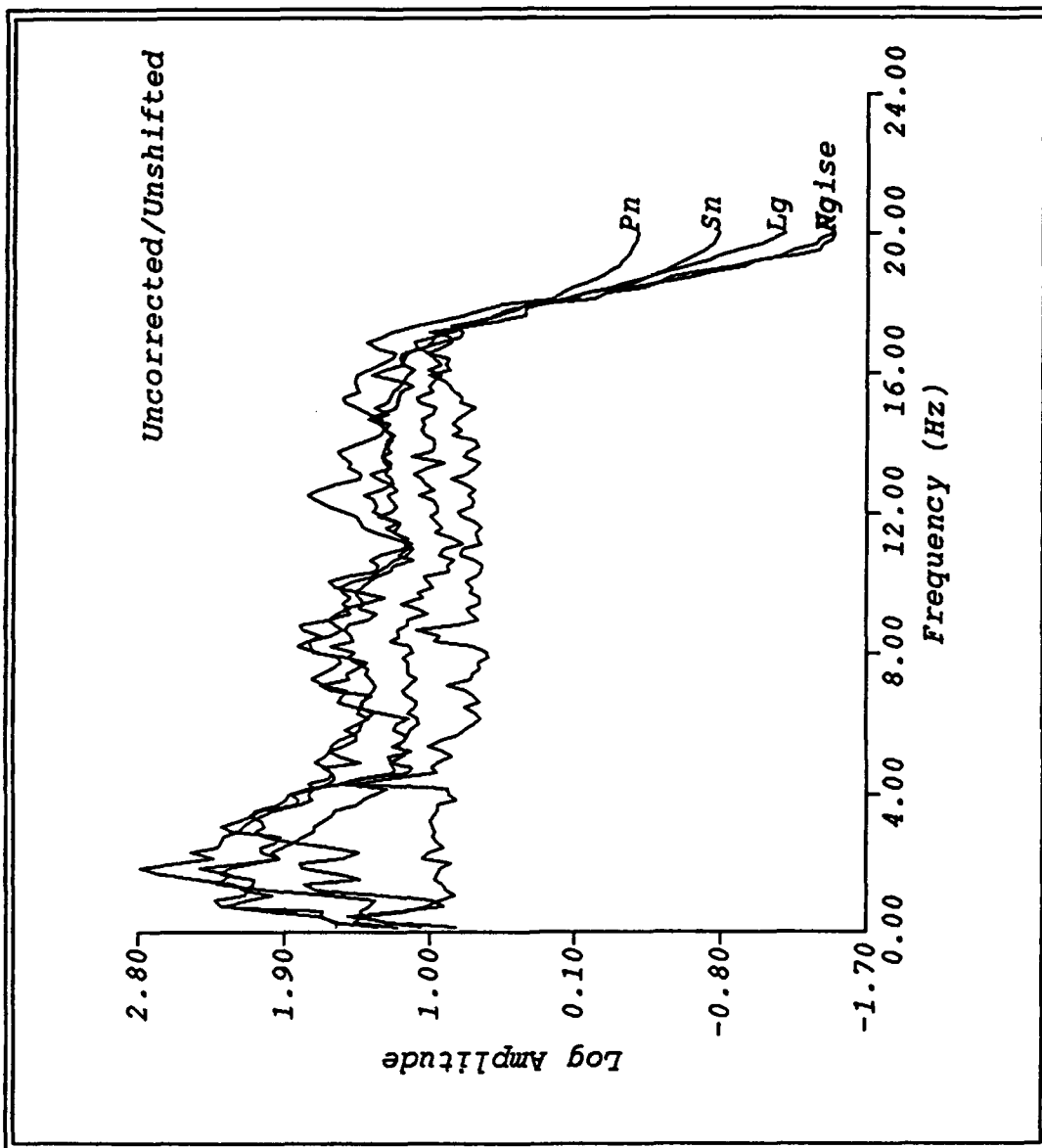


FIGURE 40(b): Plot of the spectra for the four phases and noise for a Vogtland explosion (orid=26911) recorded at GERES.

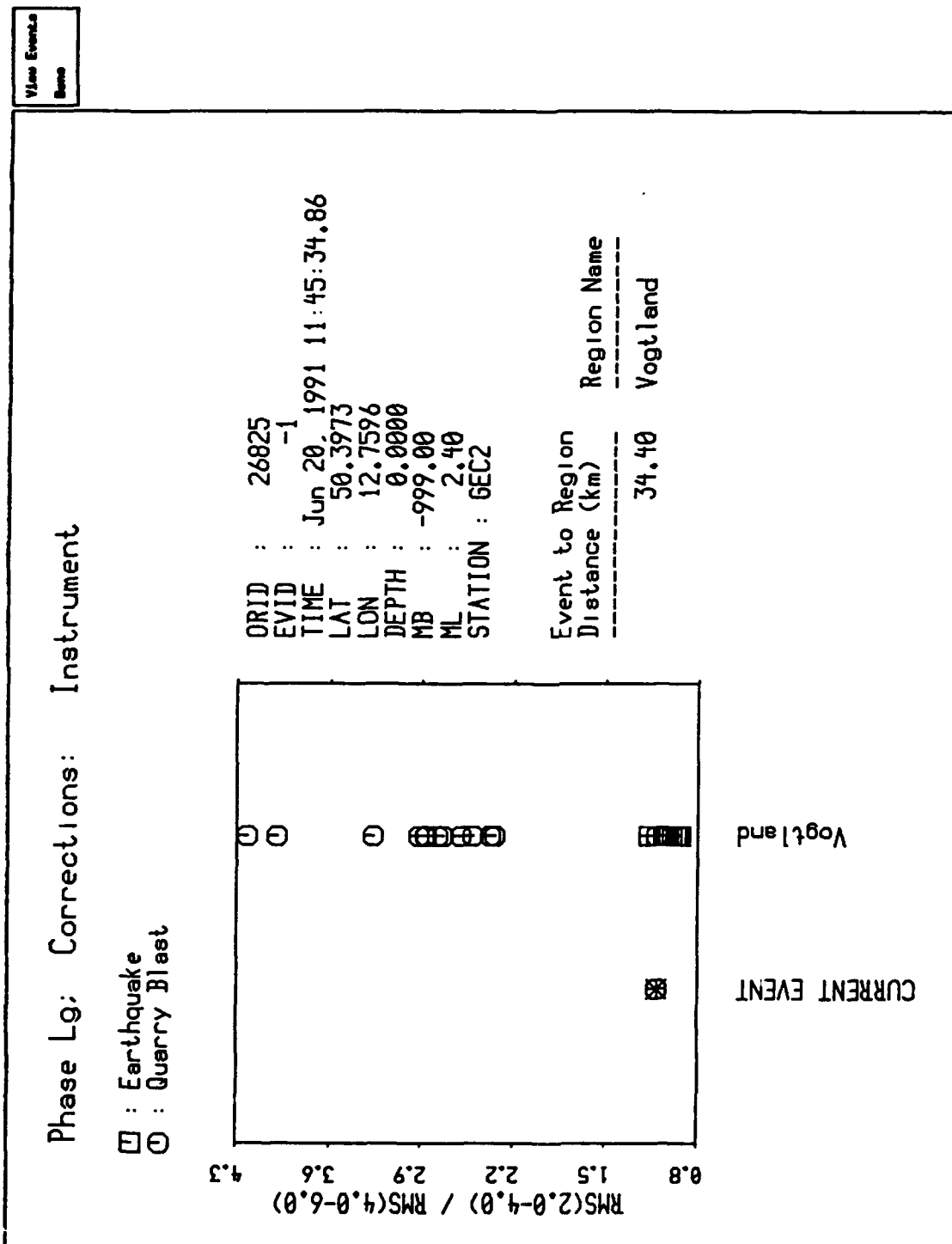


FIGURE 41: Plot of the spectral ratio for an explosion which falls in the earthquake category.

Correct Spectra  
Shift Plot  
Base

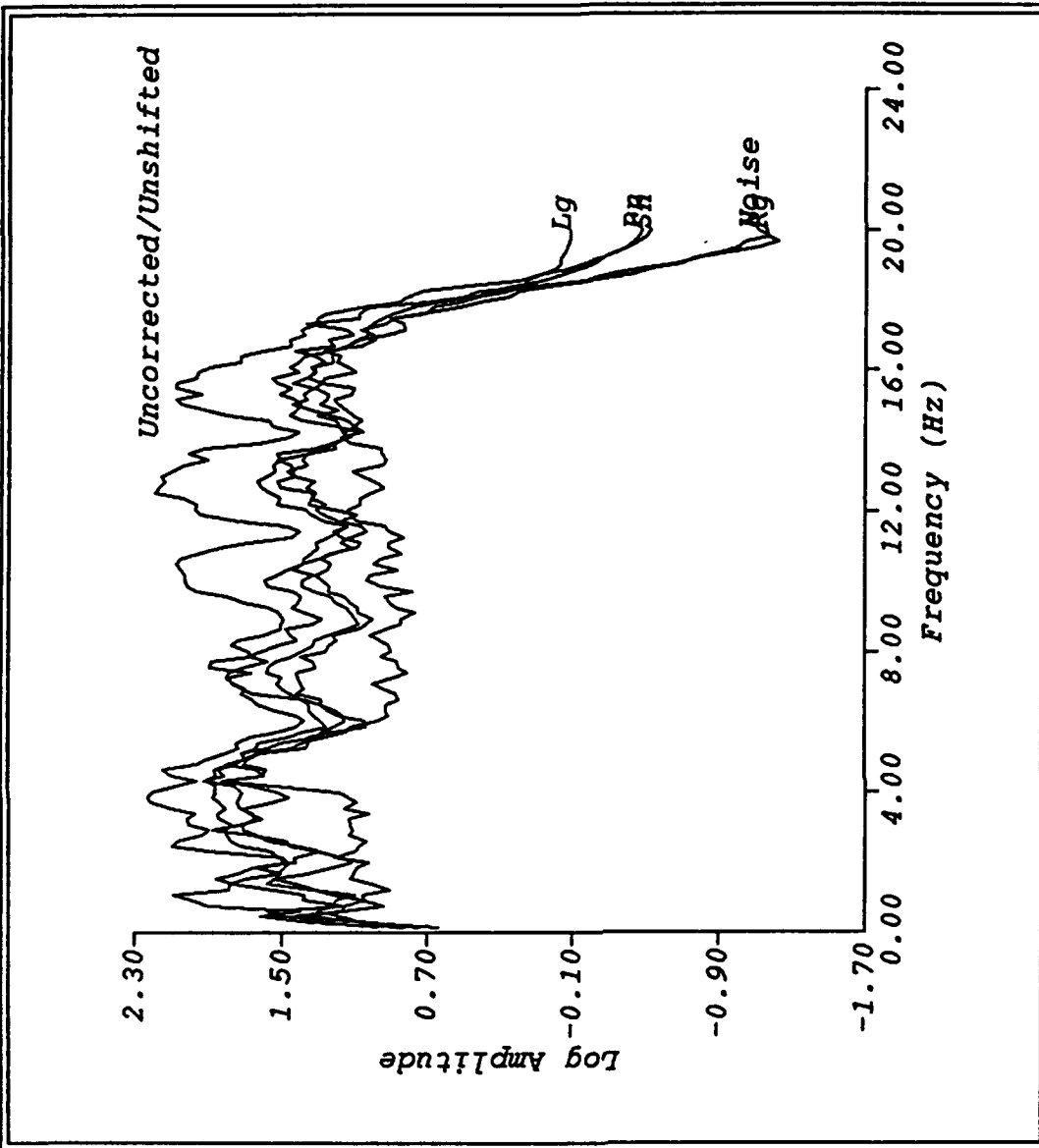


FIGURE 42: Spectra for the explosion whose spectral ratio, shown in Figure 41, fell in the earthquake category. The reason is the strong enhancement of the spectra in the 4 to 6 Hz band due to the scalloping caused by ripple fire.

event has an extremely large modulation, beginning at about 5 Hz, which continues out to the anti-alias filter cutoff. This modulation, evidently caused by a very simple, long-delay ripple-fire sequence, greatly enhances the high frequencies. This example shows how ripple-firing can affect this discriminant, as first pointed out by Baumgardt and Ziegler (1988).

These examples show that, in absence of ripple-fire effects, there appear to be significant differences in the spectral shapes of explosions and earthquakes in Germany. No such differences have been observed in Scandinavia. Taylor and Denny (1991) suggested that the *Lg* spectral-ratio discriminant works in the western U.S. because of the fact that nuclear explosions are shallower than earthquakes and the shallow explosions at NTS couple less well at high frequencies in the near-surface materials than they would have been if they had been detonated at greater depths. Moreover, the anelastic attenuation of the surface materials at NTS, where the explosions occur, may exceed that of the deeper part of the crust where the earthquakes occur. Hence, explosions may have reduced high frequencies because of the combined effects of poor high frequency coupling and low *Q*.

The models proposed by Taylor and Denny (1991) relate to large, single nuclear explosions, not ripple-fired mine explosions. Since nuclear explosions are buried and the blasting we have studied in Scandinavia and Germany accompanies surface strip mining, not deep mining, we might expect altogether different source mechanisms between buried nuclear explosions and superficial, multiple mine blasts. However, the discriminant does appear to work in Germany for strip-mine blasting, but not in Scandinavia. Also, Bennett et al (1989) found no apparent difference in *Lg* spectra from nuclear explosions and earthquakes in Kazakhstan and China, so the discriminant would apparently not work for nuclear explosions and earthquakes in Eurasia. Thus, we cannot entirely appeal to differences in source mechanism of ripple-fired mine blasts and nuclear explosions to explain why this discriminant works in some regions and not in others.

There are three possible explanations for this variability in the success of this discriminant for mine blasts. First, ripple-fire effects may obscure such differences more in Scandinavia than in Germany. Second, if the spectral ratio differences may be caused by differences in depth between explosions and earthquakes, this difference may be greater for German events than Scandinavian events. Perhaps earthquakes in Scandinavia are much more shallow than in Germany. Third, there may be differences in the shallow and deep structure in Germany that may not be present in Scandinavia.

Although, all three explanations are possible, we favor the third. Although ripple fire can greatly affect the spectral ratio, and we have seen many examples of these effects, it is unlikely that

such an effect would obscure all spectral differences. The second explanation relates to the Taylor and Denny (1991) model. However, their model relates more to the poor coupling of explosions in the near surface geology of the NTS test site than to the coupling of earthquakes. Moreover, they show that in the case of NTS explosions, overburied explosions look like earthquakes in terms of their spectral ratios. So, earthquakes do not have to be significantly deeper than explosions for them to have different spectral ratios.

The third explanation seems more likely because, in the case of IMS events, the spectral ratio discriminant has failed in shield or stable platform areas. Thus, in the Scandinavian mining districts and on the Kola Peninsula, there may be less variation in the material properties of the source region with depth and thus, no differences in spectral ratio. The ARCESS array itself is sited at the surface on hard rock. Thus, surface mine blasts and deeper earthquakes probably both occurred in hard rock. However, Germany falls in a region south of the Tornquist line, which may be tectonically more active than the Fennoscandian shield. The German blasts may have occurred in shallow materials which may be more resistant, perhaps with lower  $Q$ , than the deeper structure where the earthquakes occurred. For example, as we mentioned above, some of the GERESS sites themselves were in soft sediments. By reciprocity, we might expect the blasts to have occurred in a similar type of geology. Thus, in accordance with the source model explanation of Taylor and Denny (1991), the shallow explosions in the cratonic sedimentary cover rocks in Germany may couple less well than shallow explosions in the Fennoscandian shield, and thus, may have lower spectral ratios. We might also expect that this discriminant would not perform well in the Shagan and Novaya Zemlya test sites in the former USSR, since explosions in these regions occur in granitic type rocks. However, we might expect the discriminant to work in regions such as the Middle East, where there is more variability with depth in the crustal geology.

We thus have a possible explanation for the geographic variability of the spectral ratio discriminant. The discrimination comes from differences in depths of explosions and earthquakes combined with the nature of near surface geology in the explosion source region. In tectonically active regions, such as the western U.S. and Germany, where explosions occur in resistant, poorly coupling rocks, which may also have lower  $Q$ , the discriminant will work. In shield or platform areas, where the geology consists of hard, granitic type rocks throughout most of the geologic column, the discriminant will probably fail. All of these comments have to be qualified that the effects of ripple fire on the spectra must also be considered when interpreting the spectral ratio discriminant.

### 3.5 CONCLUSIONS

Our overall conclusion from this study are that regional waveform features will provide useful discriminants. The multivariate approach of visualization, using faces and stars, shows that there is much discriminatory information contained in multivariate vectors. This suggests that a multivariate approach, such as neural networks, may be highly useful.

As in other studies, we have found the amplitude ratio to be the most consistent discriminant. However, we have observed large variations in the mine blasts which have explained induced shear excitation in terms of explosion. We would expect less variation in nuclear explosions, and probably higher values of  $P/S$  type ratios since they are not purposely ripple-fired to induce shear. In fact, Baumgardt (1992b) observed that Novaya Zemlya explosions had much higher  $Pn/Sn$  ratios than Kola mine explosions. Finally, we have found that spectral discriminants, sensitive to spectral shape, may work better in vertically heterogeneous geologies, where explosions may be less well coupled in the shallow media. However, in shield type regions, we would not expect the discrimination. This points up the importance, in both testban and proliferation monitoring, of understanding the geology of near source regions in determining how to use and interpret regional discriminants.

#### 4.0 REFERENCES

- Anderson, J., W.E. Farrell, K. Garcia, J. Given, H. Swanger (1990). Center for Seismic Studies version 3 database: schema reference manual, Technical Report C90-01, Center for Seismic Studies, Arlington, VA.
- Bache, T.C., S.R. Bratt, J. Wang, R.M. Fung, C. Kobryn, and J.W. Given (1991). The Intelligent Monitoring System, *Bull. Seism. Soc. Am.*, **80**, 1833-1851.
- Baumgardt, D.R. (1991a). Intelligent Seismic Event Identification System, volume II: users manual, Final Report, PL-TR-91-2298(II), ENSCO, Inc, Springfield, VA.
- Baumgardt, D.R. (1991b). Possible seismic signals from a nuclear submarine accident in the Norwegian Sea, Abstract in *EOS*, **72**, 343.
- Baumgardt, D.R. (1992). Investigation of seismic discriminants in Eurasia, SBIR Phase I, Final Report, SAS-TR-92-81, ENSCO, Inc., Springfield, VA.
- Baumgardt, D.R., and K.A. Ziegler (1988). Spectral evidence of source multiplicity in explosions: application to regional discrimination of earthquakes and explosions, *Bull. Seism. Soc. Am.*, **78**, 1773-1795.
- Baumgardt, D.R., and G.B. Young (1990). Regional seismic waveform discriminants and case-based event identification using regional arrays, *Bull. Seism. Soc. Am.*, **80**, 1874-1892.
- Baumgardt, D.R., S. Carter, M. Maxson, J. Carney, K. Ziegler, and N. Matson (1991a). Design and development of the Intelligent Event Identification System, *PL-TR-91-22298(I)*, Final Report, Volumes I, II, and III, ENSCO, Inc., Springfield, VA.
- Baumgardt, D.R., G.B. Young, and K.A. Ziegler (1991b). Design and development of the Intelligent Event Identification System: design considerations and processing for regional event identification, *PL-TF-91-2211*, Scientific Report #1, ENSCO, Inc., Springfield, VA.
- Bennett, T.J., and J.R. Murphy (1986). Analysis of seismic discrimination capabilities using regional data from western United States events, *Bull. Seism. Soc. Am.*, **76**, 1069-1086.
- Bennett, T.J., B.W. Barker, K.L. McLaughlin, and J.R. Murphy (1989). Regional discrimination of quarry blasts, earthquakes, and underground nuclear explosions, Final Report, *GL-TR-89-0114*, S-Cubed, La Jolla, CA.
- Bennett, T.J., A.K. Campanella, J.F. Scheimer, and J.R. Murphy (1991). Regional discrimination of Soviet nuclear explosions, earthquakes, and mineblasts, in Papers presented at *13th Annual PL/DARPA Seismic Research Symposium*, 8-10 October 1991, Keystone, CO, 78-84.
- Bennett, T.J., J.F. Scheimer, A.K. Campanella, and J.R. Murphy (1992). Seismic discrimination of rockbursts in mines, in Papers presented at *14th Annual PL/DARPA Seismic Research Symposium*, 16-18 September 1992, Lowes Ventana Canyon Resort, Tucson, AZ, 29-35.
- Chernoff, H. (1973). The use of faces to represent points in k-dimensional space graphically, *J. Am. Stat. Assoc.*, **68**, 361-368.

Der, Z., and D. Baumgardt (1992). Automated seismic analysis using supervised machine learning (Phase I), SBIR Phase I Final Report, SAS-TR-92-92, ENSCO, Inc., Springfield, VA.

Der, Z.A., M.R. Hirano, and R.H. Shumway (1990). Coherent processing of regional signals at small seismic arrays, *Bull. Seism. Soc. Am.*, **80**, 2161-2176.

Der, Z.A., M.R. Hirano, K.A. Ziegler, and R.H. Shumway (1991). Broad-band studies of seismic sources at regional and teleseismic distances using advanced time series analysis methods, Final Report, SAS-TR-91-49, ENSCO, Inc., Springfield, VA.

Der, Z.A., R.H. Shumway, and M.R. Hirano (1992). Time domain waveform inversion - a frequency domain view: how well do we need to match waveforms?, *Bull. Seism. Soc. Am.*, **81**, 2351-2370.

Dysart, P.S., and J.J. Pulli (1990). Regional seismic event classification at the NORESS array: seismological measurements and the use of trained neural networks, *Bull. Seism. Soc. Am.*, **80**, 1910-1933.

Friedman, J.H., and L.C. Rafsky (1981). Graphics for the multivariate two-sample problem, *J. Am. Stat. Assoc.*, **76**, 277-287.

Grant, L., and J. Coyne (1992). Ground truth data for seismic discrimination research, in Papers presented at *14th Annual PL/DARPA Seismic Research Symposium*, 16-18 September 1992, Lowes Ventana Canyon Resort, Tucson, AZ, 139-145.

Harjes, H.P., N. Gestermann, M. Jost, J. Schweitzer, and J. Wuster (1992). Advanced waveform research methods for GERESS recordings, Annual Report: 15 February 1991 -14 February 1992, *PL-TR-92-2142*.

Harris, D.B. (1991). A waveform correlation method for identifying quarry explosions, *Bull. Seism. Soc. Am.*, **81**, 2395-24118.

Johnson, R.A., and D.W. Wichern (1988). *Applied Multivariate Statistical Analysis*, Prentice Hall, New Jersey.

Kandt, K., P. Yuenger, and D. Baumgardt (1987). Intelligent analysis of seismic events, *Proc. ESIG - Third Ann. Expert Systems in Government Conference*, October 19-23, 1987, Washington, D.C., 217-223.

Lynnes, C., and R. Baumstark (1991). Phase and spectral ratio discrimination in North America, *PL-TR-91-2212(II)*, Final Report, 18 July 1991, Teledyne Geotech, Alexandria, VA.

Murphy, J.R., and T.J. Bennett (1982). A discrimination analysis of short-period regional seismic data recorded at Toronto Forest Observatory, *Bull. Seism. Soc. Am.*, **72**, 1351-1366.

Mykkeltveit, S., and H. Bungum (1984). Processing of regional seismic events using data from small-aperture arrays, *Bull. Seism. Soc. Am.*, **74**, 2313-2333.

Riviere-Barbier, F., and L.T. Grant (1992). Cluster analysis of closely spaced mining blasts as a method of event location, *PL-TF-92-2006*, Science Application Intl. Corp., Arlington, VA.

Sereno, T. (1992). Personal Communication.

Taylor, S.R., and M.D. Denny (1991). An analysis of spectral differences between Nevada Test Site and Shagan River nuclear explosions, *J. Geophys. Res.*, **96**, 6237-6245.

Taylor, S.R., N.W. Sherman, and M.D. Denny (1988). Spectral discrimination between NTS explosions and western United States earthquakes at regional distances, *Bull. Seism. Soc. Am.*, **78**, 1563-1579.

Taylor, S.R., M.D. Denny, E.S. Vergino, and R.E. Glaser (1989). Regional discrimination between NTS explosions and western U.S. earthquakes, *Bull. Seism. Soc. Am.*, **79**, 1142-1176.

Wuster, J. (1992). Discrimination of chemical explosions and earthquakes in Central Europe - a case study, submitted to *Bull. Seism. Soc. Am.*